

# Oligocene-Neogene lithospheric-scale reactivation of Mesozoic terrane accretionary structures in the Alaska Range suture zone, southern Alaska, USA

## Trevor S. Waldien<sup>1,†</sup>, Sarah M. Roeske<sup>1</sup>, Jeffrey A. Benowitz<sup>2</sup>, Evan Twelker<sup>3</sup>, and Meghan S. Miller<sup>4</sup>

<sup>1</sup>Department of Earth and Planetary Sciences, University of California, Davis, 1 Shields Avenue Davis, California 95616, USA <sup>2</sup>Geophysical Institute, University of Alaska, Fairbanks, 900 Yukon Drive Fairbanks, Alaska 99775, USA <sup>3</sup>Alaska Division of Geological and Geophysical Surveys, 3354 College Road, Fairbanks, Alaska 99709, USA <sup>4</sup>Research School of Earth Sciences, Australian National University, Building 142, Mills Road, Canberra, ACT 2601 Australia

### ABSTRACT

Terrane accretion forms lithospheric-scale fault systems that commonly experience long and complex slip histories. Unraveling the evolution of these suture zone fault systems yields valuable information regarding the relative importance of various upper crustal structures and their linkage through the lithosphere. We present new bedrock geologic mapping and geochronology data documenting the geologic evolution of reactivated shortening structures and adjacent metamorphic rocks in the Alaska Range suture zone at the inboard margin of the Wrangellia composite terrane in the eastern Alaska Range, Alaska, USA. Detrital zircon uranium-lead (U-Pb) age spectra from metamorphic rocks in our study area reveal two distinct metasedimentary belts. The Maclaren schist occupies the inboard (northern) belt, which was derived from terranes along the western margin of North America during the mid- to Late Cretaceous. In contrast, the Clearwater metasediments occupy the outboard (southern) belt, which was derived from arcs built on the Wrangellia composite terrane during the Late Jurassic to Early Cretaceous. A newly discovered locality of Alaska-type zoned ultramafic bodies within the Clearwater metasediments provides an additional link to the Wrangellia composite terrane. The Maclaren and Clearwater metasedimentary belts are presently juxtaposed by the newly identified Valdez Creek fault, which is an upper crustal reactivation of the Valdez Creek shear zone, the Late Cretaceous plate boundary that initially brought them together. 40Ar/39Ar mica ages reveal independent post-collisional thermal histo-

 $^{\dagger}tswaldien@ucdavis.edu.$ 

GSA Bulletin;

ries of hanging wall and footwall rocks until reactivation localized on the Valdez Creek fault after ca. 32 Ma. Slip on the Valdez Creek fault expanded into a thrust system that progressed southward to the Broxson Gulch fault at the southern margin of the suture zone and eventually into the Wrangellia terrane. Detrital zircon U-Pb age spectra and clast assemblages from fault-bounded Cenozoic gravel deposits indicate that the thrust system was active during the Oligocene and into the Pliocene, likely as a far-field result of ongoing flat-slab subduction and accretion of the Yakutat microplate. The Valdez Creek fault was the primary reactivated structure in the suture zone, likely due to its linkage with the reactivated boundary zone between the Wrangellia composite terrane and North America in the lithospheric mantle.

#### INTRODUCTION

It has long been known that ancient intracontinental sutures are prone to structural reactivation (Dewey and Burke, 1973; Dewey, 1977). Within the crust, the orientation of inherited faults, presence of pre-existing rock fabrics, and mineral rheology are generally considered to be important factors controlling reactivation (e.g., Sibson, 1985; Ranalli, 2000; Beacom et al., 2001). However, a growing body of literature emphasizes the importance of mechanical properties of the lithospheric mantle as key factors controlling the structural evolution of polyphase accretionary orogens (Tikoff et al., 2001; Tommasi et al., 2009; Heron et al., 2016; Kelly et al., 2020; Goussin et al., 2020). If the mechanical properties of the lithospheric mantle do indeed control crustal fault reactivation, then post-collisional deformation would be more likely to focus on pre-existing crustal structures that root into inherited mantle shear zones.

Southern Alaska contains a suite of reactivated suture zone structures that likely record such linkage to an inherited lithospheric scale boundary. Rocks within the Alaska Range suture zone represent a series of marine basins that closed during the Mesozoic collision of the Wrangellia composite island arc terrane with previously accreted terranes in western North America (Ridgway et al., 2002). Decades of regional mapping, geochronology, and geophysics have identified crustal scale faults at the northern and southern boundaries of the suture zone and inferred them to be the primary collisional structures (Coney et al., 1980; Csejtey et al., 1982; Brennan et al., 2011). Recent detailed petrography and uranium-lead (U-Pb) detrital zircon analyses have shown that the marine strata and metamorphic equivalents within the suture zone may be split into a northern continental-derived succession and a southern Wrangellia composite terranederived succession (Hults et al., 2013; Yokelson et al., 2015; Box et al., 2019). A potentially deeply rooted accretionary structure has been inferred to juxtapose the two sedimentary successions and their basement in the western Alaska Range (Wallace et al., 1989; Decker et al., 1994), yet the structure has remained cryptic due to the similar rock types, prevalence of cover strata, and distributed deformation throughout the region (e.g., Box et al., 2019). Although faults at the boundaries of the suture zone appear to have no significant displacement since the Cretaceous (Wahrhaftig et al., 1975; O'Neill et al., 2001), regional seismicity (Ruppert, 2008) indicates that the interior of the suture zone is actively deforming. Thus, post-suturing deformation may have been focused on a cryptic boundary juxtaposing the distinct sedimentary successions within the suture zone. Whereas the location of these intrasuture zone structures has remained enigmatic since the early studies in the western Alaska Range (e.g., Wallace et al., 1989; Box et al.,

https://doi.org/10.1130/B35665.1; 15 figures; 2 tables; 1 supplemental file.

For permission to copy, contact editing@geosociety.org
© 2020 Geological Society of America

2019), the eastern Alaska Range contains correlative rock packages that were highly shortened during and after the collision and thus offers an opportunity to evaluate the reactivation of suture zone structures in a well-exposed focus area.

In this paper we present new bedrock geologic mapping, U-Pb geochronology, and <sup>40</sup>Ar/<sup>39</sup>Ar thermochronology from the eastern Alaska Range. We use our data to determine the burial and exhumation history of Alaska Range suture zone metamorphic rocks in the study area and then resolve the polyphase slip history of faults responsible for the burial and exhumation. Our data bear on the relative importance of Alaska Range suture zone boundary structures and intra-suture zone structures during Cenozoic reactivation.

#### GEOLOGIC BACKGROUND

#### Geology of the Alaska Range Suture Zone

The geology of the northern North American Cordillera is largely composed of allochthonous terranes that collided with the North American continent during the Mesozoic (Jones et al., 1977; Ridgway et al., 2002; Colpron et al., 2007) (Fig. 1). Major allochthonous terranes in southern Alaska and adjacent Canada include the Wrangellia, Alexander, and Peninsular terranes, which were amalgamated prior to collision with the North American Cordillera (Gardner et al., 1988; Beranek et al., 2014; Israel et al., 2014) and have thus been termed the "Wrangellia

composite terrane" (Plafker and Berg, 1994), "Insular Belt" (Monger et al., 1982), "Insular Superterrane" (Rusmore, 1987), or "Talkeetna Superterrane" (Csejtey et al., 1982). We herein refer to the amalgamated terranes as the "Wrangellia composite terrane" and distinguish the individual terranes only when necessary. A suite of Late Jurassic and Cretaceous marine basinal assemblages (Kahiltna-Nutzotin-Dezadeash-Gravina-Methow-Tyaughton basins) is discontinuously exposed along ~3000 km of the inboard (north and east) margin of the Wrangellia composite terrane throughout the northern Cordillera. These basin strata and their metamorphic equivalents are interpreted to represent south-to-north closure of a series of fringing

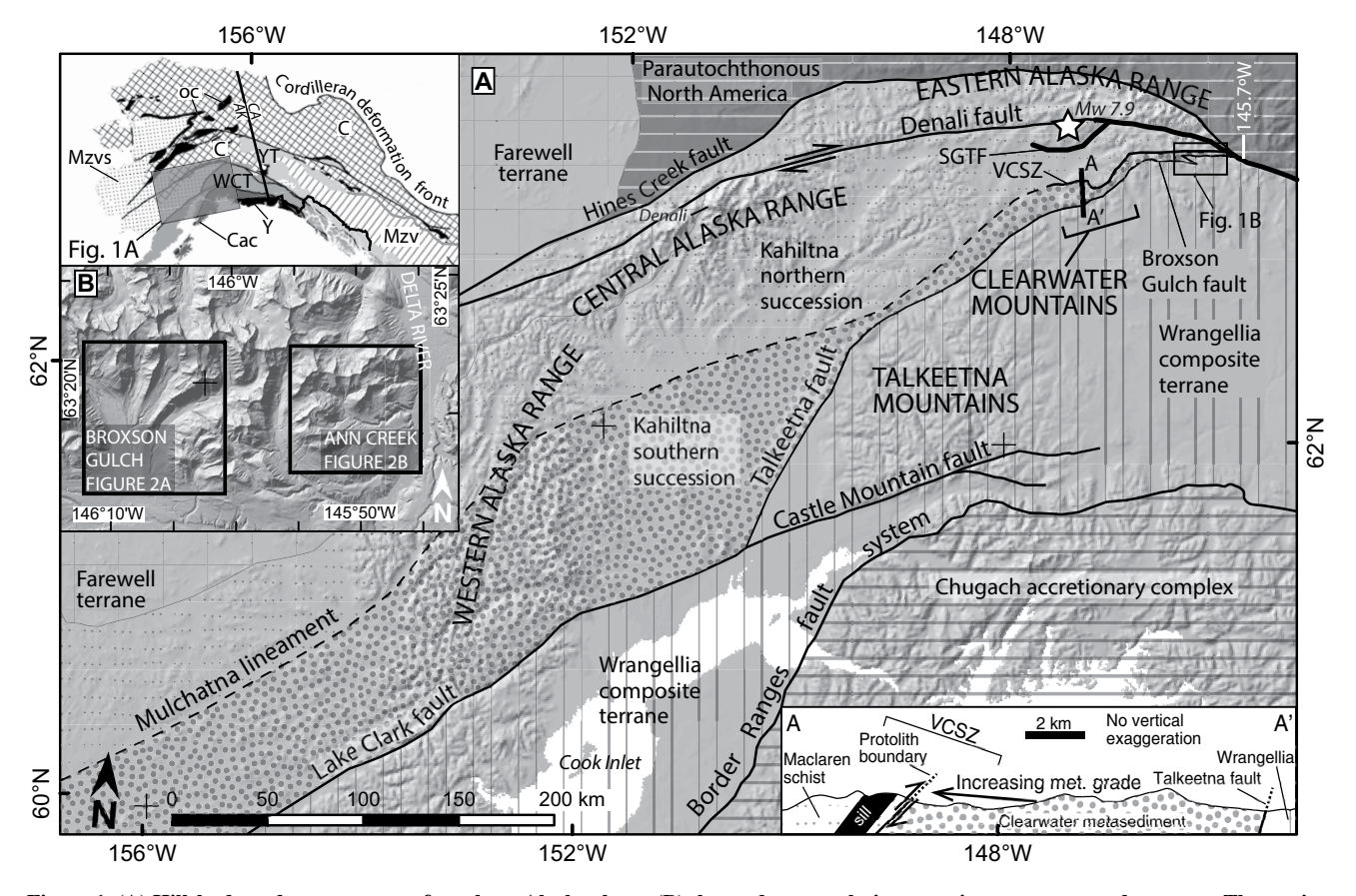


Figure 1. (A) Hillshade and terrane map of southern Alaska shows (B) the study area relative to major structures and terranes. The section of the Denali fault that had surface rupture during the 2002 M<sub>w</sub> 7.9 Denali earthquake is traced in bold. The star marks the epicenter of the main shock. SGTF—Susitna Glacier thrust fault; VCSZ—Valdez Creek shear zone. Cross section A-A' shows the structural relationships across the Valdez Creek shear zone (modified from Davidson et al., 1992). *Inset*—Terrane map of the northern North American Cordillera modified from Colpron and Nelson (2011) showing the area of Figure 1A relative to other Cordilleran terranes. C—continental crystal-line rocks and platform strata (not necessarily Laurentia); YT—Yukon-Tanana terrane; oc—ophiolites and fragments of oceanic crust; Mzv—accreted Mesozoic volcanic arcs (Stikinia, Cache Creek, Quesnellia); Mzvs—Mesozoic basinal assemblages (Kahiltna, Dezadeash, Nutzotin, Gravina, Kuskokwim) and underlying arc and sedimentary rocks; WCT—Wrangellia composite terrane (Wrangellia, Alexander, Peninsular); Cac—Chugach accretionary complex; Y—Yakutat terrane; AK—Alaska; CA—Canada. (B) Shaded relief map showing the locations of the map areas (black boxes) relative to the Delta River. The confluence of the four glacial valleys within the area of Figure 2A is referred to as Broxson Gulch. Ann Creek drains the center of the area of Figure 2B from west to east.

ocean basins between previously accreted terranes and the Wrangellia composite terrane (Rubin and Saleeby, 1991; McClelland et al., 1992; Kapp and Gehrels, 1998; Hampton et al., 2007; Manuszak et al., 2007; Surpless et al., 2014; Yokelson et al., 2015; Lowey, 2019; Trop et al., 2020). Strata in these basins were structurally imbricated, buried by thrust sheets, variably metamorphosed, and intruded by plutons during accretion of the Wrangellia composite terrane (Csejtey et al., 1982; Nokleberg et al., 1985; Rubin et al., 1990; Haeussler, 1992; Davidson and McPhillips, 2007; Trop et al., 2020). Syn- and post- collisional dextral strike-slip faulting has dismembered the basinal assemblages and contributed to northward transport of the outboard terranes (Nokleberg et al., 1985; Ridgway et al., 2002; Wyld et al., 2006).

The region between the Wrangellia composite terrane and previously accreted inboard terranes in southern Alaska presently exposes a large region of imbricated Kahiltna assemblage underlain by fragments of oceanic crust and disparate terranes (Amato et al., 2007a; Hampton et al., 2007; Nokleberg and Richter, 2007; Gilman et al., 2009). The geology in this region is interpreted to record closure of the Kahiltna basin, possibly involving a component of subduction, and has thus been named the Alaska Range suture zone (Ridgway et al., 2002).

Jurassic-Cretaceous Kahiltna strata and metamorphic equivalents within the suture zone have been split into northern and southern successions. The northern succession comprises compositionally mature sedimentary rocks with detrital zircon U-Pb age signatures that record sediment source areas in parauthochonous North America, the Yukon-Tanana terrane, and Mesozoic igneous belts built on those terranes (Kalbas et al., 2007; Hampton et al., 2010; Huff, 2012; Hults et al., 2013; Box et al., 2019; Romero et al., 2020). The southern succession consists of compositionally immature sedimentary/volcanosedimentary strata with detrital zircon U-Pb age signatures that match to Mesozoic arcs built on the Wrangellia composite terrane (Mooney, 2010; Hults et al., 2013; Box et al., 2019). In a regional mapping study of the western Alaska Range, Wallace et al. (1989) first separated the northern continental-derived strata of the Kahiltna assemblage from the southern ocean arcderived Kahiltna assemblage, which they called the Koksetna River sequence, and depicted the two successions as juxtaposed by the NE-SWstriking Mulchatna fault (Mulchatna Lineament, Fig. 1). Although the Mulchatna fault is poorly exposed, the inferred surface trace aligns with a regional aeromagnetic lineament, which may record contrasting characteristics in basement rocks across the structure (Saltus et al., 2007).

From the western Alaska Range the northern and southern Kahiltna assemblages continue northeast, where correlative structures may be covered by younger strata in the northern Talkeetna Mountains (Trop and Ridgway, 2007; Hampton et al., 2010) and are truncated by the Denali fault in the eastern Alaska Range (e.g., Hults et al., 2013) (Fig. 1).

In the eastern Alaska Range the Maclaren Glacier metamorphic belt is a highly metamorphosed portion of the Kahiltna assemblage, which has undergone major syn-collisional shortening along the Valdez Creek shear zone. The Clearwater Mountains (Fig. 1) contain the type locality of the Maclaren Glacier metamorphic belt, where it has been defined as a Barrovian inverted metamorphic belt that grades from lower greenschist facies metasedimentary strata in the south to amphibolite facies pelitic and quartzofeldspathic schist and gneiss in the north (Smith, 1981). The Valdez Creek shear zone, a ca. 75 Ma amphibolite facies S-vergent mylonitic thrust zone (Davidson et al., 1992; Ridgway et al., 2002), intersects the Maclaren Glacier metamorphic belt and marks an abrupt change in metamorphic grade between hanging wall and footwall rocks. The inverted metamorphic field gradient is restricted to the footwall of the Valdez Creek shear zone and is thus inferred to have developed during S-vergent motion on the shear zone (Smith, 1981; Davidson et al., 1992; Hollister, 1993; Beam and Fisher, 1999) (Fig. 1 cross section). Hanging wall rocks, in contrast, experienced kyanite grade metamorphism prior to development of the shear zone (Davidson et al., 1992). Recent U-Pb detrital zircon studies in the Clearwater Mountains have shown that the hanging wall rocks (Maclaren schist and gneiss) are metamorphic equivalents of the northern succession of the Kahiltna assemblage and the footwall rocks (Clearwater metasediments) are equivalent to the southern succession (Mooney, 2010; Link, 2017).

# Cenozoic Deformation in the Alaska Range Suture Zone

The Alaska Range suture zone is cut by a number of major faults, several of which likely formed during Mesozoic terrane accretion and have been reactivated in the Cenozoic. The most prominent active fault in the region is the Denali fault, which transects the suture zone west of 145.7°W and juxtaposes the Wrangellia composite terrane against inboard peri-Laurentian terranes east of 145.7°W (Fig. 1). Dextral slip in the Denali fault system has been ongoing since at least 57 Ma (Nokleberg et al., 1985; Murphy, 2018; Regan et al., 2020) and continues through the Holocene (St. Amand, 1957; Richter and

Matson, 1971; Stout et al., 1973; Matmon et al., 2006; Mériaux et al., 2009; Haeussler et al., 2017a). Surface rupture during the 2002  $M_{\rm w}$  7.9 Denali earthquake illustrates that the fault is active today (Eberhart-Phillips et al., 2003).

The Hines Creek and Talkeetna-Broxson Gulch faults are generally considered to coincide with the northern and southern boundaries of the suture zone, respectively (Fig. 1). Although geophysical observations suggest that the Hines Creek and Talkeetna faults are major crustal structures (Veenstra et al., 2006; Brennan et al., 2011; Allam et al., 2017), postcollisional deformation along these structures appears to be highly localized (cf., Wahrhaftig et al., 1975; Csejtey et al., 1982; O'Neill et al., 2001; Mooney, 2010; Bemis et al., 2012; Nokleberg et al., 2013; Koehler, 2013). The Broxson Gulch fault, in contrast, displays clear evidence for post-collisional reactivation where it marks the southern margin of the suture zone in the eastern Alaska Range (Stout and Chase, 1980; Nokleberg et al., 1985; this study).

Despite evidence for only local Cenozoic reactivation of faults at the margins of the Alaska Range suture zone, several lines of evidence indicate that post-collisional deformation has been focused within the suture zone: (1) Lowtemperature thermochronology studies show widespread fault slip-related exhumation and topographic development throughout the suture zone (Fitzgerald et al., 1993, 1995; Haeussler et al., 2008; Benowitz et al., 2011, 2012, 2014; Riccio et al., 2014; Lease et al., 2016; Lease, 2018), which has expanded Alaska Range topography (Bemis and Wallace, 2007; Ridgway et al., 2007; Bemis et al., 2015; Waldien et al., 2018; Bill et al., 2018). (2) Structural, stratigraphic, and geophysical studies show Neogene and Quaternary activity on faults at the margins on the Denali massif in the central Alaska Range (Burkett et al., 2016; Saltus et al., 2016; Haeussler et al., 2017b; Trop et al., 2019). (3) Geodetic data from southern Alaska support a model wherein upper plate deformation related to Alaska-Aleutian subduction zone convergence is concentrated in the suture zone (Freymueller et al., 2008; Kreemer et al., 2014). (4) Multiple receiver-function studies show that the suture zone crust is ~5 km to 15 km thicker than crust in adjacent terranes and suggest that a portion of this thickening developed during the Cenozoic (Veenstra et al., 2006; Brennan et al., 2011; Miller et al., 2018).

# Motivation for Re-analysis of Broxson Gulch and Ann Creek

Our map areas (Fig. 2, Broxson Gulch and Ann Creek) are the locations of the first detailed

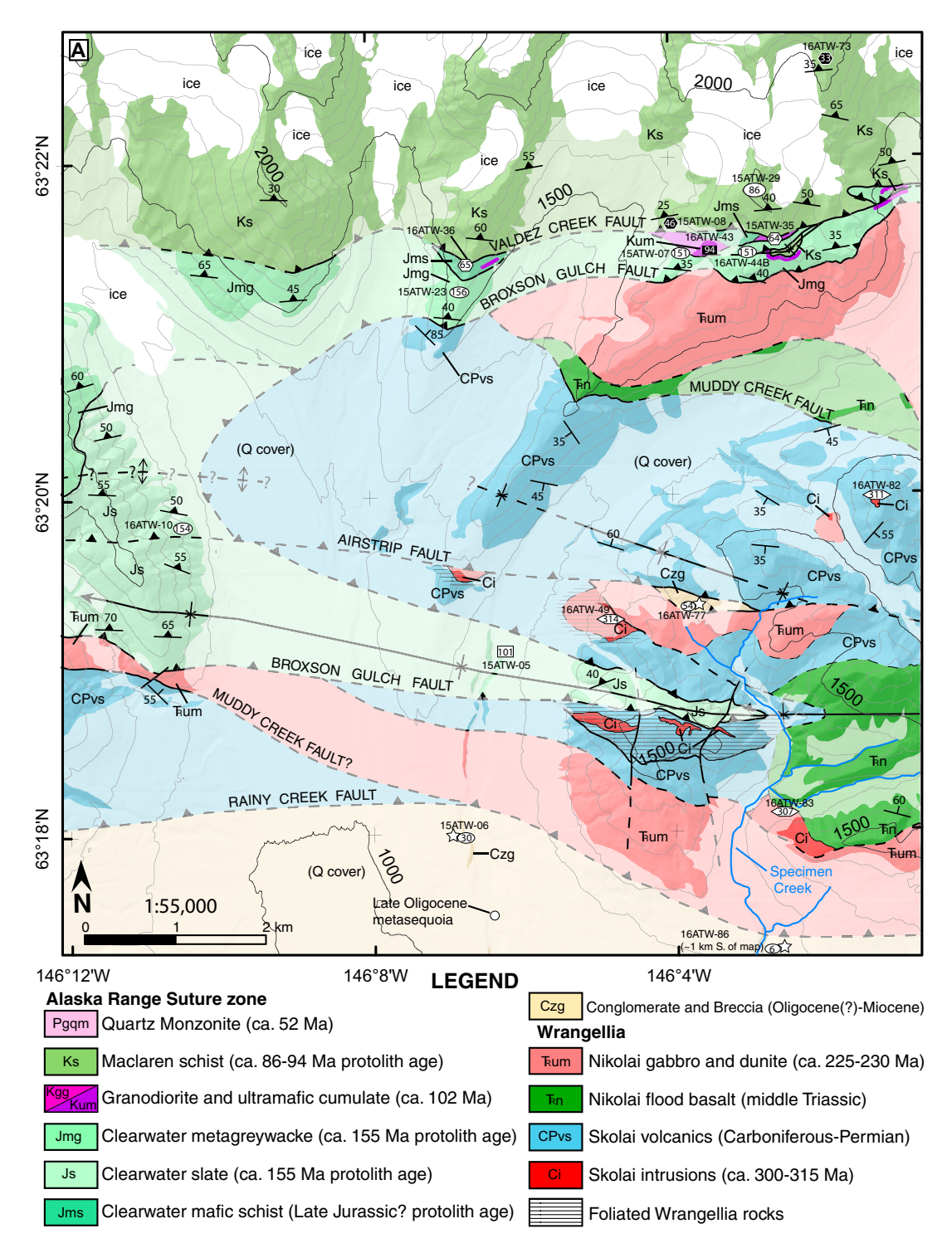


Figure 2. Hillshade and bedrock geologic maps of (A) the Broxson Gulch and (B) Ann Creek map areas are shown. The mapping presented herein is mostly original except for some areas of the Ann Creek map that are based on mapping by Stout (1965) and Twelker et al. (2020). Pastel regions (lighter than the legend) represent bedrock that is interpolated beneath Quaternary surficial deposits. Geochronology and clast assemblage sample locations are given. MDA—Maximum depositional age determined from detrital zircon U-Pb age spectra; bt—biotite; wm—white mica; hbl—hornblende; wr—whole rock. The legend applies to both maps.

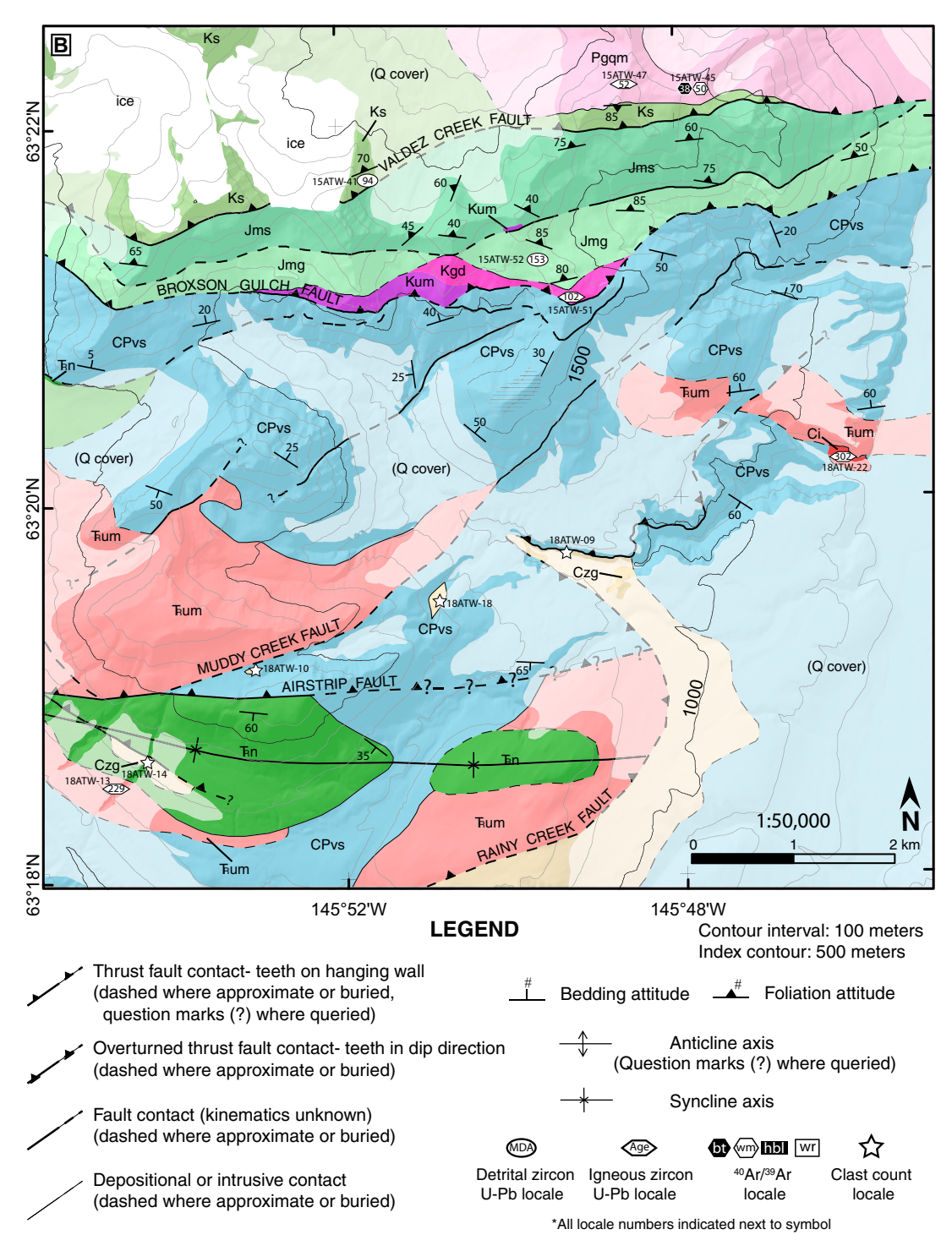


Figure 2. (Continued)

studies of the Alaska Range suture zone rocks and structures in the eastern Alaska Range (e.g., Rose, 1965, 1966; Stout, 1965). As a result, these areas contain the type locales of the Broxson Gulch fault and associated structures. Interpretations of the local geology in Broxson Gulch and the Ann Creek area fueled early analyses of strain partitioning in the Denali fault system (Stout and Chase, 1980), total slip on the Denali fault (Forbes et al., 1974), accretion of the Wrangellia composite terrane (Nokleberg et al., 1985), and ore deposit genesis associated with the Maclaren Glacier metamorphic belt (Rose, 1965, 1966; Smith, 1981). The inference of Quaternary slip on the Broxson Gulch fault (Nokleberg et al., 1985) and relocation of historic seismicity (Doser, 2004) suggest that the fault may be active.

The early geologic maps of Broxson Gulch and the Ann Creek area were foundational contributions and should continue to be viewed as useful maps. Yet, an updated examination of the map areas through the lens of modern structural analysis, geochronology, and regional tectonics is warranted. For example, Rose (1965) and Stout (1965) both recognized that metasedimentary rocks north of the Broxson Gulch fault displayed a variety of textures and mineral assemblages and thus were likely metamorphosed from multiple protolith compositions. However, the protolith age was inferred to be Devonian or older based on nearby strata containing Carboniferous fossils (Stout, 1965; Rose, 1966). Despite recognition that the metamorphic rocks had been metamorphosed from various protolith compositions, the original map units appear to have been defined based on textural features. Such unit definitions led to inconsistent inclusion of foliated greenschist grade metaigneous rocks in the hanging wall of the Broxson Gulch fault, which in turn changed the location and shape of the fault on the various maps (cf., Rose, 1966; Stout, 1976; Nokleberg et al., 1992a). A common feature of all the existing maps is the apparent offset of the Broxson Gulch fault by a buried NW-striking sinistral tear fault in the center of Broxson Gulch.

Here, we aim to resolve some of the inconsistencies in the original maps by (1) developing regionally consistent unit definitions on the basis of protolith age and composition; (2) refining the location of major structures using the new unit definitions; and (3) reinterpreting the structural evolution and resulting fault geometries of major structures using modern structural analysis and geochronology. Our analysis reveals the existence of an additional structure, which we call the Valdez Creek fault and appears to be the key Cenozoic fault in the area.

#### **METHODS**

#### **Mapping and Structural Analysis**

We conducted 1:10,000-scale bedrock and surficial mapping during the summers of 2015, 2016, and 2018 over an area of 170 km<sup>2</sup>. Our detailed mapping campaign worked in collaboration with a regional (1:100,000 scale) mapping and compilation project by the Alaska Division of Geological and Geophysical Surveys (DGGS) (Twelker et al., 2020). Due to lack of road access, we accessed the field areas by helicopter and fixed-wing aircraft. Once in the field, we mapped the areas by foot using hillshade and contour paper basemaps constructed from the 5-m-resolution Interferometric Satellite Aperture Radar (IfSAR) Alaska Digital Terrain Model (DTM). While mapping, we recorded sample locations using a handheld global positioning system.

Between the summer field mapping campaigns, we scanned our paper field maps and digitized them using Esri ArcMap. To aid our map compilation we used high-resolution (25 m pixel size) potential-field geophysical data published by the DGGS (Burns et al., 2003) and ≥1 m resolution satellite imagery (available in ArcMap) to refine our bedrock mapping in areas of poor exposure or interpolate through areas of Quaternary cover. Here we present our bedrock mapping compiled at 1:55,000, Broxson Gulch (Fig. 2A), and 1:50,000, Ann Creek (Fig. 2B).

#### **Zircon U-Pb Geochronology**

## Sample Preparation and Data Collection

We performed single-grain zircon U-Pb geochronology by Laser Ablation-Inductively Coupled-Mass Spectrometry (LA-ICP-MS) with three primary goals: (1) to fingerprint metasedimentary rocks by determining the sediment source areas of the protolith; (2) to estimate the maximum depositional age of the protolith; and (3) to date igneous intrusions in the map areas. At the University of California, Davis (UC Davis), the lead author used standard crushing techniques, a miner's gold pan, a Frantz isodynamic separator, and Lithium Polytungstate heavy liquid to concentrate zircon grains. Our mineral separation protocol for detrital zircon analysis involves concentrating zircon grains sufficiently to mount the grains by pouring, whereas for analysis of igneous grains we pick relatively large, inclusion-sparse grains. Prior to U-Pb analysis, all zircon grains and reference materials are mounted into 1" epoxy rounds, polished to expose the grain interiors, and imaged using the Cameca SX-100 Electron Microprobe housed in the Earth and Planetary Sciences Department at UC Davis. The resulting high-contrast, back-scattered electron images allow us to identify zoning and/or inherited cores in individual zircon grains, which inform our laser spot placement on each grain. We collected U-Pb data in two LA-ICP-MS laboratories: the Arizona Laserchron Center (ALC) in 2016 and 2017 and UC Davis in 2018. Supplemental File S1¹ contains detailed mineral extraction, analytical, data reduction, and data filtering methods used in the LA-ICP-MS analysis.

#### Data Representation

Our fingerprinting of metasedimentary protoliths is based on analyzing distinctive populations of detrital zircon single grain U-Pb dates. To ensure that our comparisons between samples are statistically robust, each detrital zircon age data set contains analyses on at least 117 grains (Vermeesch, 2004). We represent the data as Kernel Density Estimates (KDEs) using the Density Plotter program (Vermeesch, 2012). Because many of the rocks analyzed in our study experienced amphibolite and upper greenschist metamorphic temperatures and thus may have experienced metamorphic recrystallization and/ or lead loss (e.g., Hoskin and Schaltegger, 2003), we take a conservative approach to calculating maximum depositional ages by calculating the weighted mean of the youngest statistical population of detrital grains (Herriott et al., 2019). The ages of igneous zircon populations are determined by a weighted mean of single grain dates with propagated 2 sigma errors. Weighted mean ages are calculated and plotted using Isoplot (Ludwig, 2008). Reported uncertainties of weighted mean ages represent 95% confidence interval internal uncertainties and the quadratic addition of external uncertainties (e.g., Horstwood et al., 2016) (Supplemental Files S1 and S2; see footnote 1).

## 40Ar/39Ar Thermochronology

<sup>40</sup>Ar/<sup>39</sup>Ar analysis was performed at the Geochronology Laboratory at the University of Alaska, Fairbanks, where samples were crushed, sieved, washed, and hand-picked for a pure mineral phase of biotite, muscovite, or amphibole. The analyzed size fractions are given in Table 1. The mineral fractions and monitor mineral MMhb-1 (Samson and Alexander, 1987), which has an age of 523.5 Ma (Renne et al.,

¹Supplemental Material. U-Pb and ⁴⁰Ar/³⁰Ar data for samples presented herein. Please visit https://doi.org/10.1130/GSAB.S.12543137 to access the supplemental material, and contact editing@geosociety.org with any questions.

TABLE 1, 40 Ar/39 Ar ANALYTICAL RESULTS

Sample name	Latitude (°N)	Longitude (°W)	Rock type	Phase analyzed	Grain size analyzed (um)	Integrated age (Ma)*	Plateau age (Ma)*	Plateau information	Isochron age (Ma)	Isochron information
Maclaren So 16ATW-73	<u>chist</u> 63.3427	146.1547	Quartz-mica schist	Biotite	500–1000	32.7 ± 0.2	32.8 ± 0.3	7 of 8 fractions 98.5% <sup>39</sup> Ar release MSWD = 2.01	32.5 ± 0.4	7 of 8 fractions  40Ar/36Ar <sub>i</sub> = 324.7 ± 25.4  MSWD = 1.77
15ATW-08	63.3605	146.0647	Quartz-mica schist	Biotite	212–500	$45.8 \pm 0.2$	45.9 ± 0.3 <sup>†</sup>	2 of 8 fractions 40.7% <sup>39</sup> Ar release MSWD = 0.66	-	- 1.77 -
Clearwater I 16ATW-36	Metasedime 63.3382	ents 146.1754	Quartz-mica schist	Muscovite	212–590	63.8 ± 0.4	64.3 ± 0.7	5 of 8 fractions 94.6% <sup>39</sup> Ar release MSWD = 3.52	-	-
Alaska-type 15ATW-35	Ultramafic : 63.3380	suite 146.1759	Serpentinite	Fuchsite	125–212	$64.5\pm0.4$	65.1 ± 0.4	6 of 8 fractions 97.0% <sup>39</sup> Ar release MSWD = 1.13	-	-
16ATW-43c	63.3389	146.1718	Amphibolite	Amphibole	63–180	$88.5 \pm 0.7$	93.8 ± 0.7 <sup>†</sup>	2 of 8 fractions 65.2% <sup>39</sup> Ar release	-	-
15ATW-05	63.3172	146.1056	Amphibole- porphyry dike	Whole rock	500–1000	$94.7\pm0.9$	100.7 ± 1.6	MSWD = 0.38 5 of 8 fractions 54.5% <sup>39</sup> Ar release MSWD = 1.37	-	-
Quartz Mon 15ATW-45	zonite 63.3685	145.8110	Quartz- monzonite	Biotite	500-1000	$37.5\pm0.6$	37.7 ± 0.6	7 of 8 fractions 96.9% <sup>39</sup> Ar release	-	-
15ATW-45	63.3685	145.8110	pegmatite Quartz- monzonite pegmatite	Muscovite	500–1000	50.1 ± 0.4	50.2 ± 0.5	MSWD = 0.5 5 of 8 fractions 97.4% <sup>39</sup> Ar release MSWD = 1.65	-	-

Note: MSWD—mean square weighted deviation.

1994), were irradiated at McMaster University in Hamilton, Ontario, Canada. Upon their return from the reactor, the samples and monitors were loaded into holes 2 mm in diameter in a copper tray and then loaded in an ultra-high vacuum extraction line. The monitors were fused, and the samples were heated using a 6 W argon-ion laser following the technique described in York et al. (1981), Layer et al. (1987), and Benowitz et al. (2014). Ar isotope measurements in this system were made using a VG-3600 mass spectrometer.

Supplemental File S3 (see footnote 1) contains detailed <sup>40</sup>Ar/<sup>39</sup>Ar analytical methods and summarizes the <sup>40</sup>Ar/<sup>39</sup>Ar results, wherein all ages are quoted at the 1 sigma level and calculated using the constants of Renne et al. (2010). The integrated age is the age given by the total gas measured and is equivalent to a potassiumargon (K-Ar) age. The spectrum provides a plateau age if three or more consecutive gas fractions represent at least 50% of the total gas release and are within two standard deviations of each other (mean square weighted deviation <2.5).

### **Spinel Geochemistry**

Spinel geochemistry was determined using the Cameca SX-100 electron microprobe at UC Davis. The analysis used a beam intensity of 20 nA and voltage of 15 kV focused into a 1

 $\mu m$  spot size. Analyses were calibrated to natural spinel reference materials. Fe<sub>2</sub>O<sub>3</sub> and FeO were calculated from Fe<sub>Total</sub> using a Microsoft Excelbased calculation tool available from https://serc.carleton.edu/research\_education/equilibria/mineralformulaerecalculation.html.

#### RESULTS

# Map Unit Definitions, Protolith Ages, and Primary Structural Features

We present new bedrock mapping from two locations along the southern margin of the Alaska Range suture zone in the eastern Alaska Range: Broxson Gulch (Fig. 2A) and Ann Creek (Fig. 2B). Our mapping and definition of rock units differs from those of previous workers in the area because we defined map units based on protolith composition and age. This distinction is particularly important for metasedimentary rocks in the northern portion of the map areas. There are three primary bedrock lithologic packages in the map areas: Maclaren schist and associated felsic plutons, Clearwater metasedimentary rocks and associated intermediate-ultramafic intrusions, and Wrangellia meta-igneous rocks. A suite of N-dipping brittle faults juxtaposes these rock packages in both map areas. Here we describe the rock units and major structures from north to south.

### Geology between the Wrangellia Terrane and Denali Fault

The Maclaren schist (map unit Ks) is a dark gray, quartzofeldspathic schist that occupies the highest structural level in our map areas (Fig. 3A). Albite and, less commonly, garnet porphyroclasts contain curved or spiral inclusion trails (S<sub>1</sub>), which comprise rutile and graphite (Fig. 4A). The inclusion trails cause the albite to appear nearly black in hand sample. Phyllosilicate minerals and graphite define a strong foliation  $(S_2)$ , which is deflected by the porphyroclasts (Fig. 4A). Quartz-rich pressure shadows around the porphyroclasts create a linear fabric element contained within S2 that generally plunges down-dip to the north. Biotite parallel to the S<sub>2</sub> foliation is typically partly replaced by chlorite, except at the highest structural level (e.g., sample 16ATW-73, Fig. 2A), where biotite overgrows the  $S_2$  foliation (Fig. 4B). Meso-scale asymmetric quartz vein boudinage parallels S<sub>2</sub> and shows top-to-the-south thrust kinematics (Fig. 3B). Discontinuous cm- to m-thick carbonate-rich lozenges also parallel S2. Rare pelitic intervals contain relict kyanite, staurolite, and garnet, which are partially replaced by retrograde metamorphic assemblages. We use the peak assemblage to infer that the entire package of Maclaren schist reached amphibolite facies conditions (see also Davidson et al., 1992; Davidson and McPhillips, 2007).

<sup>\*</sup>Uncertainties are 1s.

<sup>†</sup>Did not meet all the criteria of a plateau age, hence a weighted average age is presented.

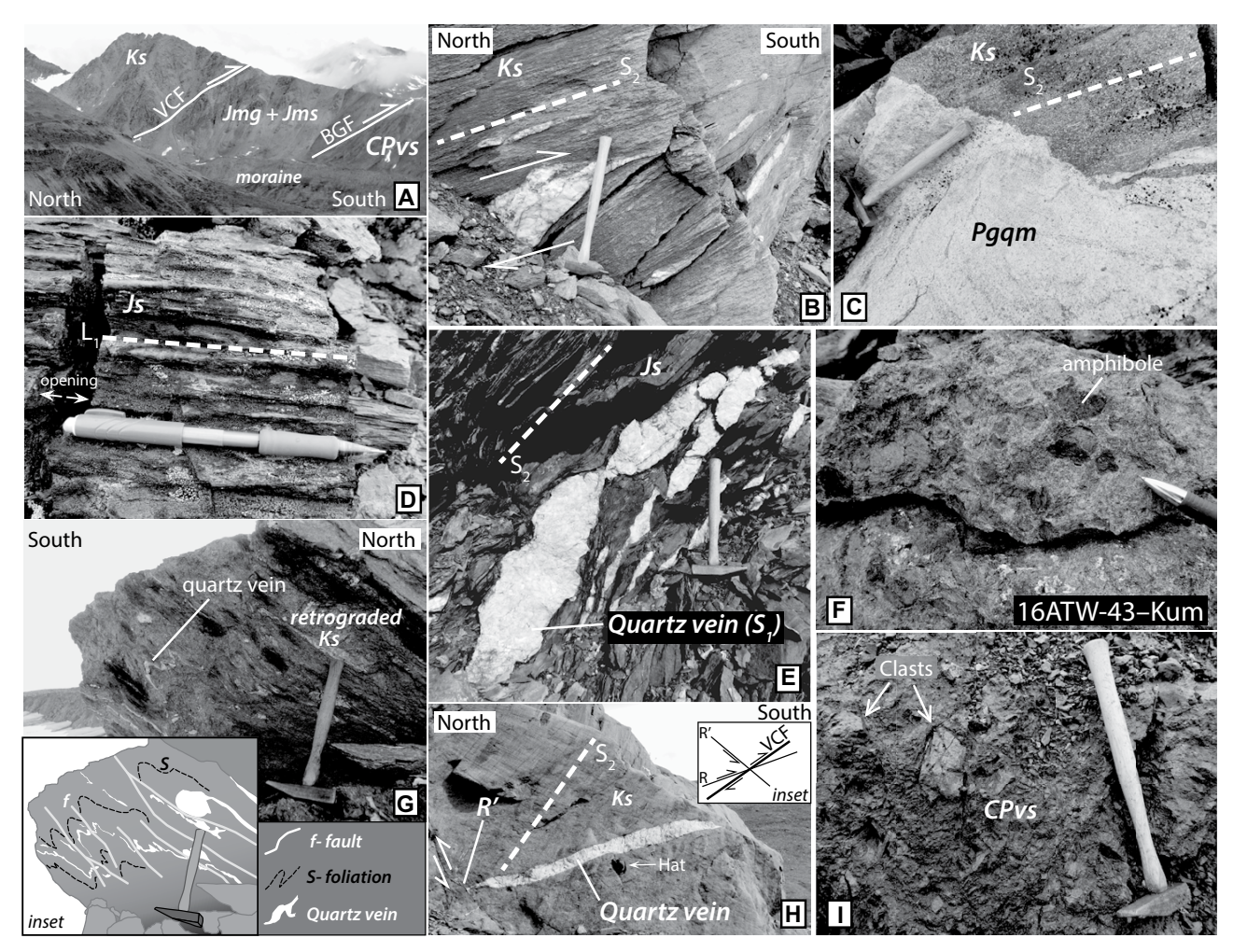


Figure 3. Field photos show key relationships on the geologic maps. Hammer for scale is 38 cm long, pencil is 12 cm long, and hat is 30 cm long. All map unit labels are the same as in Figure 2. (A) The Valdez Creek fault (VCF) and Broxson Gulch fault (BGF) create an imbricate set of N-dipping faults that juxtapose the Maclaren schist (Ks) over the Clearwater metasedimentary rocks (Jmg and Jms) and Wrangellia terrane rocks (CPvs) in the map areas. View to the NNE from western Broxson Gulch. The highest point on the ridge is ~450 m higher elevation than the moraine crest in the valley below. (B) Asymmetric boundinage of quartz veins records top-to-thesouth (thrust) shear parallel to S<sub>2</sub> in the Maclaren schist (Ks). View is to the east near location 15ATW-08 (Fig. 2A). (C) The ca. 52 Ma quartz monzonite (Pgqm) exposed in the Ann Creek area intruded across the foliation in the Maclaren gneiss (Ks). Photo is from a location south of 15ATW-47 (Fig. 2B). (D) Crenulation axes (L<sub>1</sub>) are locally well expressed in fine-grained portions of the Clearwater metasedimentary rocks. Opening fractures orthogonal to L<sub>1</sub> are commonly associated with the crenulation fabric in the Clearwater slate (Js). The opening fractures are sometimes filled with quartz veins. Photo is from an outcrop near 16ATW-10 (Fig. 2A). (E) Quartz veins in the Clearwater metasediments are stretched (boudinage) parallel to the S<sub>1</sub> foliation and isoclinally folded. Photo is from a finegrained Clearwater metagreywacke (Jmg) outcrop on the ridge depicted in Figure 3A. (F) Amphibolite (Kum) in Broxson Gulch contains coarse amphibole surrounded by a granular aggregate of greenschist facies minerals. Amphibole from this sample (16ATW-43c; Fig. 2A) yielded an 40Ar/39Ar weighted mean age of 93.8 ± 0.7 Ma (Table 1). (G) Maclaren schist (Ks) in the immediate hanging wall of the Valdez Creek fault is retrograded at lower greenschist facies conditions and contains abundant quartz veins. Both the quartz veins and retrograde fabric are folded and cut by faults. Inset-Traced photograph emphasizing the structures in the outcrop. View is to the west, ~30 m south of location 15ATW-41 (Fig. 2B). (H) Late quartz veins spatially associated with the Valdez Creek fault cross-cut the S<sub>2</sub> foliation in the Maclaren schist (Ks). The quartz vein is cut by a S-dipping reverse fault. Inset—The reverse fault that cut the quartz vein is appropriately oriented to be an R' structure splaying from the master Valdez Creek fault. View is to the east from central Broxson Gulch (Fig. 2A). (I) Primary features, such as coarse volcanic breccia, are commonly preserved in Wrangellia metavolcanic rocks (CPvs). Photo is from central Broxson Gulch (Fig. 2A).

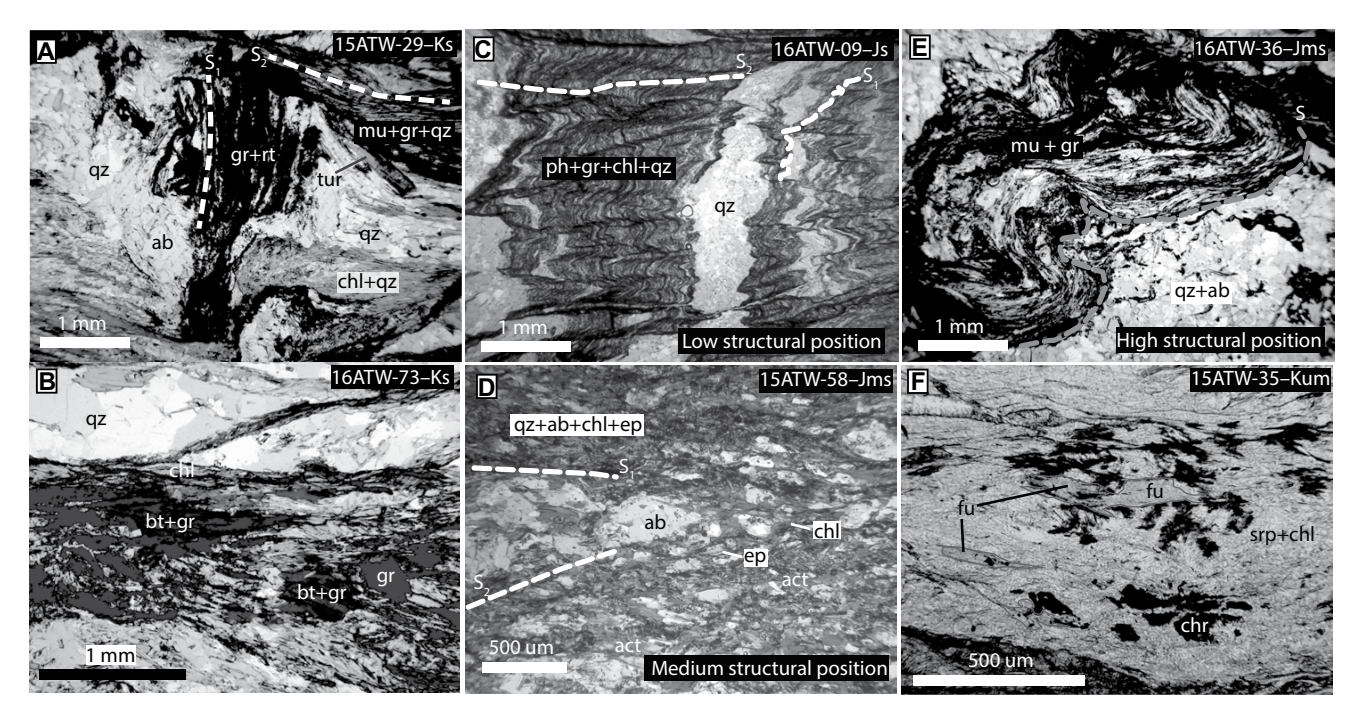


Figure 4. Photomicrographs of key mineralogical and textural features of metamorphic rocks in the hanging wall of the Broxson Gulch fault are shown. Sample names and map units are given in the upper right of each photo. Abbreviations for mineral names follow the convention defined by Whitney and Evans (2010): ab—albite, act—actinolite, bt—biotite, chl—chlorite, chr—chromite, ep—epidote, fu—fuchsite, gr—graphite, mu—muscovite, ph—phengite, qz—quartz, rt—rutile, srp—serpentine, tur—tourmaline. (A) The quartzofeldspathic portion of the Maclaren schist contains diagnostic albite porphyroclasts up to ~5 mm in diameter. The porphyroclasts contain a curved internal foliation ( $S_1$ ) defined by graphite and rutile, which is discordant with the exterior foliation ( $S_2$ ). Phyllosilicate minerals defining the  $S_2$  foliation wrap around the porphyroclasts. (B) The structurally higher portion of the Maclaren schist contains pophyroblastic biotite, which overgrew the  $S_2$  foliation. Mineral cleavage in the biotite porphyroblasts is discordant with the  $S_2$  foliation. Biotite from this sample yielded a  $^{40}$ Ar/ $^{39}$ Ar plateau age of 32.8  $\pm$  0.3 Ma (Table 1). (C) The Clearwater metasedimentary rocks display a strong transposition fabric wherein the  $S_1$  foliation is isoclinally folded into parallelism with the  $S_2$  foliation. (D) Mafic schists in the Clearwater metasediments display a strong foliation defined by greenschist facies assemblages. In this sample, chlorite defining the  $S_1$  foliation is kinked by the  $S_2$  foliation. (E) Graphite-muscovite schists interfoliated with mafic schists in the structurally highest section of the Clearwater metasediments display tight folding of mica in the foliation. Muscovite from this sample yielded a  $^{40}$ Ar/ $^{39}$ Ar plateau age of 64.3  $\pm$  0.7 Ma (Table 1). (F) Serpentinite interfoliated with the Clearwater metasediments contains fuchsite associated with relict chromite, serpentine, and Cr-rich chlorite. The fuchsite is kinked in the foliation and yielded a  $^{40}$ Ar/

A quartz monzonite body (Map unit Pgqm) intruded across the foliation in the Maclaren schist north of the Valdez Creek fault (Figs. 2B and 3C). The quartz monzonite is not foliated and contains xenoliths of Maclaren schist (Stout, 1965; our observations). Zircon separated from one sample of the quartz monzonite (15ATW-47) yielded a U-Pb date of  $51.9 \pm 0.6$  Ma (Figs. 2B and 5; Table 2). Farther west, a suite of ca. 75–70 Ma tonalitic rocks intrudes the Maclaren schist and along the Valdez Creek shear zone (Aleinikoff et al., 1981; Ridgway et al., 2002).

The Clearwater metasedimentary package (map units Jms, Jmg, Js) is a lithologically heterogeneous unit structurally below the Maclaren schist (Fig. 3A). Rock types in the Clearwater metasediments include metagreywacke, graphite-muscovite-chlorite phyllitic schist, porphy-

roblastic pyrite-graphite phyllite, argillaceous slate, and albite-actinolite-epidote-chlorite schist. We distinguish map units based on the prevalence of rock types (Jms-mafic schist, Jmg—metagreywacke, Js—slate). Our naming convention is based on that of Mooney (2010), who documented a nearly identical belt of lowgrade metasedimentary strata and inter-bedded lava flows in the Clearwater Mountains ~60 km to the west of our study area. The Clearwater metasediments in our map areas generally display an increase in flattening strain, mica content, and feldspar recrystallization from south (lowest structural level) to north (highest structural level) (Figs. 4C-4E). The nearly ubiquitous presence of chlorite, epidote, and actinolite suggests that the belt experienced greenschist facies peak metamorphic conditions. The package displays a strong transposition fabric, wherein the  $S_1$  foliation is isoclinally folded, thereby creating  $S_2$  axial surfaces parallel to  $S_1$ . Folding of the  $S_1$  foliation manifests as tight crenulation folds (Figs. 3D and 4C) and as folded quartz veins (Fig. 3E). Crenulation axes in the metasediments generally plunge modestly to the west-southwest and are interrupted by sub-vertical opening fractures (Figs. 3D and 6A).

The Clearwater metasediments are locally interfoliated with metamorphosed ultramafic rocks. Ultramafic rock types include serpentinite, amphibolite, and lesser talc-chlorite schist. The ultramafic rocks generally display a strong foliation defined by serpentine, Cr-chlorite, actinolite, and lesser fuchsite and talc (Fig. 4F). Relict chromite in the serpentinite shows reaction textures involving brucite, Cr-chlorite,

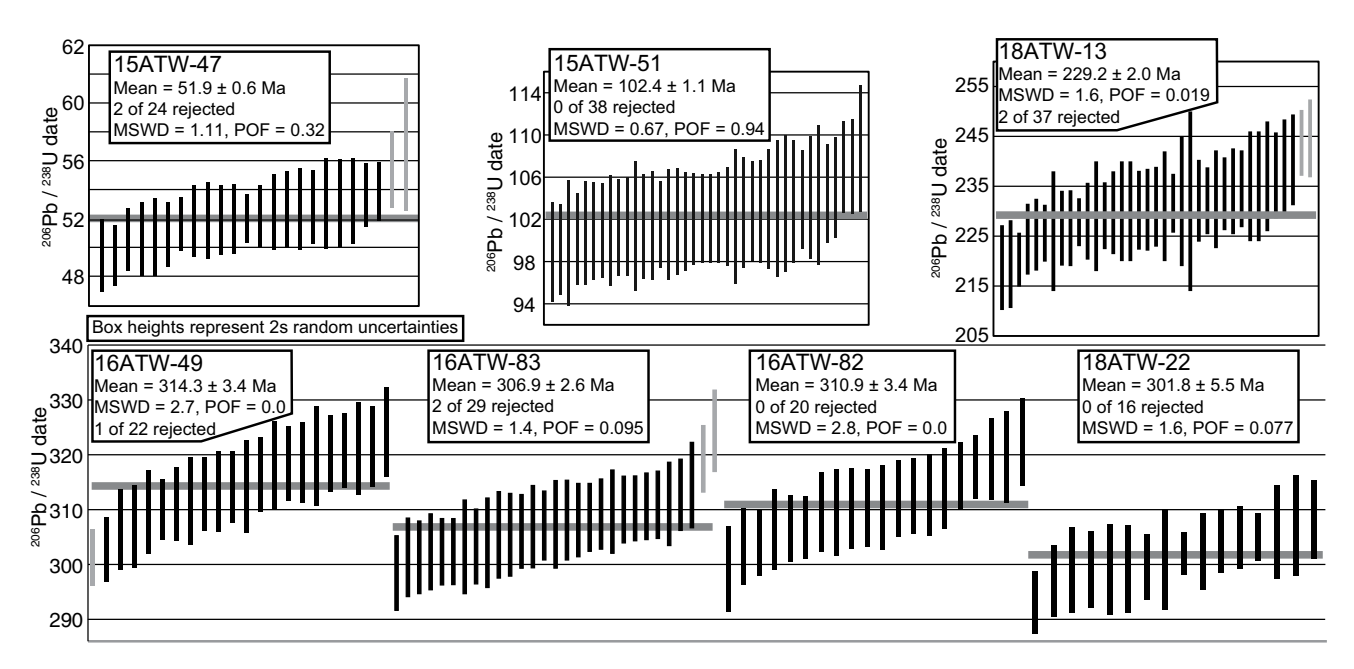


Figure 5. Weighted mean plots of U-Pb zircon dates from plutonic rocks in the map areas are shown. Each vertical bar represents a single grain analysis, which is centered on the date, and the length of the bar corresponds to the random 2s uncertainty associated with the date. Black bars are used in the age calculation, whereas gray bars passed our filtering criteria but were rejected from the age calculation by Isoplot. The weighted mean calculation uses only concordant analyses with <10% analytical uncertainty. Uncertainties quoted with the weighted mean ages of each sample include internal and external uncertainties at the 2 sigma level. POF—probability of fit; MSWD—mean square of weighted deviation. See also Table 2.

Cr-magnetite, and millerite (Supplemental File S4; see footnote 1). Broxson Gulch also contains an outcrop (~24,000 m² map area) of unfoliated amphibolite (locale 16ATW-43), which contains amphibole up to 3 cm in diameter (Fig. 3F). The coarse amphibole displays zoning consisting of hornblende cores that have reacted to patchy actinolite zones and rims (Supplemental File S4). Matrix minerals in the coarse amphibolite include titanite, epidote, chloritized biotite, and apatite (Supplemental File S4). The serpentinite and talc-chlorite schists are interfoliated and folded with the Clearwater phyllitic schist (Fig. 6A), whereas amphibolite pods are gen-

erally associated with Clearwater mafic schist (map unit Jmg).

A suite of small volume igneous bodies intruded the Clearwater metasedimentary rocks. In Broxson Gulch, these intrusive bodies are typically amphibole-bearing intermediate dikes up to one meter thick. The dikes intrude along, and locally display stretching parallel to, the  $S_1$  foliation. Chlorite and/or actinolite form pseudomorphs of primary amphibole in the dikes. One dike sample from Broxson Gulch (15ATW-05) yielded an  $^{40}$ Ar/ $^{39}$ Ar whole rock plateau age of  $100.7 \pm 1.6$  Ma (Table 1; Supplemental File S5; see footnote 1). Phyllite in the contact aureole of

another amphibole dike yielded a population of high U/Th (up to  $\sim$ 6300) zircon grains that gave a weighted mean U-Pb age of  $103.4\pm1.6$  Ma (Supplemental File S5). In the Ann Creek map area (Fig. 2B) a tabular-shaped granodiorite body intruded the metagreywacke subunit of the Clearwater metasediments (Jmg) immediately north of the Broxson Gulch fault. The granodiorite contains a weak foliation defined by the alignment of amphibole and plagioclase along a plane sub-parallel to the margins of the body. The northern contact of the granodiorite displays co-magmatic textures with a pegmatitic hornblende-biotite pyroxenite (Stout, 1965; our

T. D. E .	7100011					
TABLE 2.	ZIRCON	U-Pb	ANALY	HCAL	RESU	LIS

Map unit	Sample name	Latitude (°N)	Longitude (°W)	Rock type	Weighted mean <sup>206</sup> Pb/ <sup>238</sup> U age (Ma)*	MSWD	Number of acceptable grains in age calculation#	Total number of zircons analyzed**
Kgd	15ATW-51 <sup>†</sup>	63.3513	145.8205	Granodiorite	102.4 ± 1.1	0.67	38	40
Pgqm	15ATW-47 <sup>†</sup>	63.3678	145.8160	Quartz monzonite	51.9 ± 0.6	1.1	22	32
Trum	18ATW-13§	63.3093	145.9100	Gabbro pegmatite	229.2 ± 2.0	1.6	35	40
Ci	18ATW-22§	63.3363	145.7662	Quartz diorite	301.8 ± 5.5	1.6	16	26
Ci	16ATW-49 <sup>†</sup>	63.3397	146.1683	Diorite	314.3 ± 3.4	2.7	21	25
Ci	16ATW-82 <sup>†</sup>	63.3437	146.1502	Tonalite	310.9 ± 3.4	2.8	20	30
Ci	16ATW-83 <sup>†</sup>	63.3439	146.1497	Tonalite	$306.9 \pm 2.6$	1.4	27	33

Note: MSWD—mean square weighted deviation.

<sup>\*</sup>Weighted mean uncertainties represent quadratic addition of internal and external uncertainties at 2s.

<sup>†</sup>Analyses performed at Arizona Laserchron Center.

<sup>§</sup>Analysis performed at the University of California at Davis.

<sup>\*</sup>The number of analyses that passed the filtering criteria

<sup>\*\*</sup>The total number of analyzed grains.

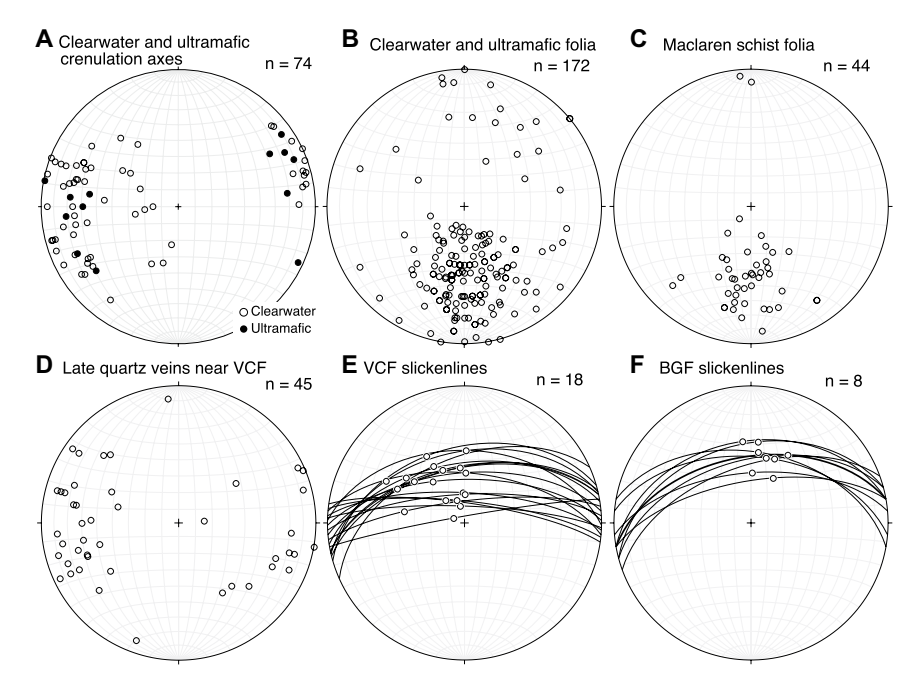


Figure 6. Lower hemisphere equal area plots show: (A) Crenulation axes from metamorphosed Alaska-type ultramafic rocks (filled circles) and the Clearwater metasedimentary rocks (open circles); (B) Poles to all foliation measurements in the Clearwater metasedimentary rocks and Alaska-type ultramafic rocks; (C) Poles to all foliation measurements in the Maclaren schist; (D) Poles to late quartz veins that cross-cut the S<sub>2</sub> foliation in the Maclaren schist (Fig. 3H); (E) Brittle fault striae (open circles) from hanging wall imbricates of the Valdez Creek fault (VCF), which occupy foliation planes (great circles) in the Maclaren schist; and (F) Brittle fault striae (open circles) from fault surfaces (great circles) in a small exposure of the Broxson Gulch fault (BGF) damage zone in northeastern Broxson Gulch. n—number of measurements shown in each plot. The plots were made using Rick Allmendinger's Stereonet program (version 9.2.1).

observations). Amphibole from the pyroxenite body yielded K-Ar dates of  $91.9 \pm 2.8$  Ma and  $97.7 \pm 2.9$  Ma (Nokleberg et al., 1992b). One sample of the granodiorite (15ATW-51) yielded a zircon U-Pb date of  $102.4 \pm 1.1$  Ma (Figs. 2B and 5; Table 2).

### Faulting between the Wrangellia Terrane and Denali Fault

Two major north-dipping brittle faults, the Valdez Creek and Broxson Gulch faults, intersect metasedimentary rock units in the map areas (Fig. 3A). Previous maps of the region emphasize the importance of the Broxson Gulch fault due to the juxtaposition of distinct rock types across it. Our mapping highlights the importance of the Valdez Creek fault as an important reactivated structure juxtaposing distinct metasedimentary rock packages north of the Broxson Gulch fault.

The herein-named Valdez Creek fault places the Maclaren schist over the Clearwater metasediments and associated ultramafic rocks. In outcrop, the Valdez Creek fault is an

~10-15-m-wide zone of clay-rich damaged rock. Hanging wall Maclaren schist adjacent to the Valdez Creek fault is intensely retrograded to lower greenschist facies assemblages and locally contains meso-scale asymmetric folds that indicate top-to-the south shear (Fig. 3G). Antithetic brittle faults and quartz veins in opening fractures near the fault zone cross the metamorphic folia in adjacent rocks at a high angle (Figs. 3H and 6B-6D). Dispersed brittle faults over a ~1-km-wide zone parallel the metamorphic foliation in the structurally lowest portion of the Maclaren schist and presumably record distributed hanging wall deformation related to slip on the Valdez Creek fault. Slickenlines on the foliation-parallel brittle slip surfaces within the Maclaren schist indicate reverse motion with a minor dextral component (Fig. 6E).

The Broxson Gulch fault places the Clearwater metasediments and associated intrusions over Wrangellia rocks and is typically marked by a 30–50-m-thick zone of brittle deformation.

The core of the Broxson Gulch fault damage zone is not well exposed in the map areas. However, one exposed cross section of the fault in northeastern Broxson Gulch contains a ~1-m-thick, clay-rich principle shear plane oriented at ~265/50°N in the core of a distributed brittle deformation zone. Brittle fault striae from the clay-rich zone at this locale plunge down dip and record reverse motion (Fig. 6F). Damage associated with slip on the Broxson Gulch fault is distributed into the hanging wall where it is localized along foliation planes within the Clearwater metasediments.

#### Geology of the Wrangellia Terrane

Wrangellia metavolcanic strata and associated intrusions occupy the footwall of the Broxson Gulch fault (Figs. 2 and 3A). Wrangellia stratigraphy in this region of the Alaska Range consists of Carboniferous volcanic and volcaniclastic strata overlain by lesser Permian carbonate strata and regionally extensive Triassic flood basalts. Both the Carboniferous and Triassic volcanic strata have intrusive igneous rocks associated with them.

Carboniferous volcanic rocks (map unit CPvs) in southern Alaska have been called the Tetelna volcanics (Mendenhall, 1905; Bond, 1973, 1976; Stout, 1976), Skolai group (Smith and MacKevett, 1970), and Slana Spur-Eagle Creek formation (Nokleberg et al., 1985; 1992a). Nomenclature aside, the strata provide a record of a Carboniferous island arc, which has been named the Skolai arc (Bond, 1973; Beard and Barker, 1989); thus, we herein refer to them as the Skolai arc strata. The stratigraphy of the Skolai arc in Broxson Gulch and Ann Creek is similar to that documented by Bond (1973) for a region ~20 km to the east: massive mafic volcanic rocks lower in the section, intermediate volcanic rocks and pyroclastic flow deposits in the middle of the section, and volcaniclastic and carbonate strata near the top of the >3000-m-thick section. Some of the carbonate strata contain Early Permian fossils (Bond, 1973; Nokleberg et al., 1992b; Richter and Dutro, 1975). We combined these strata with the Carboniferous strata for the purpose of our mapping. Igneous bodies of diorite-to-tonalite composition intruded the lower and middle portion of the Skolai arc strata (map unit Ci). Primary biotite and hornblende in the intrusions show reaction textures involving chlorite and actinolite. Skolai strata in the contact aureoles of the intrusions display a strong foliation defined primarily by chlorite, which parallels the margins of the intrusion (Fig. 2A). Primary volcanic features are preserved farther from the intrusive rocks (Fig. 3I). Three samples of representative intrusive igneous rock types from Broxson Gulch yielded

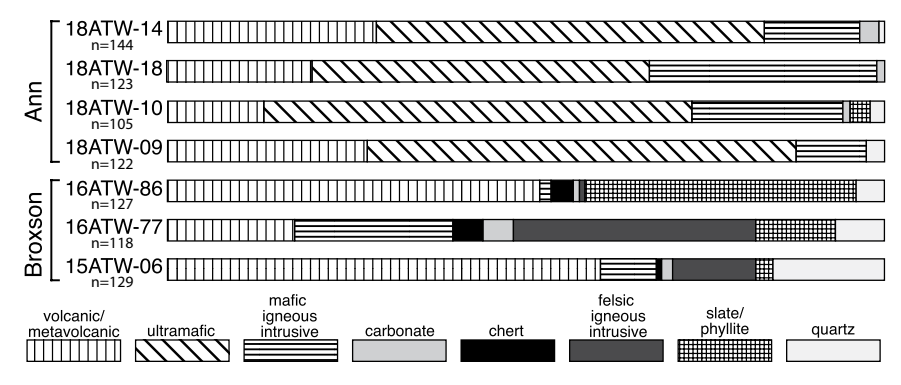


Figure 7. Normalized clast population histograms with number (n) of clasts from Cenozoic gravel deposits in the map areas are shown. The samples are grouped by map area.

zircon suitable for analysis by LA-ICP-MS: 16ATW-49-diorite- $314.3\pm3.4$  Ma; 16ATW-82-tonalite- $310.9\pm3.4$  Ma; and 16ATW-83-tonalite- $306.9\pm2.6$  Ma (Figs. 2A and 5; Table 2). Zircon from one quartz diorite body exposed at the mouth of Ann Creek (18ATW-22) yielded a U-Pb date of  $301.8\pm5.5$  Ma (Figs. 2B and 5; Table 2).

Massive aphanitic basalt flows and lesser interbedded carbonate unconformably overlie the Skolai arc rocks. The basalt flows belong to the Upper Triassic Nikolai flood basalt province (map unit Trn), which has been described in detail to the southwest and southeast of our study area (e.g., Greene et al., 2008, 2010). Large (>1 km across) bodies of gabbro and dunite (map unit Trum) related to the flood basalts are present within the Skolai and Nikolai strata. Twelker et al. (2020) documented at least one location where Nikolai lava flows were deposited unconformably onto the gabbro-dunite complex. Secondary chlorite, actinolite, and serpentine indicate that both intrusive and extrusive Nikolai rocks experienced greenschist facies metamorphic conditions. Biostratigraphic and radiometric (U-Pb and 40Ar/39Ar) age determinations yield dates of ca. 225-230 Ma for Nikolai strata (see Greene et al., 2010). Gabbro bodies in the region yielded 40Ar/39Ar biotite and hornblende dates of ca. 225-228 Ma (Bittenbender et al., 2007; Benowitz et al., 2017). We discovered an outcrop of pegmatitic hornblende-biotite-gabbro within the Nikolai gabbro-dunite complex in the Ann Creek map area (18ATW-13; Fig. 2B). Zircon from this sample yielded a U-Pb date of  $229.2 \pm 2.0$  Ma (Fig. 5; Table 2).

## Cenozoic Cover Strata

Isolated exposures of fluvial and alluvial gravels (map unit Czg) unconformably overlie Skolai and Nikolai rocks in the central and southern portions of the map areas. Most exposures are clast supported, poorly bedded, and

poorly-to-moderately sorted (Supplemental File S6; see footnote 1). Exposures in the Ann Creek map area (Fig. 2B) generally contain subangular to subrounded clasts, whereas exposures in Broxson Gulch (Fig. 2A) contain subrounded to rounded clasts. The clasts are composed of various proportions of volcanic, intrusive igneous, carbonate, and low-grade metamorphic rocks (Fig. 7). Clasts of volcanic and metavolcanic rock are common among all exposures. Dunite and gabbro clasts are abundant in gravel exposures in the Ann Creek map area. Gravel exposures in the Broxson Gulch map area lack ultramafic clasts and instead contain a significant proportion of felsic intrusive igneous rocks. Low-grade metasedimentary rocks, carbonate, and quartz constitute subordinate clast populations in all the exposures. Although the clast rounding, clast composition, detrital zircon age spectra, and structural position differ for each gravel exposure, we classify all the gravel deposits into a single map unit for the purpose of this study.

### Faulting within the Wrangellia Terrane

Three major structures offset the Wrangellia bedrock and cover strata. From north to south, these structures are the Muddy Creek, Airstrip, and Rainy Creek faults.

The herein named Muddy Creek fault cuts through Wrangellia strata and associated intrusive rocks. Good exposures of the fault are found in the cliffs above Muddy Creek (Ann Creek map area: Fig. 2B) and on a ridge in the central part of Broxson Gulch (Fig. 2A). The fault can be accessed easily in Broxson Gulch, where it is a narrow (<10 m) zone of serpentinized and cataclasized Nikolai flood basalt that dips to the northeast. A hanging wall imbricate carrying the gabbro-dunite complex steps up from the Muddy Creek fault ~500 m north of this locale, suggestive of duplexing within the Nikolai ultramafic rocks. The Alaska DGGS mapped a structure

in the Amphitheater Mountains ~10 km to the south of our map areas that we interpret to be an equivalent structure because it juxtaposes the same suites of rocks and also displays evidence of duplexing. They call this the Fish Lake fault (Twelker et al., 2020). Evidence for duplexing and stratigraphic duplication associated with the Fish Lake-Muddy Creek fault suggests topto-the-southwest thrust kinematics (Twelker et al., 2020). The Broxson Gulch and Airstrip faults both appear to cut at a low angle or merge with the Muddy Creek fault (Fig. 2). We favor a cross-cutting relationship because the Muddy Creek fault strikes more northwesterly than other faults in the map areas and has no demonstrable Cenozoic slip.

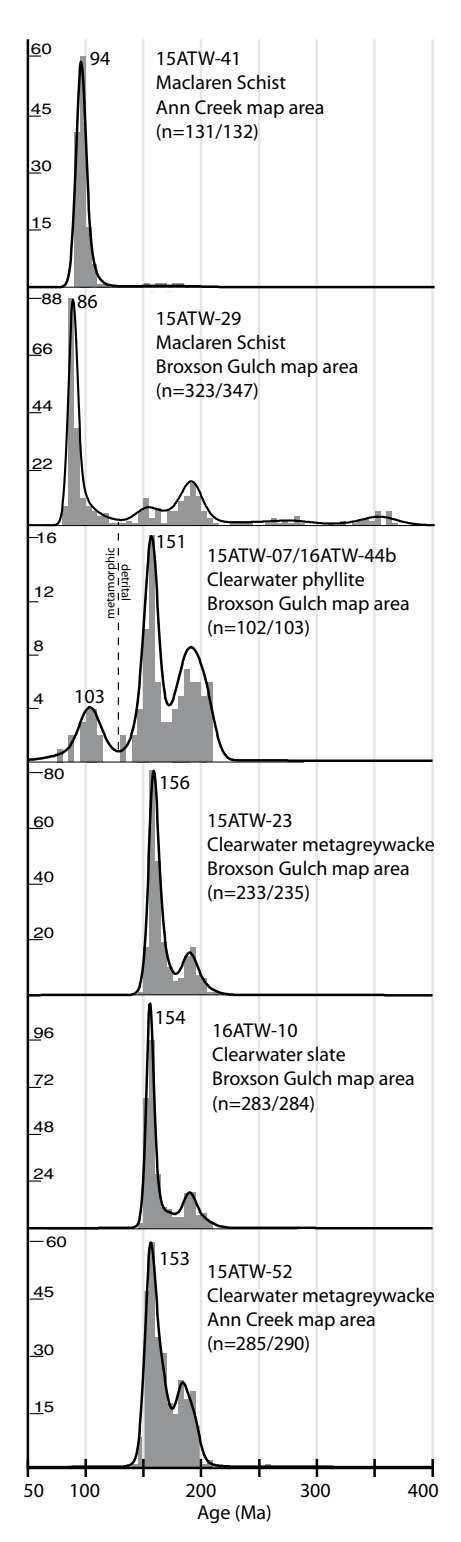
The Airstrip fault, first named by Rose (1965), places Skolai rocks and intrusive Nikolai rocks over Nikolai flood basalts and overlying Cenozoic gravel deposits in the center of the map areas. Our mapping of the Airstrip fault in Broxson Gulch is similar to that of Rose (1965), yet we were able to track the fault to both the east and west. Parallel to the strike of the fault, we mapped a synform in the footwall of the Airstrip fault, which contains Wrangellia meta-igneous rocks, Clearwater slate, and possibly the Muddy Creek fault (Fig. 2). Despite an ~50-m-thick zone of damaged rock associated with the fault trace, the core of the Airstrip fault damage zone is not well enough exposed to yield reliable kinematic indicators. However, we infer top-to-thesouth reverse kinematics based on the associated synform and preservation of Cenozoic gravels in the footwall of the fault (Fig. 2).

The Rainy Creek fault, first named by Nokleberg et al. (1985), is the range-bounding fault in the region. It is not exposed in Broxson Gulch and is poorly exposed in Ann Creek, but it shows up in both regions as a significant aeromagnetic and resistivity boundary because it places Triassic ultramafic rocks over Cenozoic gravels (Nokleberg et al., 1992a) (Fig. 2; Supplemental File S7; see footnote 1). Our mapping of the Rainy Creek fault is similar to that of Nokleberg et al. (2015). We do not have kinematic information for the Rainy Creek fault due to the lack of exposure. However, we infer primarily top-tothe-south thrust slip due to the location of the fault at the topographic range front, the shallow dip of the fault, and the juxtaposition of Wrangellia rocks in the hanging wall against Cenozoic gravels in the footwall.

## **Detrital Zircon U-Pb Geochronology**

### Age Spectra from Metasedimentary Rocks

Detrital zircon U-Pb age spectra from two samples of Maclaren schist primarily display grains of Jurassic and Cretaceous age (Fig. 8;



Supplemental File S2). Grains with dates of ca. 85–95 Ma constitute the largest age population in each sample (45%–85%). Other Phanerozoic age populations include ca. 160 Ma, 185 Ma,

Figure 8. Kernel density estimate (KDE) and 5 m.y. histogram plots of <400 Ma detrital zircon U-Pb dates from the Clearwater metasedimentary rocks and Maclaren schist are shown. Sample numbers, map unit, map area, and the number of analyses constituting the plot out of total acceptable analyses (n) are indicated with each plot. The youngest statistical population of detrital dates, which is taken as the maximum depositional age, is labeled for each plot. Where applicable, the cutoff between detrital and postdepositional metamorphic grains is marked by a vertical broken line. Each vertical axis corresponds to the histogram in each plot. The plots were created using the Density-Plotter program (Vermeesch, 2012).

and 330–350 Ma. A distribution of Precambrian grains ranging from ca. 620–2800 Ma accounts for less than 10% of either Maclaren schist sample (Fig. 9).

Detrital zircon U-Pb age spectra from all four samples of the Clearwater metasediments

display nearly identical bimodal detrital age populations centered at ca. 155-160 Ma and 185-190 Ma (Fig. 8; Supplemental File S2). The Late Jurassic age population comprises the majority (55%-75%) of the grains in all samples. Pre-Mesozoic grains are uncommon in the Clearwater metasediments, yet each sample yielded five or fewer grains at ca. 425 Ma and ca. 1100-1700 Ma (Fig. 9). Sample 15ATW-52 yielded one grain with a date of 2785 Ma. Zircon grains extracted from Clearwater phyllite in the contact aureoles of the ca. 100 Ma amphibole-bearing dikes (samples 15ATW-07 and 16ATW-44b) display a sieve texture around the rims of the crystals and typical igneous zoning patterns in the interiors of the crystals (Supplemental File S5). Laser spots placed on the concentric- or sector-zoned interiors of the zircon crystals yielded Jurassic dates commensurate with the other Clearwater samples. Laser spots placed near regions of sieve texture generally yielded dates of ca. 80-120 Ma and cluster at ca. 100 Ma. These dates are associated with elevated and variable U/Th ratios (Supplemental Files S2 and

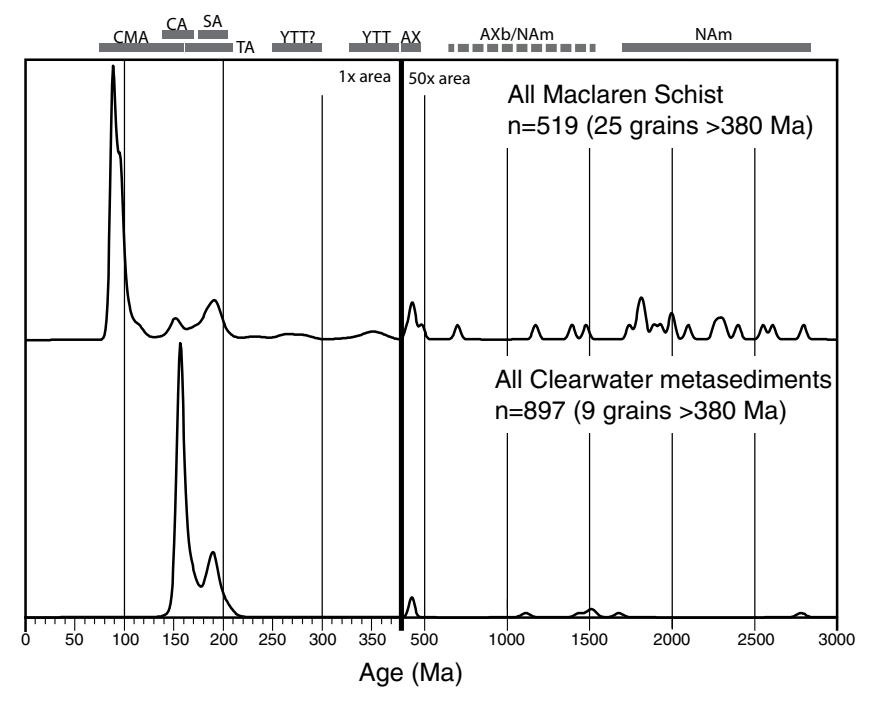


Figure 9. Combined kernel density estimate (KDE) plots of all acceptable detrital zircon U-Pb dates for the Clearwater metasedimentary rocks and Maclaren schist are shown. Note the change in horizontal scale at 380 Ma. The area under the curve from 380 Ma to 3000 Ma is increased by 50x. The KDE plots were created using the DensityPlotter program (Vermeesch, 2012). Sediment source areas: CMA—Coast Mountains Arc; CA—Chitina Arc; SA—Stikine Arc; TA—Talkeetna Arc; YTT—Yukon-Tanana Terrane; AXb—Alexander terrane (basement); NAm—North American strata and basement.

S5). The population of Cretaceous high U/Th grains yielded a weighted mean U-Pb date of  $103.4 \pm 1.6$  Ma (Fig. 8; Supplemental File S5).

#### Age Spectra from Cenozoic Gravel Deposits

Cenozoic and Mesozoic grains dominate the detrital zircon U-Pb age spectra from three samples of Cenozoic gravel deposits in Brox-

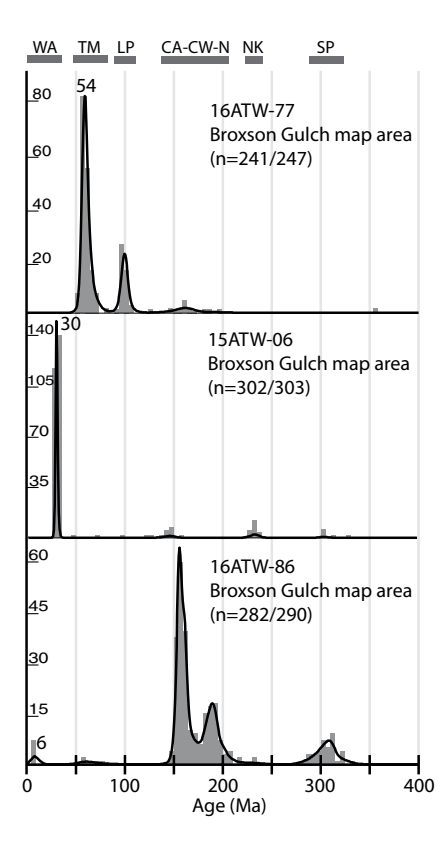


Figure 10. Kernel density estimate (KDE) and 5 m.y. histogram plots of <400 Ma detrital zircon U-Pb dates from the Cenozoic gravel deposits in Broxson Gulch are shown. Sample numbers and the number of analyses constituting the plot out of total acceptable analyses (n) are indicated with each plot. The youngest statistical population, which is taken as the maximum depositional age, is labeled for each plot. Each vertical axis corresponds to the histogram in each plot. The KDE plots were created using the DensityPlotter program (Vermeesch, 2012). Sediment source areas: WA—Wrangell Arc; TM—Talkeetna Mountains plutonic rocks; LP-local Mesozoic plutonic rocks; CA-Chitina Arc; CW-Clearwater metasedimentary rocks; N-Nutzotin Mountains Sequence; NK-Nikolai igneous rocks; SP-Skolai arc plutonic rocks.

son Gulch (Fig. 10; Supplemental File S2). The structurally highest sample (16ATW-77) displays a nearly bimodal distribution of grain dates split between ca. 60 Ma (63%) and ca. 100 Ma (20%) populations. Jurassic-aged grains compose a minor age population at ca. 160 Ma (4%). In the intermediate structural position, sample 15ATW-06 displays a nearly unimodal age distribution wherein 83% of the analyzed grains constitute a single age population at ca. 30 Ma. Grains with ages of ca. 145 Ma (5%), 230 Ma (7%), and 305 Ma (3%) constitute subordinate age populations in this sample. Sample 16ATW-86 occupies the lowest structural position and displays the most heterogeneity in detrital ages from the dated Cenozoic gravel deposits. A bimodal distribution of Jurassic grains comprises the majority (79%) of the analyzed grains. The Jurassic population contains modes at ca. 155 Ma and 185 Ma. The remaining grains compose smaller populations at ca. 310 Ma (13%), 60 Ma (2%), and 6 Ma (3%; n = 7). Grains with dates older than 400 Ma constitute less than 3% of analyzed zircon grains from all samples. Recurring >400 Ma age populations include: 430-470 Ma, 1500-1800 Ma, and 2300-2700 Ma.

#### <sup>40</sup>Ar/<sup>39</sup>Ar Thermochronometry

We dated K-bearing mineral phases from samples in the hanging wall of the Broxson Gulch fault using the <sup>40</sup>Ar/<sup>39</sup>Ar method, which resulted in one amphibole, three white mica, and three biotite dates (Table 1; Supplemental File S3).

## Broxson Gulch Map Area

Biotite and muscovite from the Maclaren schist in Broxson Gulch yield late Eocene-Oligocene dates (Fig. 11). The  $S_2$  foliation in the structurally highest sample (16ATW-73) is defined by intergrown muscovite, chlorite, and graphite. Biotite in this sample overgrows the  $S_2$  foliation with a porphyroblastic texture (Fig. 4B) and yielded a plateau age of  $32.8 \pm 0.3$  Ma. Sample 15ATW-08 is located at a low structural level in the Maclaren schist near the Valdez Creek fault (Fig. 2A). Biotite in this sample is oriented sub-parallel to the  $S_2$  foliation, shows reaction textures involving chlorite, and yielded a weighted mean age of  $45.9 \pm 0.3$  Ma.

Amphibole and mica from Clearwater metasediments and ultramafic rocks in Broxson Gulch yield mid-Cretaceous-earliest Paleogene dates (Fig. 12). The zoned amphibole from the coarse amphibolite block (Supplemental File S4) in Broxson Gulch (16ATW-43c) yielded an <sup>40</sup>Ar/<sup>39</sup>Ar release spectrum that displays a loss pattern, which is matched by the K/Ca spectrum over the same range of gas release steps

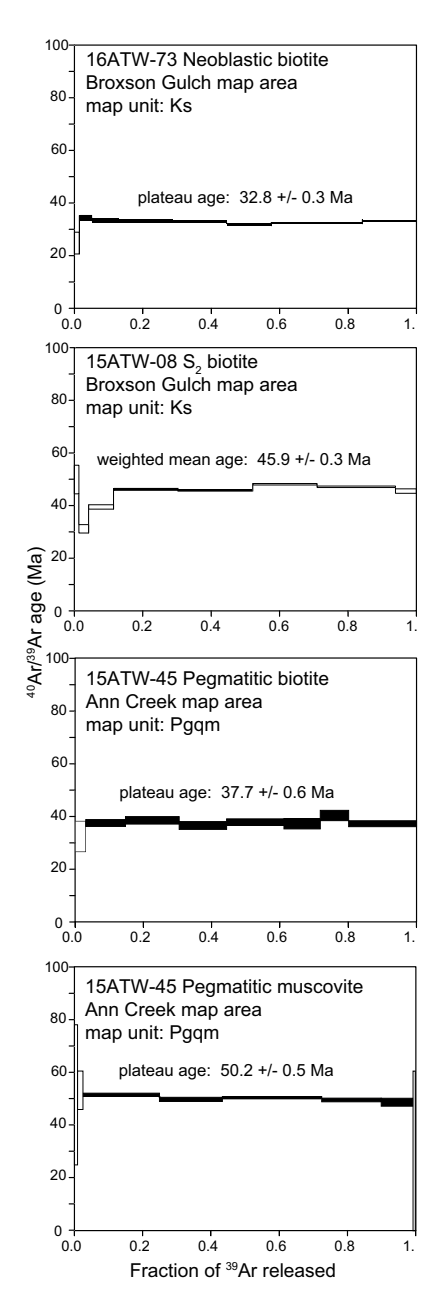


Figure 11. Mica <sup>40</sup>Ar/<sup>39</sup>Ar age spectra for samples north of the Valdez Creek fault are shown. The sample number, mineral phase dated, map unit, and plateau or weighted mean age determinations are given for each sample. Only filled Ar release steps are used to calculate plateau or weighted mean ages. See also Table 1.

(Fig. 12). Our preferred date for the amphibole is the  $93.8 \pm 0.7$  Ma weighted mean date because the duration of consistent gas release defining the date corresponds to a constant

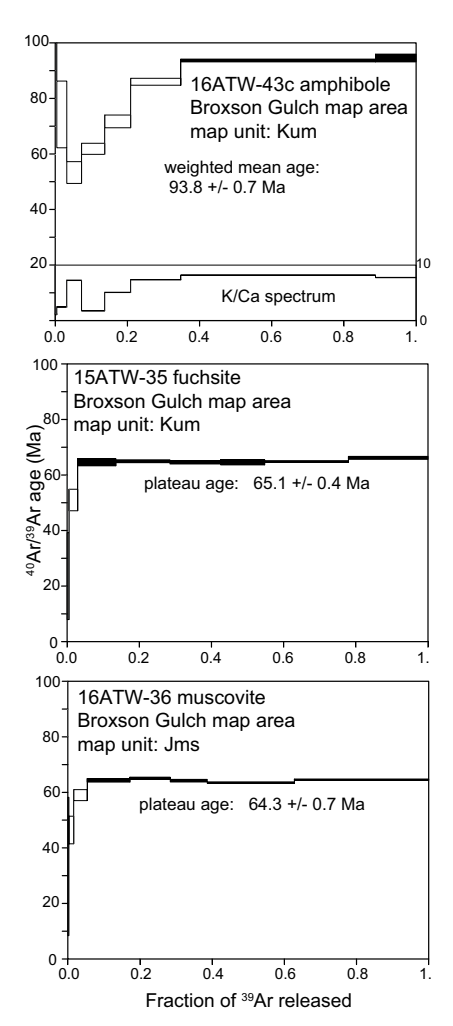


Figure 12. Mica and amphibole <sup>40</sup>Ar/<sup>39</sup>Ar age spectra for samples south of the Valdez Creek fault are shown. The sample number, mineral phase dated, map unit, and plateau or weighted mean age determinations are given for each sample. Only filled Ar release steps are used to calculate plateau or weighted mean ages. The K/Ca spectrum for sample 16ATW-43c is also given. Also see Table 1.

K/Ca ratio, which we infer to record Ar release from the K-bearing hornblende cores of the amphibole crystals. Sample 15ATW-35 is a serpentine-chlorite-brucite schist with minor kinked fuchsite sub-parallel to the foliation (Fig. 4F). The fuchsite yielded a plateau age of  $65.1 \pm 0.4$  Ma. One sample of muscovite graphite schist (16ATW-36) interfoliated with Clearwater mafic schist yielded a similar plateau age of  $64.3 \pm 0.7$  Ma. Muscovite in this sample is folded with the foliation and is partially recrystallized only locally into tabular grains near the crenulation axes (Fig. 4D).

#### Ann Creek Map Area

In the Ann Creek map area, the ca. 52 Ma quartz monzonite pluton carried in the hanging wall of the Valdez Creek fault contains a network of late, cross-cutting pegmatite dikes. One sample of pegmatite (15ATW-45) yielded biotite and muscovite suitable for  $^{40}$ Ar/ $^{39}$ Ar analysis. Biotite from this sample yielded a plateau age of  $37.7 \pm 0.6$  Ma, whereas the muscovite gave a plateau age of  $50.2 \pm 0.5$  Ma (Fig. 11).

#### Spinel Geochemistry

Ultramafic rocks hosted within the Clearwater metasediments contain minor (≤10%) proportions of opaque minerals including spinel group minerals, ilmenite, millerite, and chalcopyrite. The spinel group minerals display a variety of compositions ranging from chromite to magnetite with minor to moderate substitution of Ti, Mn, Mg, and Zn. Chromite-rich grains display reaction textures involving millerite, magnetite, and brucite (Supplemental File S4). Chromite cores and rims display Cr# (Cr/  $[Cr + Ti + Al + Fe^{3+}]$ ) values ranging from 0.5 to 0.8 and  $Fe^{2+}$ # ( $Fe^{2+}$ /[ $Mg + Mn + Fe^{2+}$ ]) ranging from 0.4 to 0.95 (Fig. 13). Magnetite-rich grains display Cr# less than 0.3 and Fe2+# values near 1 (Fig. 13). Supplemental File S8 (see footnote 1) contains electron microprobe data of the spinel group phases.

### DISCUSSION

# Interpretation of Geochronology and Thermochronology

### Sediment Source Areas, Unit Ages, and Terrane Associations

Mesozoic metamorphic rocks. Although the detrital zircon U-Pb age spectra for both the Maclaren schist and Clearwater metasedimentary rocks are dominated by Mesozoic ages, each unit records sediment input from distinct source areas inboard and outboard of the Denali fault. It is important to recognize that the eastern Denali fault has experienced more than 400 km of Cenozoic dextral displacement (Nokleberg et al., 1985). Moreover, stratigraphic studies of the Kahiltna assemblage demonstrate the predominance of margin parallel sediment transport as the strata were deposited (Ridgway et al., 2002; Kalbas et al., 2007). Therefore, sediment provenance areas for metasedimentary rocks in our study area may be located several hundred kilometers along strike to the southeast.

Key detrital zircon U-Pb age populations in the Maclaren schist include: 85–100 Ma, 140–210 Ma, and 330–370 Ma (Fig. 9). The distri-

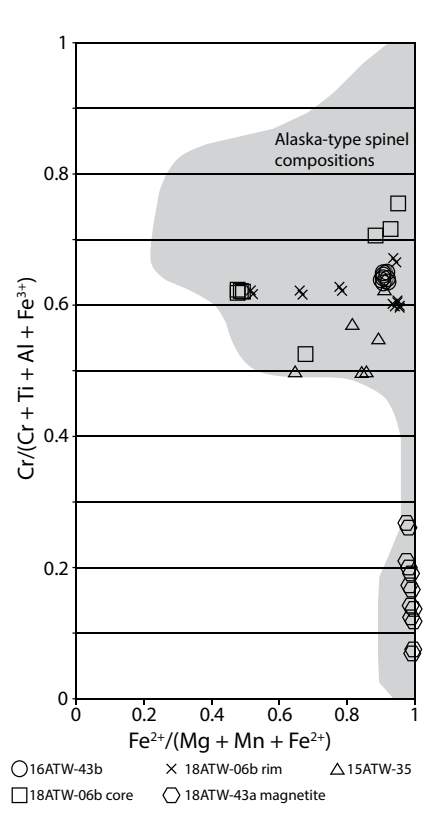


Figure 13. Plot of Cr# (Cr/[Cr+Ti+Al+Fe³+]) versus  $Fe^{2+}\#(Fe^{2+}/[Mg+Mn+Fe^{2+}])$  is shown for spinel group minerals (chromite unless otherwise noted) from ultramafic rocks within the Clearwater metasediments. Each sample is represented as a different symbol. The analytical uncertainty is smaller than the symbol. The shaded region represents the compositions of spinel group minerals from Alaska-type ultramafic complexes compiled by Barnes and Roeder (2001).

bution of Paleoproterozoic zircon grains and quartzofeldspathic-to-pelitic composition together suggest that the Maclaren schist protolith received detritus from a continental source area inboard of the Denali fault. Cretaceous and Jurassic igneous belts are abundant throughout British Columbia and Yukon (Gehrels et al., 2009; Allan et al., 2013) and represent a likely source area for Mesozoic age populations in the Maclaren schist. Devonian to early Mississippian igneous rocks are widespread in the Yukon-Tanana terrane in east-central Alaska and Yukon (Dusel-Bacon and Williams, 2009) and are a likely source for the mid-Paleozoic zircon population in the Maclaren schist. A Yukon-Tanana terrane source for the mid-Paleozoic grains is also supported by the presence of ca. 1.7-2.8 Ga detrital grains

because the Yukon-Tanana terrane igneous rocks intruded into Paleozoic and Neoproterozoic Laurentian continental margin rocks, which contain abundant Paleoproterozoic detrital zircon grains (Dusel-Bacon and Williams, 2009; Piercey and Colpron, 2009; Gehrels and Pecha, 2014; Pecha et al., 2016; Dusel-Bacon et al., 2017). In sum, detrital zircon age data suggest that the protolith of the Maclaren schist was principally sourced from Jurassic and Cretaceous igneous belts that were built on the western margin of North America. Considering the maximum depositional ages of ca. 94 Ma and 86 Ma (Fig. 8) places the Maclaren schist protolith in a basin system along the western margin of North America after 94 Ma. By ca. 75 Ma, the Maclaren schist was undergoing regional amphibolite facies metamorphism (Davidson et al., 1992; Ridgway et al., 2002).

The Clearwater metasedimentary rocks contain two major detrital zircon U-Pb age populations: 150-160 Ma and 175-200 Ma (Fig. 9). Although sediment source areas of this age range are present inboard of the Denali fault (e.g., Gehrels et al., 2009; Allan et al., 2013), the dearth of Paleozoic and Precambrian zircon grains and generally mafic composition of the Clearwater metagreywacke suggest a sediment source within oceanic arc terranes outboard of the Denali fault. Jurassic source areas outboard of the Denali fault include Chitina arc rocks (ca. 140-160 Ma, Roeske et al., 2003; Day et al., 2016; Beranek et al., 2017) and Talkeetna arc rocks (ca. 150-205 Ma, Roeske et al., 1989; Amato et al., 2007b; Rioux et al., 2007). The scant Paleozoic (ca. 415 Ma) and Precambrian (ca. 1100 Ma, 1500 Ma, 2800 Ma) grains can be traced to Paleozoic sedimentary and igneous rocks within the Alexander terrane (e.g., Gehrels et al., 1996; Kapp and Gehrels, 1998; Beranek et al., 2013; White et al., 2016) or to the Tlikakila complex in the western Alaska Range (Amato et al., 2007a). Based on these data, we infer that the protolith of the Clearwater metasedimentary rocks was sourced primarily from Chitina and Talkeetna arc rocks and thus was likely deposited along the paleo-eastern margin of the Wrangellia composite terrane. The protolith age is bracketed to 142-151 Ma by the maximum depositional ages of individual samples of the Clearwater metasediments (151–156 Ma, Fig. 8) and intrusion of a ca. 142 Ma alkali gabbro in the Clearwater Mountains (Mooney, 2010).

Association between the Clearwater metasediments and the Wrangellia composite terrane is also supported by the presence of ca. 100 Ma ultramafic to intermediate magmatism within the metasediments. Our data indicate that the Clearwater metasediments host a suite of ca. 100 Ma intermediate igneous intrusions and ultramafic cumulates (the aforementioned

hornblende-biotite-pyroxenite). Similar, albeit somewhat older (ca. 120 Ma), ultramafic and intermediate intrusive rocks have been mapped as intruding into Wrangellia rocks and Nutzotin basin strata ~30-50 km to the southeast of the Ann Creek map area (Bittenbender et al., 2007; Snyder and Hart, 2007; Wilson et al., 2015). Farther to the southeast, ca. 100-115 Ma, ultramafic and intermediate rocks have been described in southeast Alaska (Duke Island suite) and in the Yukon Territory (Pyroxenite Creek and Shorty Creek suites), where they form a series of compositionally zoned intrusions within the western Gravina belt, Alexander terrane, and Dezadeash formation (Eisbacher, 1976; Saleeby, 1992; Himmelberg and Loney, 1995). The zoned ultramafic intrusions in southeast Alaska and adjacent Yukon are geochemically distinct among ultramafic magmatic suites globally and have thus earned their own classification as "Alaska-type" ultramafic suites (Barnes and Roeder, 2001). Although the ca. 100 Ma magmatic suite in the Clearwater metasediments does not clearly display the zoned structure common of other Alaska-type ultramafic localities, the spinel compositions from ultramafic rocks in our study areas plot among the Cr# and Fe2+# values from other Alaska-type zoned ultramafic complexes (e.g., Barnes and Roeder, 2001) (Fig. 13). The age, spinel geochemistry, petrography, and distribution of rock types together make a strong case that ultramafic cumulates and associated intermediate composition intrusive rocks within the Clearwater metasediments represent a faulted and metamorphosed portion of an Alaska-type ultramafic intrusion rather than a structurally entrained fragment of lithospheric mantle or Nikolai intrusive rocks. Due to the clear connection between the Dezadeash formation and western Gravina belt with the Wrangellia composite terrane (e.g., Lowey, 1998, 2011, 2019; Yokelson et al., 2015) and the presence of Early Cretaceous ultramafic bodies within Wrangellia in the Alaska Range (Bittenbender et al., 2007), it appears that the Alaska-type zoned magmatic suite formed across the paleo-eastern margin of the Wrangellia composite terrane.

The similarity in detrital zircon U-Pb age spectra between the Clearwater metasediments, Dezadeash formation, and western Gravina belt (cf., Mooney, 2010; Yokelson et al., 2015; Link, 2017; Lowey, 2019; this study) suggests that the Clearwater metasediments are part of the dismembered Late Jurassic–Early Cretaceous basin system at the inboard margin of the Wrangellia composite terrane. The proximity of the hornblende-biotite-pyroxenite in the Ann Creek map area to the Denali fault suggests that it may be an offset portion of the Pyrox-

enite Creek ultramafic body, which intrudes the Dezadeash formation and is cut by the Denali fault in southwestern Yukon Territory (Eisbacher, 1976). Such correlation is consistent with other estimates of >400 km of Cenozoic dextral separation on the Denali fault (Nokleberg et al., 1985).

Cenozoic gravel deposits. Exposures of Cenozoic gravels at the southern flank of the Alaska Range display a variety of clast compositions and detrital zircon U-Pb age spectra that suggest a range of proximal and distal source areas. Clast populations from exposures in the Ann Creek map area indicate that Paleozoic and Triassic rocks within Wrangellia were the primary sediment source areas (Fig. 7). Alternatively, clast assemblages from exposures in Broxson Gulch suggest more heterogeneous source areas that include felsic intrusive rocks and low-grade metasedimentary rocks. We infer that the heterogeneity in the characteristics of the Cenozoic gravel deposits in the map areas reflects variability in depositional setting for each of these deposits. For example, 18ATW-14 (Fig. 2B) contains angular clasts of underlying Wrangellia rock (Fig. 7) and therefore may represent a preserved portion of a local alluvial deposit. In contrast, 16ATW-77 (Fig. 2A) contains rounded clasts of rock types that are not found near the sample location and thus were likely carried to their present location by a larger fluvial system. Aside from evidence for both local and distal sediment sources, the lack of Maclaren schist detritus in the gravel deposits suggests that the sediment source areas feeding the basins did not intersect the Maclaren schist.

The detrital zircon U-Pb age spectrum for 16ATW-77 displays a predominance of ca. 60 Ma and 100 Ma grains. Given the abundance of felsic igneous clasts in the deposit (Fig. 7), we infer that these age populations record input from a source area rich in Paleogene and Cretaceous plutonic rocks. The population of ca. 100 Ma plutonic rocks may be locally sourced from the granodiorite body exposed in the Ann Creek map area (sample 15ATW-51-102.4  $\pm$  1.1 Ma). The nearest potential source area for the Paleogene plutonic clasts is west of our study area in the northern Talkeenta Mountains (Csejtey et al., 1986; Davidson and McPhillips, 2007). In the northern Talkeetna Mountains, Paleogene plutons intruded into metasedimentary strata that contain Jurassic detrital zircon grains (cf. Davidson and McPhillips, 2007; Hults et al., 2013; Link, 2017; Hampton et al., 2010). These Late Jurassic metasedimentary rocks provide a probable source for the low-grade metamorphic clasts and Late Jurassic detrital zircon grains in sample 16ATW-77. Given that the youngest age population of detrital zircons (ca. 60 Ma) in sample 16ATW-77 is likely derived from plutonic rocks, it is tenable that the true depositional age is significantly younger than the maximum depositional age determined from the detrital zircon U-Pb age distribution (ca. 54 Ma; Fig. 10).

Sample 15ATW-06 also contains a suite of detrital zircon U-Pb dates that suggest derivation from a distal source area. The primary ca. 30 Ma age population in this sample cannot be traced to any local source in the Alaska Range or Talkeetna Mountains but does coincide with the onset of volcanism in the Wrangell Arc to the southeast of our study area and may reflect deposition of airfall ash deposits, although none were identified in the field (Berkelhammer et al., 2019; Brueseke et al., 2019). The minor ca. 145 Ma age population may be sourced from Chitina arc igneous rocks or Early Cretaceous strata exposed in the Nutzotin Mountains (e.g., Manuszak et al., 2007; Trop et al., 2020). Both low-grade metasedimentary and plutonic clasts are present in 15ATW-06 (Fig. 7), thus allowing for either source area. Triassic (ca. 230 Ma) and Carboniferous (ca. 300-310 Ma) zircon grains constitute the remaining minor age populations in the sample. These ages correlate well with the known ages of Nikolai and Skolai igneous provinces, which are widespread throughout the Wrangellia terrane (e.g., Beard and Barker, 1989; Greene et al., 2010; this study). As such, either proximal or distal source areas for Triassic and Carboniferous zircon grains are permissible. The maximum depositional age determined from the youngest population of zircon ages (ca. 30 Ma) is in agreement with Oligocene and Late Oligocene biostratigraphic ages (Metasequoia fossils) from an outcrop ~1 km to the south of 15ATW-06 (Stout, 1976; Locality #12 of Nokleberg et al., 1992b). We thus assign an Oligocene age to the deposit.

The southernmost sample (16ATW-86) represents the most heterogeneous zircon age distribution of the Cenozoic gravel deposits. However, the age populations can generally be traced to local source areas. Unlike the 16ATW-77 and 15ATW-06, the youngest age population (ca. 6 Ma) in sample 16ATW-86 is not the largest. Instead, the largest population comprises a ca. 155 Ma and 185 Ma bimodal distribution of Jurassic grains, which are identical to the ages and relative proportions of detrital zircon grains in the Clearwater metasediments (cf. Figs. 9 and 10). The presence of low-grade metamorphic clasts in 16ATW-86 further supports the inference that the Jurassic grains were derived from the Clearwater metasedimentary rocks. A moderate-sized population of ca. 310 Ma zircon grains suggests that intrusive igneous clasts in the deposit were sourced from Skolai arc plutons. Intrusive igneous clasts may also have been recycled into the deposit from 16ATW-77, which would account for the small population of Paleogene zircon grains. An isolated cluster of seven grains give late Miocene ages and constitute the youngest age population at ca. 6 Ma. The late Miocene marks a time of major expansion of the Wrangell Arc (Preece and Hart, 2004), and several late Miocene-Pliocene tephras have been found throughout the eastern Alaska Range (Kunk, 1995; Allen, 2016). Because no tephra is exposed near the sample, we infer that the late Miocene zircon grains in sample 16ATW-86 were recycled into the deposit from a tephra sourced from the Wrangell Arc and thus brackets the age of the deposit to be late Miocene or younger.

The clast assemblages and detrital zircon U-Pb age spectra for the Cenozoic gravel deposits contain a record of sediment recycling and landscape evolution in response to Cenozoic faulting along the south flank of the eastern Alaska Range. We discuss the implications of these data below in the context of the reactivation and evolution of major structures in the map areas.

## 40Ar/39Ar ages

Mica and amphibole <sup>40</sup>Ar/<sup>39</sup>Ar ages from metamorphic rocks in the hanging wall of the Broxson Gulch fault record over 60 m.y. of metamorphism and cooling. The <sup>40</sup>Ar/<sup>39</sup>Ar ages reveal that each thrust panel of metamorphic rocks in the study area experienced unique thermal histories that may be used to reconstruct the structural evolution of faults bounding the thrust sheets.

Mica ages from the Maclaren schist record two phases of cooling. The older phase of cooling is recorded by sample 15ATW-08 in Broxson Gulch (45.9  $\pm$  0.3 Ma biotite). Earlymid Eocene mica K-Ar and 40Ar/39Ar ages are widespread in the Maclaren schist to the west of Broxson Gulch (Turner and Smith, 1974; Riccio et al., 2014) and likely record cooling from early Eocene magmatism within the Maclaren schist. Because the quartz monzonite pluton in the Ann Creek map area appears to also be a part of the early Eocene magmatic suite, we infer that the Maclaren schist in our study area experienced the thermal effects of early Eocene magmatism and that the ca. 46 Ma 40 Ar/39 Ar biotite age on sample 15ATW-08 records cooling from that thermal event. A younger phase of cooling is recorded by sample 16ATW-73 in Broxson Gulch  $(32.8 \pm 0.3 \text{ Ma biotite plateau age})$ . Ca. 32 Ma K-Ar and 40Ar/39Ar ages are widespread near the Denali fault in the eastern and northern regions of the Maclaren schist and are interpreted to record thermal resetting and subsequent cooling from intrusion of a suite of ca. 32-40 Ma plutons throughout the eastern and central Alaska Range (Benowitz et al., 2011, 2019; Trop et al.,

2019). We infer that the biotite porphyroblasts in 16ATW-73 formed during heating associated with the 32-40 Ma magmatism. Sample 15ATW-45 in Ann Creek (37.7 ± 0.6 Ma biotite,  $50.2 \pm 0.5$  Ma muscovite) contains evidence for both thermal resetting/cooling events. The similarity between the muscovite age and the U-Pb zircon age of the quartz monzonite pluton  $(51.9 \pm 0.6 \text{ Ma})$  suggests that the muscovite records rapid post-emplacement cooling. The biotite age from 15ATW-45 may either record that the post-emplacement cooling rate slowed during the late Eocene or that the sample had cooled below argon closure in biotite prior to 40 Ma and the thermal effects of the 32-40 Ma magmatic event were significant enough to reset the biotite age. A third intermediate scenario wherein the thermal effect of the late Eocene magmatism provided enough heat to slow the cooling rate of sample 15ATW-45 is also viable. The mica cooling ages collectively indicate that the Maclaren schist maintained temperatures in excess of ~350 °C (Ar closure for coarse biotite during typical orogenic cooling rates; Harrison et al., 1985; Hodges, 2014) until the early Oligocene.

There is presently no evidence that any of the rocks south of the Valdez Creek fault experienced the thermal pulses of Eocene magmatism recorded by mica ages in the Maclaren schist. Instead, white mica ages from metamorphosed ultramafic rocks and the Clearwater muscovitegraphite schist record a single phase of prograde regional metamorphism and development of the inverted metamorphic gradient. The inference that white mica ages in the ultramafic rocks and Clearwater schist record the timing of peak metamorphism is supported by our observations of feldspar deformation textures, amphibole compositions, and mineral assemblages, suggesting that peak regional metamorphic conditions in the inverted metamorphic belt did not exceed middle-to-upper greenschist facies conditions. White mica in the structurally highest position of the inverted metamorphic belt (i.e., the dated samples) is kinked parallel to the dominant foliation and displays undulose extinction due to the deformation (Figs. 4E and 4F). The size fraction of the dated white mica grains (200-500 um) corresponds to an Ar closure temperature exceeding 425 °C for typical orogenic cooling rates (e.g., Harrison et al., 2009; Hodges, 2014). By considering the above petrographic observations and inferred Ar closure temperature together, we argue that the dated white mica samples have retained Ar since final recrystallization and deformation at middle-to-upper greenschist facies conditions. Thus, the mica ages from both 16ATW-36 (64.3  $\pm$  0.7 Ma muscovite) and 15ATW-35 (65.1  $\pm$  0.4 Ma fuchsite) record the peak of regional metamorphism and

associated deformation in the earliest Paleogene. This timing compares well with age data from the Valdez Creek shear zone, where post-75 Ma ductile thrusting of the Maclaren schist over the Clearwater metasedimentary rocks is inferred to have developed an inverted metamorphic gradient in the footwall rocks (Davidson et al., 1992; Hollister, 1993; Ridgway et al., 2002). Biotite <sup>40</sup>Ar/<sup>39</sup>Ar cooling ages record uniform cooling across the Valdez Creek shear zone by ca. 61–64 Ma (Ridgway et al., 2002).

Amphibole from the amphibolite body (16ATW-43c) in Broxson Gulch provides a record of both mid-Cretaceous magmatism and Late Cretaceous metamorphism within the Clearwater metasediments. The size of the amphibole in the sample (Fig. 3F), lack of feldspar, and association with serpentinite suggest that the protolith of the amphibolite was a coarsely crystalline ultramafic rock. The amphibole 40Ar/39Ar weighted mean age of  $93.8 \pm 0.7$  Ma from sample 16ATW-43c is similar to a ca. 92 Ma K-Ar amphibole age from the pegmatitic hornblendebiotite-pyroxenite (Alaska-type ultramafic cumulate) in the Ann Creek map area (Nokleberg et al., 1992b). Considering that the petrographic observations suggest a coarsely crystalline protolith and the similarity in amphibole age between 16ATW-43c and the pyroxenite body in the Ann Creek area, we infer that the amphibolite in Broxson Gulch was metamorphosed from a protolith composed of coarse ultramafic cumulate. The actinolite zones within the coarse amphibole and greenschist facies matrix minerals indicate that the rock experienced greenschist facies metamorphism following emplacement. This inference is consistent with the age and grade of metamorphism of the Clearwater metasediments recorded by the muscovite and fuchsite ages.

# Synthesis of Mapping, Cooling Ages, and Structural Evolution

Our revision of the regional geologic framework is based on the recognition of district metasedimentary rock units in the study area. Similar to the early work by Rose (1965, 1966) and Stout (1965), our mapping and petrography indicate that the Maclaren schist and Clearwater metasediments are distinguishable on the basis of protolith composition and rock fabrics. Moreover, detrital zircon age spectra (Figs. 8 and 9) and ages of intrusive igneous rocks within the metasedimentary rocks (Figs. 2 and 5) reveal that the protoliths of the Clearwater metasediments and Maclaren schist cannot be the same. Although the Clearwater metasediments display internal variation in protolith composition, the detrital zircon age spectra from zircon-bearing rock types throughout the package suggest that

the various sedimentary protoliths were derived from the same sediment source area. Accordingly, the ages of the protoliths are likely similar across the various rock types in the Clearwater metasediments.

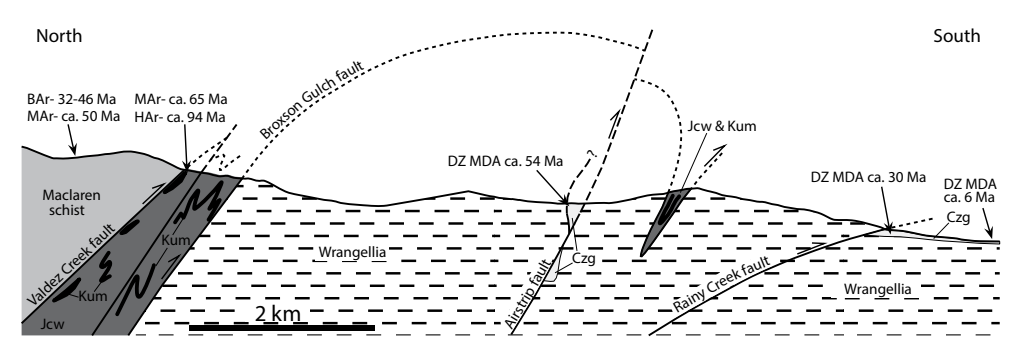
Our recognition of the Valdez Creek fault and the separate thermal histories of the rocks on either side further require that the Maclaren schist and Clearwater metasediments be split into distinct metasedimentary packages that evolved independently until structural juxtaposition. Our naming of the Valdez Creek fault is based on the Valdez Creek shear zone in the Clearwater Mountains ~60 km to the southwest of our study area. 40Ar/39Ar biotite cooling ages across the Valdez Creek shear zone suggest there has been little or no slip across it since ca. 60 Ma (Ridgway et al., 2002). The same structural relationship is observed in the Ann Creek map area, Broxson Gulch map area, and the Clearwater Mountains: the Maclaren schist is thrust southward over the Clearwater metasediments. However, the Maclaren schist in the Ann Creek and Broxson Gulch areas lacks the mylonitic fabric of the Valdez Creek shear zone and instead has a significant retrograde metamorphic fabric defined by a strong chlorite-muscovite penetrative foliation (e.g., Fig. 3G), which intensifies down-section to the Valdez Creek fault. Thus, we interpret that the Cenozoic Valdez Creek fault developed within the hanging wall of the Late Cretaceous-early Cenozoic Valdez Creek shear zone as a lowerdip, lower-grade shear zone, which evolved into a brittle fault with continued slip and exhumation. In our naming of the Valdez Creek fault, we keep the location name "Valdez Creek" because the structural relations are the same as those observed in the type locality. Our use of the word fault rather than shear zone is intended to convey that the boundary between the two units is a discrete zone of cataclastic deformation.

The timing of reactivation of the Valdez Creek shear zone as the Valdez Creek fault is recorded by the disparate thermal histories of rocks juxtaposed by the fault. Biotite and muscovite cooling ages from the hanging wall record multiple thermal pulses that held the Maclaren schist above ~350 °C until ca. 32 Ma. Contrarily, rocks in the structurally highest section of the footwall cooled from peak metamorphic temperatures of ~350-450 °C after ca. 65 Ma and had passed though the 350 °C isotherm by 60 Ma (Ridgway et al., 2002). Map-based evidence highlighting the independent thermal histories comes from the Ann Creek map area where both the ca. 52 Ma quartz monzonite intrusion and sillimanite-bearing Maclaren gneiss in the contact aureole are cut by the Valdez Creek fault (Stout, 1965) (Fig. 2B). Footwall rocks in this area display no textural evidence of static recrystallization and therefore

apparently did not experience any significant heating by the quartz monzonite intrusion. The field, textural, and thermochronological evidence together indicate that the Maclaren schist and Clearwater metasediments experienced independent thermal paths until juxtaposition by the Valdez Creek fault after ca. 32 Ma.

The thermal evolution of the Clearwater metasediments is also distinct from Wrangellia rocks, which leads to refinement of the location of the Broxson Gulch fault. We define the Broxson Gulch fault as the boundary between low-grade metasedimentary rocks containing ca. 100 Ma ultramafic-intermediate intrusions (Clearwater) and pre-Jurassic metavolcanic rocks with associated intrusions (Skolai and Nikolai). Previous mappers had included intermediate intrusions and foliated Skolai rocks in the hanging wall of the Broxson Gulch fault due to similarities in metamorphic grade and rock fabrics. However, the Carboniferous age of the intrusions (Figs. 2 and 5; Table 2) and location of the fabric only in the contact aureole of the intrusions (Fig. 2A) indicate that these rocks experienced a different metamorphic history than the Clearwater metasediments. Our reinterpretation of the map units near the Broxson Gulch fault is supported by the observation that the boundary between the Clearwater metasediments and Skolai rocks is always marked by a ~30-m-thick zone of sheared rock, which we infer to mean that the rocks are juxtaposed by a large structure (i.e., the Broxson Gulch fault). Our re-mapping of the fault generally places it farther north in the northern portions of both map areas and refines the location of it near the range front in Broxson Gulch (cf. Fig. 2 and Stout, 1976).

The structural evolution of Cenozoic faulting within Wrangellia yields additional insight into the geometry of the Broxson Gulch fault. Because the Muddy Creek fault does not appear to have Cenozoic displacement, the Airstrip fault is the structurally highest fault within Wrangellia with clear evidence for Cenozoic slip. In both the Broxson Gulch and Ann Creek map areas, we map a shallowly west-plunging footwall synform associated with the Airstrip fault (Figs. 2 and 14). The core of the synform in Broxson Gulch contains Clearwater slate, and because the slate is always underlain by the Broxson Gulch fault in this area, the fold must also involve that fault (Fig. 2A). Although previous mappers had recognized the Clearwater slate in southeastern Broxson Gulch, they attributed the apparent offset of the Broxson Gulch fault to a NW-striking sinistral tear fault that was inferred to exist beneath Quaternary surficial deposits (Rose, 1965; Stout, 1976; Nokleberg et al., 1992a). We contend that the presence of the synform in the footwall of the Airstrip fault implies the presence of a



Czg—Cenozoic gravel deposit; DZ MDA—Detrital zircon maximum depositional age; BAr—biotite <sup>40</sup>Ar/<sup>39</sup>Ar age. HAr—hornblende <sup>40</sup>Ar/<sup>39</sup>Ar age.

Figure 14. Schematic cross section shows key features compiled from both map areas. Broken lines represent faults projected above the surface. Each thrust panel is annotated with 40Ar/39Ar ages to show the diverse thermal histories of the individual thrust sheets. Kum—Alaska-type ultramafic rocks; Jcw—Clearwater metasedimentary rocks; 40Ar/39Ar age; MAr—muscovite

companion hanging wall antiform (e.g., Mitra, 1990); however, the section of the Broxson Gulch fault that would display the inferred antiform is buried beneath glacial deposits (Fig. 2A). We argue that because the synform is known from our mapping, the sinuous map pattern of the Broxson Gulch fault is better explained by erosion of an antiform-synform pair rather than offset of the Broxson Gulch fault by a younger NW-SE-striking fault. Our new interpretation of the map pattern implies that the Airstrip fault became active before the overlying thrust sheets carried by the Broxson Gulch fault were completely eroded. As a result, accumulated slip on the Airstrip fault folded and eventually cut through the overlying Broxson Gulch fault (Fig. 14).

The Rainy Creek fault is the southernmost and structurally lowest fault in the study area. Its position near the topographic range front and projected trace between Oligocene and late Miocene fluvial gravel deposits strongly suggest that the Rainy Creek fault is the most recently active fault in the map areas. Such an inference is supported by geophysical evidence in the Ann Creek area, where the Rainy Creek fault appears to cross-cut the Airstrip fault (Fig. 2B; Supplemental File S7; see footnote 1).

The geologic evolution of both map areas suggests that structural reactivation initiated on the Valdez Creek fault and progressed into the Wrangellia terrane. 40Ar/39Ar cooling ages reveal that the Valdez Creek fault formed after ca. 32 Ma. The lack of Maclaren schist detritus in the Cenozoic gravel deposits further suggests that either the reactivation did not happen until after ca. 30 Ma and/or the Valdez Creek thrust sheet was topographically separated from the watersheds that fed the ca. 30 Ma and 6 Ma gravel deposits. Evidence for southward progression of thrusting is present in Broxson Gulch, where slip on a subsidiary footwall structure within the Clearwater metasediments folded and cut an overlying klippe of Maclaren schist (Fig. 2A, south of 15ATW-35, and Fig. 14). Slip on the Broxson Gulch fault is inferred to post-date the

Valdez Creek fault because only cataclastic deformation is associated with slip on the Broxson Gulch fault and because all rocks in the hanging wall of the Broxson Gulch fault appear to share a Miocene cooling history below ~200 °C (Waldien et al., 2017). Folding of the Broxson Gulch fault over the Airstrip fault requires that slip on the Airstrip fault post-dates slip on the Broxson Gulch fault and the burial of the northernmost Cenozoic gravel deposit (16ATW-77). Erosion related to slip on the Airstrip fault likely exhumed a portion of the <54 Ma gravel deposit (16ATW-77), which may have been recycled into the ca. 6 Ma gravel deposit (sample 16ATW-86) presently exposed at the range front (e.g., Figs. 7 and 10). Such an inference requires the Airstrip fault to have been active during the Miocene. The Rainy Creek fault cuts the gravel deposit at the range front (Fig. 2B; Supplemental File S6), which suggests that the Rainy Creek fault has been active since ca. 6 Ma.

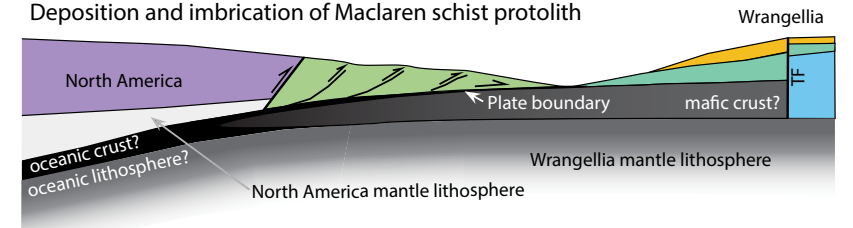
In summary, our mapping, petrography, geochronology, and thermochronology demonstrate that the Valdez Creek and Broxson Gulch faults are key structures that bound distinct packages of rocks with independent structural, metamorphic, and magmatic histories prior to juxtaposition. As such, each fault likely represents the Cenozoic reactivation of structures that formed individually during Mesozoic terrane accretion. Structural reactivation initiated on the Valdez Creek fault after ca. 32 Ma and has since shifted to the Broxson Gulch fault and then into Wrangellia (Fig. 14). It is possible that the Broxson Gulch fault and imbricate Cenozoic structures within Wrangellia are restricted to the upper crust and root into the Valdez Creek fault at depth via some décollement system. Offset of the youngest fluvial gravel deposit by the Rainy Creek fault indicates that shortening in the system lasted until at least 6 Ma.

## Regional Significance

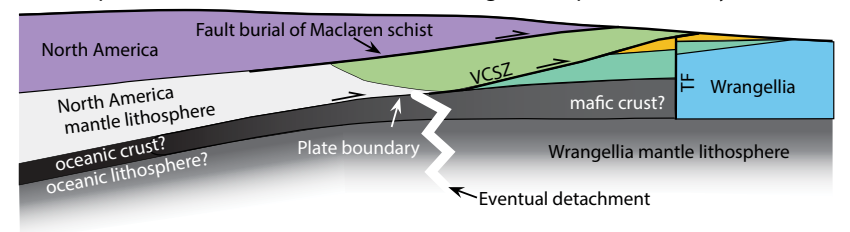
A major shift in the tectonic configuration of southern Alaska took place between 30 Ma

and 20 Ma. The shift is recorded throughout southern Alaska by regional exhumation within the Alaska Range suture zone (Finzel et al., 2011; Lease et al., 2016; Terhune et al., 2019), onset of focused exhumation along the Denali fault (Benowitz et al., 2011, 2014), cessation of magmatism along the Denali fault (Trop et al., 2019), drainage reorganization related to topographic development (Ridgway et al., 2007; Finzel et al., 2015, 2016; Brennan and Ridgway, 2015; Benowitz et al., 2019), initiation of Wrangell Arc volcanism (Richter et al., 1990; Berkelhammer et al., 2019; Brueseke et al., 2019), and development of the St. Elias fold and thrust belt (Bruhn et al., 2004; Pavlis et al., 2012). These events are generally considered to be upper plate responses to increased plate coupling and eventual collision of the Yakutat block with the southern Alaska subduction zone (e.g., Enkelmann et al., 2008, 2010; Jadamec et al., 2013; Haynie and Jadamec, 2017). The post-32 Ma onset of slip on the Valdez Creek fault is contemporaneous with the above events and suggests that it, too, is related to Yakutat convergence. It is again important to convey that the rocks and structures in our study area were likely ~200-300 km along strike to the southeast at the time of reactivation and have since moved into the curved section of the Denali fault. Therefore, reactivation could not have initiated due to interaction with the curved section of the Denali fault and is inconsistent with models of thrust (re)activation in the core of the Alaska orocline (e.g., Glen, 2004). Instead, reactivation of the Valdez Creek fault and associated structures is better explained by translation along the Denali fault system into increased alignment with the Queen Charlotte-Fairweather transform fault system (e.g., Riccio et al., 2014) in concert with strain transfer from the Yakutat collision zone to the mechanical contrast at the inboard margin of the Wrangellia terrane (e.g., Saltus and Hudson, 2007).

#### A Ca. 90 Ma-

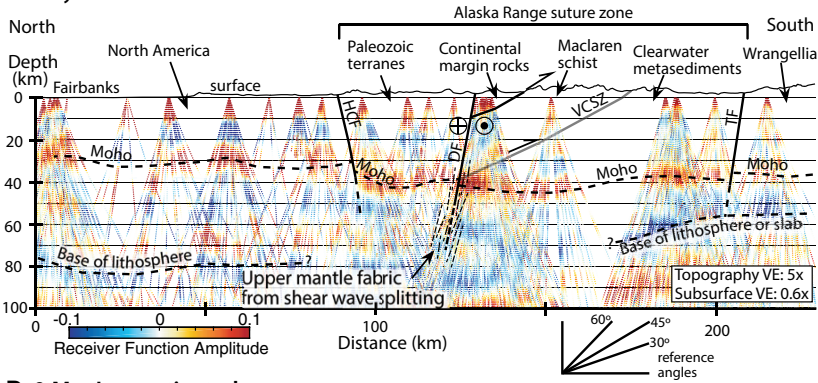


**B Ca. 75 Ma**-Development of Valdez Creek shear zone along former plate boundary



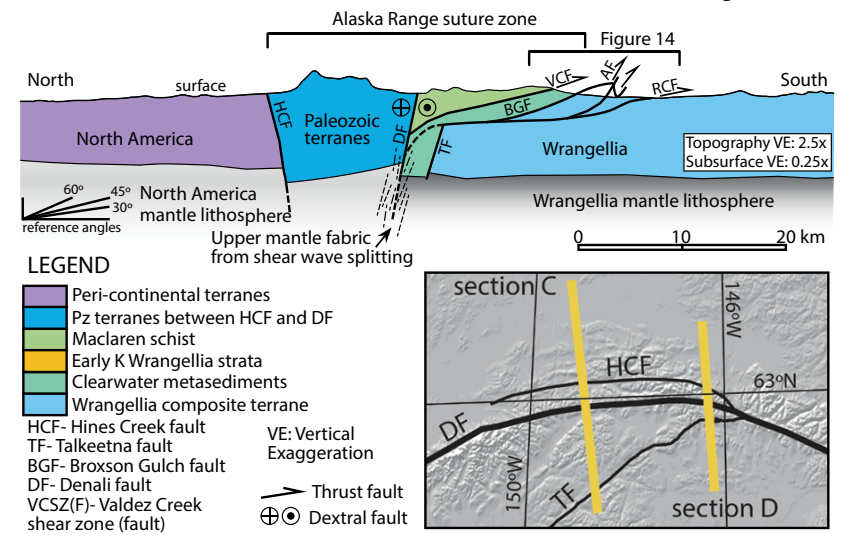
#### C 0 Ma- West of reactivated zone

- -P receiver functions suggest Denali fault and Valdez Creek shear zone root into upper mantle shear zone
- -Proxy for ca. 32 Ma crustal structure south of the Denali fault



## D 0 Ma- In reactivated zone

Imbricate Cenozoic structures shorten suture zone and northern Wrangellia



Geological Society of America Bulletin

Figure 15. Proposed evolutionary model shows the formation of the Valdez Creek shear zone and subsequent reactivation as the Valdez Creek fault. The vertical scale for all profiles is based on profile C. The horizontal distances in profiles A and B are schematic and not related to the vertical scale. Topography and subsurface geology in profiles C and D have been vertically exaggerated (VE); reference angles for each profile are given to help visualize the true dip of the structures. The locations of profiles C and D are shown as yellow lines on the accompanying map. (A) The Maclaren schist was deposited into a contractional basin on the western margin of North America at ca. 90 Ma. Shortening structures in the basin likely rooted into an E-dipping plate boundary fault zone, possibly a subduction zone, that consumed the marine basin between the Wrangellia composite terrane and North America. The Clearwater metasediments were previously deposited on the paleoeastern margin of the Wrangellia composite terrane and were brought to North America with the terrane. (B) The Valdez Creek shear zone (VCSZ) developed along the pre-existing plate boundary after the Maclaren schist was buried and metamorphosed beneath the North American margin. Note that it remains unclear whether oceanic lithosphere was attached to the inboard margin of the Wrangellia composite terrane during the Cretaceous. If oceanic lithosphere were present, it would have likely detached in the latest Cretaceous. (C) Cross section showing depth-converted P receiver functions from seismic stations across interior Alaska, the Alaska Range suture zone, and the Wrangellia terrane annotated with crustal faults, interpreted Moho conversions (strong positive amplitude; red colors), interpreted asthenosphere-lithosphere conversions (negative amplitude; blue colors), and inferred anisotropic fabrics from shear wave splitting (Rasendra et al., 2014) along the Denali fault at depth. The receiver function data were processed using the methods of Miller et al. (2018) and updated for this study. The steep northward dip of the Denali fault is inferred from thermochronological data (Benowitz et al., 2011). (D) Schematic cross section along a profile from interior Alaska through our study area and into the Wrangellia terrane. The Denali fault juxtaposes crust and lithosphere of different thicknesses and geophysical properties belonging to the Wrangellia terrane and peri-continental terranes to the north. Alaska Range suture zone metamorphic rocks discussed herein occupy a highly shortened domain adjacent to the south side of the Denali fault. The location of the Figure 14 cross section is given for reference.

# Deep-Seated Structural Reactivation of a Cryptic Suture

Our data indicate that the Valdez Creek shear zone formed as a primary Mesozoic collisional structure between the North American continent and the allochthonous Wrangellia composite terrane. The characteristics of rocks in the hanging wall of the Valdez Creek shear zone (Maclaren schist) place them along the western margin of North America at ca. 90 Ma. Contrarily, footwall rocks (Clearwater metasediments) accumulated along the paleo-eastern margin of the Wrangellia composite terrane at ca. 150 Ma. These distinctive assemblages were presumably brought together by a plate boundary fault system, possibly a subduction zone, that existed between them (Fig. 15A). After tectonic burial of the Maclaren schist beneath the North American continental margin, the Valdez Creek shear zone formed along the former plate boundary and brought the Maclaren schist and Clearwater metasediments into contact by ca. 75 Ma, at which time they were deformed together during the peak of the collision (Fig. 15B). Regional Late Cretaceous exhumation of rocks northeast of the Denali fault in eastern Alaska and central Yukon (Dusel-Bacon et al., 2002, 2016) and Paleogene extensionrelated magmatism (Bacon et al., 1990; Moll-Stalcup, 1994) may be upper plate responses to underplating of the Maclaren schist and inferred slab detachment following collision.

The collision of the Wrangellia composite terrane marked a massive addition of juvenile lithosphere to the western margin of North America (Samson et al., 1990; Trop and Ridgway, 2007). The differences in crustal composition, age, thickness, and structure between the Wrangellia composite terrane and North American margin terranes correlate with unique geophysical characteristics in the crust and lithospheric mantle underlying each region (e.g., Glen et al., 2007; Saltus et al., 2007; O'Driscoll and Miller, 2015; Allam et al., 2017; Miller et al., 2018; Miller and Moresi, 2018; Feng and Ritzwoller, 2019; Berg et al., 2020). The P receiver function profile in Figure 15C illustrates the correlation between terrane boundaries and distinct changes in crust and lithosphere thickness. The transition in lithospheric architecture across the eastern Alaska Range also coincides with a well-defined zone of fault parallel seismic anisotropy in the lower crust and upper mantle that is inferred to record rock fabrics in the roots of the Denali fault system (Rasendra et al., 2014; Audet et al., 2016). These geophysical data sets together suggest that the eastern Denali fault formed along a lithospheric boundary between the Wrangellia composite terrane and previously accreted terranes to the north and east. Because structures

south of the Denali fault along the profile in Figure 15C have experienced limited activity since 32 Ma, we infer that the lithospheric structure of that region revealed by the P receiver functions approximates the geometry of the Denali fault, Valdez Creek shear zone, and Talkeetna fault prior to reactivation.

One key outcome of this study is that the Valdez Creek shear zone, rather than the Talkeetna fault, was the main reactivated structure. Both structures intersect the Moho (Fig. 15C). Yet, the Talkeetna fault in most places marks one of the most profound geophysical boundaries in southern Alaska due to differences in crustal thickness (Veenstra et al., 2006; Brennan et al., 2011; Miller et al., 2018) and strongly contrasting crustal gravity/magnetic properties across the fault (Glen et al., 2007; Saltus et al., 2007). These features of the Talkeetna fault may record differences in crustal strength across the fault (e.g., Saltus and Hudson, 2007), which would imply that it would localize reactivation. However, the data synthesized herein indicate that reactivation nucleated on the Valdez Creek shear zone. Our preferred reconciliation of these data sets is that the history of the Valdez Creek shear zone as a former convergent plate boundary implies that it penetrates the crust and links to the Denali fault in the upper mantle (Fig. 15C). Such connectivity of major structures highlights the Valdez Creek shear zone as a lithospheric-scale zone of weakness that focused shortening when the Denali fault system transitioned from transcurrent to transpressional deformation. Post-32 Ma shortening on the Valdez Creek fault and imbricate structures resulted in underthrusting of the Wrangellia terrane, possibly as far north as the Denali fault (Allam et al., 2017) (Fig. 15D).

Reactivation of suture zone structures is observed at all crustal levels in polyphase orogens worldwide (Sykes, 1978; Bailey et al., 2000; Tikoff et al., 2001; Taylor et al., 2003; Jones et al., 2013; Cavazza et al., 2017; and numerous others). Although the boundary between allochthonous terranes may manifest in the upper crust as a wide zone of distributed deformation between the disparate terranes, we have shown herein that rocks within a suture zone sensu lato may be parsed and assigned to terranes on either side of the collision zone. As a result, the main deformation zone marking the juxtaposition of rocks with independent histories may be relatively discrete. We further argue that the independent lithospheric evolution of each terrane prior to collision will result in a lithospheric scale boundary along the length of the collision zone. Post-collisional deformation is likely to focus on the inherited lithospheric boundary in response to evolving plate boundary conditions.

The reactivated fault system will grow initially by reactivation of major crustal structures that link through the lithosphere and eventually by incorporation of subordinate regional structures.

#### CONCLUSION

We documented the polyphase structural and thermal evolution of metamorphic rocks within the Alaska Range suture zone in the eastern Alaska Range. Our analysis illuminates the Valdez Creek fault as the primary reactivated structure in the area, which formed by reactivation of the Valdez Creek shear zone after ca. 32 Ma. Subordinate Cenozoic faults include the Broxson Gulch fault at the northern boundary of the Wrangellia terrane and the Airstrip and Rainy Creek faults within Wrangellia. The Maclaren schist in the hanging wall of the Valdez Creek fault likely formed along the western margin of North America at ca. 90 Ma, whereas the protolith of the Clearwater metasediments in the footwall was deposited on the paleo-eastern margin of the Wrangellia composite terrane at ca. 150 Ma. The Valdez Creek fault thus appears to have reactivated along the collisional boundary between North American lithosphere and allochthonous Wrangellia composite terrane lithosphere. Shortening subsequently progressed southward from the Valdez Creek fault to the Broxson Gulch fault and then into the Wrangellia terrane. The timing and style of deformation documented herein suggest that reactivation of structures in the Alaska Range suture zone is a far-field result of Yakutat flat slab subduction and accretion along the southern Alaska convergent margin in concert with the Denali fault tectonic conveyor belt system.

#### ACKNOWLEDGMENTS

This work was funded by grants from the American Association of Petroleum Geologists, Alaska Geological Society, Geological Society of America, and UC Davis Durrell Fund (T.S. Waldien), U.S. Geological Survey National Cooperative Geologic Mapping Program award #G16AC00206 (S.M. Roeske and T.S. Waldien), National Science Foundation (NSF) Tectonics award #EAR-1828737 to S.M. Roeske and #EAR-1828023 to LA Benowitz and the State of Alaska Strategic and Critical Minerals Assessment program (E. Twelker). Analyses at the Arizona Laserchron Center were partially supported by NSF award #EAR-1649254 to that facility. We are grateful to Wing Air and Alaska Land Exploration for transportation to and from the field areas, T.S. Waldien appreciates assistance in the field from Daniel Baldassare, Tyler Schlieder, and Sonny Hutchinson and in the lab from Cait Livsey, Kojo Plange, and Nicky Geissler. Robert Zierenberg provided valuable advice on chromite analyses and interpretation. Jim Stout graciously shared thin sections and words of advice upon starting this project. We thank Richard Lease, Terry Pavlis, and an anonymous reviewer for feedback on this manuscript.

#### REFERENCES CITED

- Aleinikoff, J.N., Nokleberg, W.J., and Herzon, P.L., 1981, Age of intrusion and metamorphism of the East Susitna batholith. Mount Hayes B-6 quadrangle, eastern Alaska Range, Alaska: Geological Survey Circular, v. 844, p. 100–102.
- Allam, A.A., Schulte-Pelkum, V., Ben-Zion, Y., Tape, C., Ruppert, N., and Ross, Z.E., 2017, Ten kilometer vertical Moho offset and shallow velocity contrast along the Denali fault zone from double-difference tomography, receiver functions, and fault zone head waves: Tectonophysics, v. 721, p. 56–69, https://doi.org/10.1016/ j.tecto.2017.09.003.
- Allan, M.M., Mortensen, J.K., Hart, C.J.R., Bailey, L.A., Sánchez, M.G., Ciolkiewicz, W., McKenzie, G.G., and Creaser, R.A., 2013, Magmatic and metallogenic framework of west-central Yukon and eastern Alaska, in Colpron, M., Bissig, T., Rusk, B.G., and Thompson, J.F.H., eds., Tectonics, Metallogeny, and Discovery: The North American Cordillera and Similar Accretionary Settings: Society of Economic Geologists Special Publication 17, p. 111–168.
- Allen, W.K., 2016, Miocene-Pliocene strike-slip basin development along the Denali fault system in the eastern Alaska Range: Chronostratigraphy and provenance of the McCallum formation and implications for displacement [M.S. thesis]: West Lafayette, Indiana, Purdue University, 160 p.
- Amato, J.M., Bogar, M.J., Gehrels, G.E., Farmer, G.L., and McIntosh, W.C., 2007a, The Tlikakila complex in southern Alaska: A suprasubduction-zone ophiolite between the Wrangellia composite terrane and North America, in Ridgway, K.D., Trop, J.M., Glen, J.M.G., and O'Neill, M.O., eds., Tectonic Growth of a Collisional Continental Margin: Crustal Evolution of Southern Alaska: Geological Society of America Special Paper 431, p. 227–252, https://doi.org/10.1130/2007.2431(10).
- Amato, J.M., Rioux, M.E., Keleman, P.B., Gehrels, G.E., Clift, P.D., Pavlis, T.L., and Draut, A.E., 2007b, U-Pb geochronology of volcanic rocks from the Jurassic Talkeetna Formation and detrital zircons from preare and postarc sequences: Implications for the age of magmatism and inheritance in the Talkeetna Arc, in Ridgway, K.D., Trop, J.M., Glen, J.M.G., and O'Neill, M.O., eds., Tectonic Growth of a Collisional Continental Margin: Crustal Evolution of Southern Alaska: Geological Society of America Special Paper 431, p. 253–271, https:// doi.org/10.1130/2007.2431(11).
- Audet, P., Sole, C., and Schaeffer, A.J., 2016, Control of lithospheric inheritance on neotectonic activity in northwestern Canada?: Geology, v. 44, no. 10, p. 807– 810, https://doi.org/10.1130/G38118.1.
- Bacon, C.R., Foster, H.L., and Smith, J.G., 1990, Rhyolitic calderas of the Yukon-Tanana Terrane, east central Alaska: Volcanic remnants of a mid-Cretaceous magmatic arc: Journal of Geophysical Research: Solid Earth, v. 95, B13, p. 21451–21461, https://doi.org/10.1029/ JB095iB13p21451.
- Bailey, W.R., Holdsworth, R.E., and Swarbrick, R.E., 2000, Kinematic history of a reactivated oceanic suture: The Mamonia Complex Suture Zone, SW Cyprus: Journal of the Geological Society, v. 157, no. 6, p. 1107–1126, https://doi.org/10.1144/jgs.157.6.1107.
- Barnes, S.J., and Roeder, P.L., 2001. The range of spinel compositions in terrestrial mafic and ultramafic rocks: Journal of Petrology, v. 42, no. 12, p. 2279–2302, https://doi.org/10.1093/petrology/42.12.2279.
- Beacom, L.E., Holdsworth, R.E., McCaffrey, K.J.W., and Anderson, T.B., 2001, A quantitative study of the influence of pre-existing compositional and fabric heterogeneities upon fracture-zone development during basement reactivation, in Holdsworth, R.E., Strachan, R.A., Magloughlin, G.F., and Knipe, R.J., eds., The Nature and Significance of Fault Zone Weakening: Geological Society, London, Special Publication 186, no. 1, p. 195–211, https://doi.org/10.1144/GSL. SP.2001.186.01.12.
- Beam, E.C., and Fisher, D.M., 1999, An estimate of kinematic vorticity from rotated elongate porphyroblasts: Journal of Structural Geology, v. 21, no. 11, p. 1553– 1559, https://doi.org/10.1016/S0191-8141(99)00110-8.

- Beard, J.S., and Barker, F., 1989, Petrology and tectonic significance of gabbros, tonalites, shoshonites, and anorthosites in a late Paleozoic arc-root complex in the Wrangellia terrane, southern Alaska: The Journal of Geology, v. 97, p. 667–683, https://doi.org/10.1086/629351.
- Bemis, S.P., and Wallace, W.K., 2007, Neotectonic framework of the north-central Alaska Range foothills, in Ridgway, K.D., Trop, J.M., Glen, J.M.G., and O'Neill, M.O., eds., Tectonic Growth of a Collisional Continental Margin: Crustal Evolution of Southern Alaska: Geological Society of America Special Paper 431, p. 549–572, https://doi.org/10.1130/2007.2431(21).
- Bemis, S.P., Carver, G.A., and Koehler, R.D., 2012, The Quaternary thrust system of the northern Alaska Range: Geosphere, v. 8, no. 1, p. 196–205, https://doi. org/10.1130/GES00695.1.
- Bemis, S.P., Weldon, R.J., and Carver, G.A., 2015, Slip partitioning along a continuously curved fault: Quaternary geologic controls on Denali fault system slip partitioning, growth of the Alaska Range, and the tectonics of south-central Alaska: Lithosphere, v. 7, no. 3, p. 235–246, https://doi.org/10.1130/L352.1.
- Benowitz, J.A., Layer, P.W., Armstrong, P., Perry, S.E., Haeussler, P.J., Fitzgerald, P.G., and Vanlaningham, S., 2011, Spatial variations in focused exhumation along a continental-scale strike-slip fault: The Denali fault of the eastern Alaska Range: Geosphere, v. 7, no. 2, p. 455–467, https://doi.org/10.1130/GES00589.1.
- Benowitz, J.A., Haeussler, P.J., Layer, P.W., O'Sullivan, P.B., Wallace, W.K., and Gillis, R.J., 2012, Cenozoic tectono-thermal history of the Tordrillo Mountains, Alaska: Paleocene-Eocene ridge subduction, decreasing relief, and late Neogene faulting: Geochemistry Geophysics Geosystems, v. 13, p. 1–22, https://doi .org/10.1029/2011GC003951.
- Benowitz, J.A., Layer, P.W., and Vanlaningham, S., 2014, Persistent long-term (c. 24 Ma) exhumation in the Eastern Alaska Range constrained by stacked thermochronology, in Jordan, F., Mark, D.F., and Verati, C., eds, Advances in 40 Arr/39 Ar Dating: from Archaeology to Planetary Sciences: Geological Society, London, Special Publication 378, p. 225–243, https://doi .org/10.1144/SP378.12.
- Benowitz, J.A., Layer, P.W., Wypych, A., and Twelker, E., 2017, <sup>40</sup>Ar/<sup>59</sup>Ar data from rocks collected in the 2015 Wrangellia mineral assessment project area, Mount Hayes A-5, Mount Hayes B-6, and Talkeetna Mountains D-2 quadrangles, Alaska: Alaska Division of Geological and Geophysical Surveys Raw Data File 2017–1, p. 9, https://doi.org/10.14509/29699.
- Benowitz, J.A., Davis, K., and Roeske, S., 2019, A river runs through it both ways across time: <sup>40</sup>Ar/<sup>39</sup>Ar detrital and bedrock muscovite geochronology constraints on the Neogene paleodrainage history of the Nenana River system, Alaska Range: Geosphere, v. 15, no. 3, p. 682–701, https://doi.org/10.1130/GES01673.1.
- Beranek, L.P., van Staal, C.R., McClelland, W.C., Israel, S., and Mihalynuk, M.G., 2013, Detrital zircon Hf isotopic compositions indicate a northern Caledonian connection for the Alexander terrane: Lithosphere, v. 5, no. 2, p. 163–168. https://doi.org/10.1130/L255.1.
- Beranek, L.P., van Staal, C.R., McClelland, W.C., Joyce, N., and Israel, S., 2014, Late Paleozoic assembly of the Alexander-Wrangellia-Peninsular composite terrane, Canadian and Alaskan Cordillera: Geological Society of America Bulletin, v. 126, no. 11–12, p. 1531–1550, https://doi.org/10.1130/31066.1.
- Beranek, L.P., McClelland, W.C., van Staal, C.R., Israel, S., and Gordee, S.M., 2017, Late Jurassic flare-up of the Coast Mountains arc system, NW Canada, and dynamic linkages across the northern Cordilleran orogen: Tectonics, v. 36, no. 5, p. 877–901, https://doi .org/10.1002/2016TC004254.
- Berg, E.M., Lin, F.C., Allam, A., Schulte-Pelkum, V., Ward, K.M. and Shen, W., 2020, Shear velocity model of Alaska via joint inversion of Rayleigh Wave ellipticity, phase velocities, and receiver functions across the Alaska transportable array: Journal of Geophysical Research: Solid Earth, v. 125, no. 2, e2019JB018582.
- Berkelhammer, S.E., Brueseke, M.E., Benowitz, J.A., Trop, J.M., Davis, K., Layer, P.W., and Weber, M., 2019, Geochemical and geochronological records of tectonic changes along a flat-slab arc-transform junction:

- Circa 30 Ma to ca. 19 Ma Sonya Creek volcanic field, Wrangell Arc, Alaska: Geosphere, v. 15, no. 5, p. 1508–1538, https://doi.org/10.1130/GES02114.1.
- Bill, N.S., Mix, H.T., Clark, P.U., Reilly, S.P., Jensen, B.J., and Benowitz, J.A., 2018, A stable isotope record of Late Cenozoic surface uplift of southern Alaska: Earth and Planetary Science Letters, v. 482, p. 300–311, https://doi.org/10.1016/j.epsl.2017.11.029.
- Bittenbender, P.E., Bean, K.W., Kurtak, J.M., and Deininger, J., 2007, Mineral assessment of the Delta River mining district area, east-central Alaska: U.S. Bureau of Land Management Alaska Technical Report 57, 697 p.
- Bond, G.C., 1973, A late Paleozoic volcanic arc in the eastern Alaska Range, Alaska: The Journal of Geology, v. 81, p. 575–576, https://doi.org/10.1086/627907.
- Bond, G.C., 1976, Geology of the Rainbow Mountain-Gulkana Glacier Area, Eastern Alaska Range, with Emphasis on Upper Paleozoic Strata: State of Alaska Geologic Division of Geological and Geophysical Surveys Geologic Report 45, scale 1:40:000, 3 sheets, 47 p.
- Box, S.E., Karl, S.M., Jones, J.V., Bradley, D.C., Haeussler, P.J., and O'Sullivan, P.B., 2019, Detrital zircon geochronology along a structural transect across the Kahiltna assemblage in the western Alaska Range: Implications for emplacement of the Alexander-Wrangellia-Peninsular terrane against North America: Geosphere, v. 15, no. 6, p. 1774–1808, https://doi.org/10.1130/GES02060.1.
- Brennan, P.R.K., Gilbert, H., and Ridgway, K.D., 2011, Crustal structure across the central Alaska Range: Anatomy of a Mesozoic collisional zone: Geochemistry Geophysics Geosystems, v. 12, no. 4, Q04010, https:// doi.org/10.1029/2011GC003519.
- Brennan, P.R.K., and Ridgway, K.D., 2015, Detrital zircon record of Neogene exhumation of the central Alaska Range: A far-field upper plate response to flat-slab subduction: Geological Society of America Bulletin, v. 127, no. 7–8, p. 945–961, https://doi.org/10.1130/B31164.1.
- Brueseke, M.E., Benowitz, J.A., Trop, J.M., Davis, K.N., Berkelhammer, S.E., Layer, P.W., and Morter, B.K., 2019, The Alaska Wrangell Arc: -30 Ma of subductionrelated magmatism along a still active arc-transform junction: Terra Nova, v. 31, no. 1, p. 59-66.
- Bruhn, R.L., Pavlis, T.L., Plafker, G., and Serpa, L., 2004, Deformation during terrane accretion in the Saint Elias orogen, Alaska: Geological Society of America Bulletin, v. 116, no. 7–8, p. 771–787, https://doi.org/10.1130/B25182.1.
- Burkett, C.A., Bemis, S.P., and Benowitz, J.A., 2016, Along-fault migration of the Mount McKinley restraining bend of the Denali fault defined by late Quaternary fault patterns and seismicity, Denali National Park and Preserve, Alaska: Tectonophysics, v. 693, p. 489–506, https://doi.org/10.1016/j.tecto.2016.05.009.
- Burns, L.E., U.S. Bureau of Land Management, Fugro Airborne Surveys, and Stevens Exploration Management Corp, 2003, Total magnetic field and detailed electromagnetic anomalies of the southern Delta River area, east-central Alaska, parts of Mt. Hayes A-3, A-4, B-3, and B-4 quadrangles, in Burns, L.E., U.S. Bureau of Land Management, Fugro Airborne Surveys, and Stevens Exploration Management Corp., Plot files of the airborne geophysical survey data of the southern Delta River area, east-central Alaska: Alaska Division of Geological and Geophysical Surveys Geophysical Report 2003–5-2C, scale 1:31,680, 1 sheet, http://doi.org/10.14509/3219.
- Cavazza, W., Albino, I., Zattin, M., Galoyan, G., Imamverdiyev, N., and Melkonyan, R., 2017, Thermochronometric evidence for Miocene tectonic reactivation of the Sevan–Akera suture zone (Lesser Caucasus): A far-field tectonic effect of the Arabia–Eurasia collision?, in Sosson, M., Stephenson, R.A., and Adamia, S.A., eds., Tectonic Evolution of the Eastern Black Sea and Caucasus: Geological Society, London, Special Publication 428, no. 1, p. 187–198, https://doi.org/10.1144/SP428.4.
- Colpron, M., and Nelson, J.L., 2011, A Digital Atlas of Terranes for the Northern Cordillera: British Columbia Ministry of Energy and Mines, British Columbia Geological Survey GeoFile 2011-11.
- Colpron, M., Nelson, J.L., and Murphy, D.C., 2007, Northern Cordilleran terranes and their interactions through time: GSA Today, v. 17, no. 4/5, p. 4, https://doi.org/10.1130/ GSAT01704-5A.1.

- Coney, P.J., Jones, D.L., and Monger, J.W., 1980, Cordilleran suspect terranes: Nature, v. 288, no. 5789, p. 329, https://doi.org/10.1038/288329a0.
- Csejtey, B., Cox, D.P., Evarts, R.C., Stricker, G.D., and Foster, H.L., 1982, The Cenozoic Denali fault system and the Cretaceous accretionary development of southern Alaska: Journal of Geophysical Research: Solid Earth, v. 87, no. B5, p. 3741–3754, https://doi.org/10.1029/JB087iB05p03741.
- Csejtey, B., Mullen, M.W., Cox, D.P., Gilbert, W.G., Yeend, W.E., Smith, T.E., Wahrhaftig, C., Craddock, C., Brewer, W.M., Sherwood, K.W., Hickman, R.G., Stricker, G.D., St. Aubin, D.R., and Goerz, D.J., III, 1986, Geology and geochronology of the Healy Quadrangle, Alaska: U.S. Geological Survey Open-File Report 86-396, scale 1:250.000. 4 sheets, 92 p.
- 396, scale 1:250,000, 4 sheets, 92 p.
  Davidson, C., and McPhillips, D., 2007, Along strike variations in metamorphism and deformation of the strata of the Kahiltna basin, south-central Alaska, *in* Ridgway, K.D., Trop, J.M., Glen, J.M.G., and O'Neill, M.O., eds., Tectonic Growth of a Collisional Continental Margin: Crustal Evolution of Southern Alaska: Geological Society of America Special Paper 431, p. 439–453, https://doi.org/10.1130/2007.2431(17).
- Davidson, C., Hollister, L.S., and Schmid, S.M., 1992, Role of Melt in the Formation of a Deep-crustal Compressive Shear zone: The Maclaren Glacier Metamorphic Belt, south central Alaska: Tectonics, v. 11, no. 2, p. 348– 359, https://doi.org/10.1029/91TC02907.
- Day, E.M., Pavlis, T.L., and Amato, J.M., 2016, Detrital zircon ages indicate an Early Cretaceous episode of blueschist-facies metamorphism in southern Alaska: Implications for the Mesozoic paleogeography of the northern Cordillera: Lithosphere, v. 8, no. 5, p. 451– 462, https://doi.org/10.1130/L525.1.
- Decker, J., Bergman, S.C., Blodgett, R.B., Box, S.E., Bundtzen, T.K., Clough, J.G., Coonrad, W.L., Gilbert, W.G., Miller, M.L., Murphy, J.M., Robinson, M.S., and Wallace, W.K., 1994, Geology of southwestern Alaska, in Plafker, G., and Berg, H.C., eds., The Geology of Alaska: Boulder, Colorado, Geological Society of America, Geology of North America, v. G-1, p. 285–310, https://doi.org/10.1130/DNAG-GNA-G1.285.
- Dewey, J.F., 1977, Suture zone complexities: A review: Tectonophysics, v. 40, no. 1, p. 53–67, https://doi.org/10.1016/0040-1951(77)90029-4.
- Dewey, J.F., and Burke, K.C., 1973, Tibetan, Variscan, and Precambrian basement reactivation: Products of continental collision: The Journal of Geology, v. 81, no. 6, p. 683–692, https://doi.org/10.1086/627920.
- Doser, D.I., 2004, Seismicity of the Denali-Totschunda fault zone in central Alaska (1912–1988) and its relation to the 2002 Denali fault earthquake sequence: Bulletin of the Seismological Society of America, v. 94, p. 132– 144, https://doi.org/10.1785/0120040611.
- Dusel-Bacon, C., and Williams, I.S., 2009, Evidence for prolonged mid-Paleozoic plutonism and ages of crustal sources in east-central Alaska from SHRIMP U-Pb dating of syn-magmatic, inherited, and detrital zircon: Canadian Journal of Earth Sciences, v. 46, no. 1, p. 21–39, https://doi.org/10.1139/E09-005.
- Dusel-Bacon, C., Lanphere, M.A., Sharp, W.D., Layer, P.W., and Hansen, V.L., 2002, Mesozoic thermal history and timing of structural events for the Yukon-Tanana Upland, east-central Alaska: 40Ar/39Ar data from metamorphic and plutonic rocks: Canadian Journal of Earth Sciences, v. 39, no. 6, p. 1013–1051, https://doi.org/10.1139/e02-018.
- Dusel-Bacon, C., Bacon, C.R., O'Sullivan, P.B., and Day, W.C., 2016, Apatite fission-track evidence for regional exhumation in the subtropical Eocene, block faulting, and localized fluid flow in east-central Alaska: Canadian Journal of Earth Sciences, v. 53, no. 3, p. 260–280, https://doi.org/10.1139/cies-2015-0138.
- https://doi.org/10.1139/cjes-2015-0138.

  Dusel-Bacon, C., Holm-Denoma, C.S., Jones, J.V., Aleini-koff, J.N., and Mortensen, J.K., 2017, Detrital zircon geochronology of quartzose metasedimentary rocks from parautochthonous North America, east-central Alaska: Lithosphere, v. 9, no. 6, p. 927–952, https://doi.org/10.1130/L672.1.
- Eberhart-Phillips, D., Haeussler, P.J., Freymueller, J.T., Frankel, A.D., Rubin, C.M., Craw, P., Ratchkovski, N.A., Anderson, G., Carver, G.A., Crone, A.J., Daw-

- son, T.E., Fletcher, H., Hansen, R., Harp, E.L., et al., 2003, The 2002 Denali fault earthquake, Alaska: A large magnitude, slip-partitioned event: Science, v. 300, p. 1113–1118, https://doi.org/10.1126/science.1082703.
- Eisbacher, G.H., 1976, Sedimentology of the Dezadeash flysch and its implications for strike-slip faulting along the Denali fault, Yukon Territory and Alaska: Canadian Journal of Earth Sciences, v. 13, no. 11, p. 1495–1513, https://doi.org/10.1139/e76-157.
- Enkelmann, E., Garver, J.I., and Pavlis, T.L., 2008, Rapid exhumation of ice-covered rocks of the Chugach–St. Elias orogen, Southeast Alaska: Geology, v. 36, p. 915–918, https://doi.org/10.1130/G2252A.1.
- Enkelmann, E., Zeitler, P.K., Garver, J.I., Pavlis, T.L., and Hooks, B.P., 2010, The thermochronological record of tectonic and surface process interaction at the Yakutat–North American collision zone in southeast Alaska: American Journal of Science, v. 310, no. 4, p. 231–260, https://doi.org/10.2475/04.2010.01.
- Feng, L., and Ritzwoller, M.H., 2019, A 3-D shear velocity model of the crust and uppermost mantle beneath Alaska including apparent radial anisotropy: Journal of Geophysical Research: Solid Earth, v. 124, no. 10, p. 10468–10497, https://doi.org/10.1029/2019JB018122.
- Finzel, E.S., Ridgway, K.D., and Trop, J.M., 2015, Provenance signature of changing plate boundary conditions along a convergent margin: Detrital record of spreading-ridge and flat-slab subduction processes, Cenozoic foreare basins, Alaska: Geosphere, v. 11, no. 3, p. 823–849, https://doi.org/10.1130/GES01029.1.
- Finzel, E.S., Enkelmann, E., Falkowski, S., and Hedeen, T., 2016, Long-term fore-arc basin evolution in response to changing subduction styles in southern Alaska: Tectonics, v. 35, no. 7, p. 1735–1759, https://doi. org/10.1002/2016TC004171.
- Finzel, E.S., Trop, J.M., Ridgway, K.D., and Enkelmann, E., 2011, Upper plate proxies for flat-slab subduction processes in southern Alaska: Earth and Planetary Science Letters, v. 303, p. 348–360, https://doi.org/10.1016/ j.epsl.2011.01.014.
- Fitzgerald, P.F., Sorkhabi, R.B., Redfield, T.F., and Stump, E., 1995, Uplift and denudation of the central Alaska Range: A case study in the use of apatite fission track thermochronology to determine absolute uplift parameters: Journal of Geophysical Research: Solid Earth, v. 100, p. 20,175–20,191.
- Fitzgerald, P.G., Stump, E., and Redfield, T.E., 1993, Late Cenozoic uplift of Denali and its relation to relative plate motion and fault morphology: Science, v. 259, p. 497–499, https://doi.org/10.1126/science.259.5094.497.
- Forbes, R.B., Smith, T.E., and Turner, D.L., 1974, Comparative petrology and structure of the Maclaren, Ruby Range, and Coast Range belts: Implications for offset along the Denali fault system: Geological Society of America Abstracts with Programs, v. 6, p. 177.
- Freymueller, J.T., Cohen, S.C., Cross, R., Elliott, J., Fletcher, H., Larsen, C., Hreinsdóttir, S., and Zweck, C., 2008, Active deformation processes in Alaska, based on 15 years of GPS measurements, in Freymueller, J.T., Haeussler, P.J., Wesson, R.L., and Ekström,G., eds., Active Tectonics and Seismic Potential of Alaska: Washington, D.C., American Geophysical Union, p. 1–42, https://doi.org/10.1029/GM179.
- Gardner, M.C., Bergman, S.C., Cushing, G.W., MacKevett, E.M., Jr., Plafker, G., Campbell, R.B., Dodds, C.J., McClelland, W.C., and Mueller, P.A., 1988, Pennsylvanian pluton stitching of Wrangellia and the Alexander Terrane, Wrangell Mountains, Alaska: Geology, v. 16, no. 11, p. 967–971, https://doi.org/10.1130/0091-7613(1988)016<0967:PPSOWA>2.3.CO;2.
- Gehrels, G., and Pecha, M., 2014, Detrital zircon U-Pb geochronology and Hf isotope geochemistry of Paleozoic and Triassic passive margin strata of western North America: Geosphere, v. 10, no. 1, p. 49–65, https://doi. org/10.1130/GES00889.1.
- Gehrels, G.E., Butler, R.F., and Bazard, D.R., 1996, Detrital zircon geochronology of the Alexander terrane, southeastern Alaska: Geological Society of America Bulletin, v. 108, no. 6, p. 722–734, https://doi.org/10.1130/0016-7606(1996)108

- Gehrels, G., Rusmore, M., Woodsworth, G., Crawford, M., Andronicos, C., Hollister, L., Patchett, J., Ducea, M., Butler, R., Klepeis, K., and Davidson, C., 2009, U-Th-Pb geochronology of the Coast Mountains batholith in north-coastal British Columbia: Constraints on age and tectonic evolution: Geological Society of America Bulletin, v. 121, no. 9–10, p. 1341–1361, https://doi. org/10.1130/B26404.1.
- Gilman, T., Feineman, M., and Fisher, D., 2009, The Chulitna terrane of south-central Alaska: A rifted volcanic arc caught between the Wrangellia composite terrane and the Mesozoic margin of North America: Geological Society of America Bulletin, v. 121, no. 7–8, p. 979–991, https://doi.org/10.1130/B26400.1.
- Glen, J.M.G., 2004, A kinematic model for the southern Alaska orocline based on regional fault patterns, in Sussman, A. and Weil, A.B., eds., Orogenic Curvature: Geological Society of America Special Paper 383, p. 161–172, https://doi.org/10.1130/0-8137-2383-3(2004)383[161:AKMFTS]2.0.CO;2.
- Glen, J.M.G., Schmidt, J., Pellerin, L., McPhee, D.K., and O'Neill, J.M., 2007, Crustal structure of Wrangellia and adjacent terranes inferred from geophysical studies along a transect through the northern Talkeetna Mountains, in Ridgway, K.D., Trop, J.M., Glen, J.M.G., and O'Neill, M.O., eds., Tectonic Growth of a Collisional Continental Margin: Crustal Evolution of Southern Alaska: Geological Society of America Special Paper 431, p. 21–41, https://doi.org/10.1130/2007.2431(02).
- Goussin, F., Riel, N., Cordier, C., Guillot, S., Boulvais, P., Roperch, P., Replumaz, A., Schulmann, K., Dupont-Nivet, G., Rosas, F. and Guo, Z., 2020, Carbonated inheritance in the Eastern Tibetan lithospheric mantle: Petrological evidences and geodynamic implications: Geochemistry, Geophysics, Geosystems, v. 21, e2019GC008495.
- Greene, A.R., Scoates, J.S., and Weiss, D., 2008, Wrangellia flood basalts in Alaska: A record of plume-lithosphere interaction in a Late Triassic accreted oceanic plateau: Geochemistry Geophysics Geosystems, v. 9, https://doi. org/10.1029/2008GC002092.
- Greene, A.R., Scoates, J.S., Weis, D., Katvala, E.C., Israel, S., and Nixon, G.T., 2010, The architecture of oceanic plateaus revealed by the volcanic stratigraphy of the accreted Wrangellia oceanic plateau: Geosphere, v. 6, no. 1, p. 47–73, https://doi.org/10.1130/GES00212.1.
- Haeussler, P.J., 1992, Structural evolution of an arc-basin: The Gravina Belt in central southeastern Alaska: Tectonics, v. 11, no. 6, p. 1245–1265, https://doi.org/10.1029/92TC01107.
- Haeussler, P.J., O'Sullivan, P., Berger, A.L., and Spotila, J.A., 2008, Neogene exhumation of the Tordrillo Mountains, Alaska, and correlations with Denali (Mount McKinley), in Freymueller, J.T., Haeussler, P.J., Wesson, R.L., and Ekström, G., eds., Active Tectonics and Seismic Potential of Alaska: Washington, D.C., American Geophysical Union Monograph 179, p. 269–285, doi: https://doi.org/10.1029/179GM15.
- Haeussler, P.J., Saltus, R.W., Stanley, R.G., Ruppert, N., Lewis, K., Karl, S.M., and Bender, A., 2017a, The Peters Hills basin, a Neogene wedge-top basin on the Broad Pass thrust fault, south-central Alaska: Geosphere, v. 13, p. 1464–1488, https://doi.org/10.1130/ GFS01487.1.
- Haeussler, P.J., Matmon, A., Schwartz, D.P., and Seitz, G.G., 2017b, Neotectonics of interior Alaska and the late Quaternary slip rate along the Denali fault system: Geosphere, v. 13, p. 1445–1463, https://doi.org/10.1130/ GFS01447 1
- Hampton, B.A., Ridgway, K.D., O'Neill, J.M., Gehrels, G.E., Schmidt, J., and Blodgett, R.B., 2007, Pre-, syn-, and postcollisional stratigraphic framework and provenance of Upper Triassic-Upper Cretaceous strata in the northwestern Talkeetna Mountains, Alaska, in Ridgway, K.D., Trop, J.M., Glen, J.M.G., and O'Neill, M.O., eds., Tectonic Growth of a Collisional Continental Margin: Crustal Evolution of Southern Alaska: Geological Society of America Special Paper 431, p. 401–438, https:// doi.org/10.1130/2007.2431(16).
- Hampton, B.A., Ridgway, K.D., and Gehrels, G.E., 2010, A detrital record of Mesozoic island are accretion and exhumation in the North American Cordillera: U-Pb geochronology of the Kahiltna basin,

- southern Alaska: Tectonics, v. 29, TC4015, https://doi.org/10.1029/2009TC002544.
- Harrison, T.M., Duncan, I., and McDougall, I., 1985, Diffusion of <sup>40</sup>Ar in biotite: Temperature, pressure and compositional effects: Geochimica et Cosmochimica Acta, v. 49, no. 11, p. 2461–2468, https://doi.org/10.1016/0016-7037(85)90246-7.
- Harrison, T.M., Célérier, J., Aikman, A.B., Hermann, J., and Heizler, M.T., 2009, Diffusion of <sup>40</sup>Ar in muscovite: Geochimica et Cosmochimica Acta, v. 73, p. 1039– 1051, https://doi.org/10.1016/j.gca.2008.09.038.
- Haynie, K.L., and Jadamec, M.A., 2017, Tectonic drivers of the Wrangell block: Insights on fore-arc sliver processes from 3-D geodynamic models of Alaska: Tectonics, v. 36, no. 7, p. 1180–1206, https://doi.org/10.1002/2016TC004410.
- Heron, P.J., Pysklywec, R.N., and Stephenson, R., 2016, Lasting mantle scars lead to perennial plate tectonics: Nature Communications, v. 7, article no. 11834, https://doi.org/10.1038/ncomms11834.
- Herriott, T.M., Crowley, J.L., Schmitz, M.D., Wartes, M.A., and Gillis, R.J., 2019, Exploring the law of detrital zircon: LA-ICP-MS and CA-TIMS geochronology of Jurassic forearc strata, Cook Inlet, Alaska, USA: Geology, v. 47, no. 11, p. 1044–1048, https://doi.org/10.1130/G46312.1.
- Himmelberg, G.R., and Loney, R.A., 1995, Characteristics and petrogenesis of Alaskan-type ultramafic-mafic intrusions, southeastern Alaska: U.S. Geological Survey Professional Paper 1564, https://doi.org/10.3133/ pp1564.
- Hodges, K.V., 2014, Thermochronology in orogenic systems, in Holland, H.D., and Turekian, K.K., eds., Treatise on Geochemistry, Second Edition: Elsevier, p. 281–308.
- Hollister, L.S., 1993, The role of melt in the uplift and exhumation of orogenic belts: Chemical Geology, v. 108, no. 1–4, p. 31–48, https://doi.org/10.1016/0009-2541(93)90316-B.
- Horstwood, M.S., Košler, J., Gehrels, G., Jackson, S.E., McLean, N.M., Paton, C., Pearson, N.J., Sircombe, K., Sylvester, P., Vermeesch, P., and Bowring, J.F., 2016, Community-derived standards for LA-ICP-MS U-(Th-) Pb geochronology–Uncertainty propagation, age interpretation and data reporting: Geostandards and Geoanalytical Research, v. 40, no. 3, p. 311–332, https://doi .org/10.1111/j.1751-908X.2016.00379.x.
- Hoskin, P.W., and Schaltegger, U., 2003, The composition of zircon and igneous and metamorphic petrogenesis: Reviews in Mineralogy and Geochemistry, v. 53, no. 1, p. 27–62.
- Huff, C.J., 2012, Paleozoic to Neogene stratigraphic and structural history of the Alaska Range suture zone, north of the Denali fault, east central Alaska Range [M.S. thesis]: Davis, University of California, 149 p.
- Hults, C.P., Wilson, F.H., Donelick, R.A., and O'Sullivan, P.B., 2013, Two flysch belts having distinctly different provenance suggest no stratigraphic link between the Wrangellia composite terrane and the paleo-Alaskan margin: Lithosphere, v. 5, no. 6, p. 575–594, https:// doi.org/10.1130/L310.1.
- Israel, S., Beranek, L., Friedman, R.M., and Crowley, J.L., 2014. New ties between the Alexander terrane and Wrangellia and implication for North America Cordilleran evolution: Lithosphere, v. 6, no. 4, p. 270–276, https://doi.org/10.1130/L364.1.
- Jadamec, M.A., Billen, M.I., and Roeske, S.M., 2013, Threedimensional numerical models of flat slab subduction and the Denali fault driving deformation in south-central Alaska: Earth and Planetary Science Letters, v. 376, p. 29–42, https://doi.org/10.1016/j.epsl.2013.06.009.
- Jones, D.L., Silberling, N.J., and Hillhouse, J., 1977, Wrangellia—A displaced terrane in northwestern North America: Canadian Journal of Earth Sciences, v. 14, no. 11, p. 2565–2577, https://doi.org/10.1139/e77-222.
- Jones, D.S., Barnes, C.G., Premo, W.R., and Snoke, A.W., 2013, Reactivation of the Archean-Proterozoic suture along the southern margin of Laurentia during the Mazatzal orogeny: Petrogenesis and tectonic implications of ca. 1.63 Ga granite in southeastern Wyoming: Geological Society of America Bulletin, v. 125, no. 1–2, p. 164–183, https://doi.org/10.1130/B30577.1.
- Kalbas, J.L., Ridgway, K.D., and Gehrels, G.E., 2007, Stratigraphy, depositional systems, and provenance of the Lower Cretaceous Kahiltna assemblage, west-

- ern Alaska Range: Basin development in response to oblique collision, *in* Ridgway, K.D., Trop, J.M., Glen, J.M.G., and O'Neill, M.O., eds., Tectonic Growth of a Collisional Continental Margin: Crustal Evolution of Southern Alaska: Geological Society of America Special Paper 431, 307–343, doi: https://doi.org/10.1130/2007.2431(13).
- Kapp, P.A., and Gehrels, G.E., 1998, Detrital zircon constraints on the tectonic evolution of the Gravina belt, southeastern Alaska: Canadian Journal of Earth Sciences, v. 35, no. 3, p. 253–268, https://doi.org/10.1139/e97-110.
- Kelly, S., Beaumont, C., and Butler, J.P., 2020, Inherited terrane properties explain enigmatic post-collisional Himalayan-Tibetan evolution: Geology, v. 48, no. 1, p. 8–14, https://doi.org/10.1130/G46701.1.
- Koehler, R.D., 2013, Quaternary Faults and Folds (QFF), Alaska Division of Geological and Geophysical Surveys Digital Data Series 3, http://doi.org/10.14509/ qff, http://doi.org/10.14509/249566.
- Kreemer, C., Blewitt, G., and Klein, E.C., 2014, A geodetic plate motion and Global Strain Rate Model: Geochemistry Geophysics Geosystems, v. 15, no. 10, p. 3849– 3889, https://doi.org/10.1002/2014GC005407.
- Kunk, M.J., 1995, 40Ar Age-spectrum data for Horn-blende, Plagioclase and Biotite from tephras collected at Dan Creek and McCallum Creek, Alaska and in the Klondike Placer District Near Dawson, Yukon Territory: U.S. Geological Survey Open-File Report 95–217 h, 52 p.
  Layer, P.W., Hall, C.M., and York, D., 1987, The derivation
- Layer, P.W., Hall, C.M., and York, D., 1987, The derivation of <sup>40</sup>Ar/<sup>39</sup>Ar age spectra of single grains of hornblende and biotite by laser step heating: Geophysical Research Letters, v. 14, p. 757–760, https://doi.org/10.1029/ GL014i007p00757.
- Lease, R.O., 2018, Pliocene erosional pulse and glacier-landscape feedbacks in the western Alaska Range: Earth and Planetary Science Letters, v. 497, p. 62–68, https://doi .org/10.1016/j.epsl.2018.06.009.
- Lease, R.O., Haeussler, P.J., and O'Sullivan, P.B., 2016, Changing exhumation patterns during Cenozoic growth and glaciation of the Alaska Range: Insights from detrital thermochronology and geochronology: Tectonics, v. 35, p. 934–955, https://doi .org/10.1002/2015TC004067.
- Link, B.J., 2017, From deposition to deformation within an accretionary suture zone: An example from the Clearwater and Talkeetna Mountains, Alaska Range Suture Zone [M.S. thesis]: West Lafayette, Indiana, Purdue University, 55 p.
- Lowey, G.W., 1998, A new estimate of the amount of displacement on the Denali fault system based on the occurrence of carbonate megaboulders in the Dezadeash Formation (Jura-Cretaceous), Yukon, and the Nutzotin Mountains sequence (Jura-Cretaceous), Alaska: Bulletin of Canadian Petroleum Geology, v. 46, no. 3, p. 379–386.
- Lowey, G.W., 2011, Volcaniclastic gravity flow deposits in the Dezadeash Formation (Jura-Cretaceous), Yukon, Canada: Implications regarding the tectonomagmatic evolution of the Chitina arc in the northern Cordillera of North America: Lithos, v. 125, no. 1–2, p. 86–100, https://doi.org/10.1016/j.lithos.2011.0.114.
- Lowey, G.W., 2019, Provenance analysis of the Dezadeash Formation (Jurassic–Cretaceous), Yukon, Canada: Implications regarding a linkage between the Wrangellia composite terrane and the western margin of Laurasia: Canadian Journal of Earth Sciences, v. 56, no. 1, p. 77–100, https://doi.org/10.1139/cjes-2017-0244.
- Ludwig, K., 2008, Isoplot 3.6: Berkeley Geochronology Center Special Publication 4, 77 p.
- Manuszak, J.D., Ridgway, K.D., Trop, J.M., and Gehrels, G.E., 2007, Sedimentary record of the tectonic growth of a collisional continental margin: Upper Jurassic–Lower Cretaceous Nutzotin Mountains sequence, eastern Alaska Range, Alaska, in Ridgway, K.D., Trop, J.M., Glen, J.M.G., and O'Neill, M.O., eds., Tectonic Growth of a Collisional Continental Margin: Crustal Evolution of Southern Alaska: Geological Society of America Special Paper 431, p. 345–377, https://doi.org/10.1130/2007.2431(14).
- Matmon, A., Schwartz, D.P., Haeussler, P.J., Finkel, R., Lienkaemper, J.J., Stenner, H.D., and Dawson, T.E., 2006, Denali fault slip rates and Holocene-late Pleistocene ki-

- nematics of central Alaska: Geology, v. 34, p. 645–648, https://doi.org/10.1130/G22361.1.
- McClelland, W.C., Gehrels, G.E., Samson, S.D., and Patchett, P.J., 1992, Protolith relations of the Gravina belt and Yukon-Tanana terrane in central southeastern Alaska: The Journal of Geology, v. 100, no. 1, p. 107–123, https://doi.org/10.1086/629574.
- Mendenhall, W.C., 1905, Geology of the central Copper River region, Alaska (No. 41): U.S. Geological Survey Professional Paper 41, 133 p.
- Mériaux, A.-S., Sieh, K., Finkel, R.C., Rubin, C.M., Taylor, M.H., Meltzner, A.J., and Ryerson, F.J., 2009, Kinematic behavior of southern Alaska constrained by westward decreasing postglacial slip rates on the Denali Fault, Alaska: Journal of Geophysical Research: Solid Earth, v. 114, B03404, https://doi.org/10.1029/2007JB005053.
- Miller, M.S., and Moresi, L., 2018, Mapping the Alaskan Moho: Seismological Research Letters, v. 89, no. 6, p. 2430–2436, https://doi.org/10.1785/0220180222.
- Miller, M.S., O'Driscoll, L.J., Porritt, R.W., and Roeske, S.M., 2018, Multiscale crustal architecture of Alaska inferred from P receiver functions: Lithosphere, v. 10, no. 2, p. 267–278, https://doi.org/10.1130/L701.1.
- Mitra, S., 1990, Fault-propagation folds: Geometry, kinematic evolution, and hydrocarbon traps: The American Association of Petroleum Geologists Bulletin, v. 74, p. 921–945.
- Moll-Stalcup, E.J., 1994, Latest Cretaceous and Cenozoic magmatic rocks of Alaska, in Plafker, G., and Berg, H.C., eds., The Geology of Alaska: Boulder, Colorado, Geological Society of America, p. 589–619, https://doi. org/10.1130/DNAG-GNA-G1.589.
- Monger, J.W.H., Price, R.A., and Tempelman-Kluit, D.J., 1982, Tectonic accretion and the origin of the two major metamorphic and plutonic welts in the Canadian Cordillera: Geology, v. 10, no. 2, p. 70–75, https://doi.org/10.1130/0091-7613(1982)10<70:TAATOO>2.0.
- Mooney, P.R., 2010, Geology of the Clearwater Mountains and southern boundary of the Alaska Range Suture Zone [M.S. thesis]: Davis, University of California, 93 p.
- Murphy, D.C., 2018, Latest Cretaceous-early Eocene Pacific-Arctic?—Atlantic connection: Co-evolution of strike-slip fault systems, oroclines, and transverse foldand-thrust belts in the northwestern North American Cordillera, in Piepjohn, K., Strauss, J.V., Reinhardt, L., and McClelland, W.C., eds., Circum-Arctic Structural Events: Tectonic Evolution of the Arctic Margins and Trans-Arctic Links with Adjacent Orogens: Geological Secretary of America Structural Events.
- Society of America Special Paper 541, 665 p.

  Nokleberg, W.J., and Richter, D.H., 2007, Origin of narrow terranes and adjacent major terranes occurring along the Denali fault in the Eastern and Central Alaska Range, Alaska, *in* Ridgway, K.D., Trop, J.M., Glen, J.M.G., and O'Neill, M.O., eds., Tectonic Growth of a Collisional Continental Margin: Crustal Evolution of Southern Alaska: Geological Society of America Special Paper 431, p. 129–154, https://doi.org/10.1130/2007.2431(06).
- Nokleberg, W.J., Jones, D.L., and Silberling, N.J., 1985, Origin and tectonic evolution of the Maclaren and Wrangellia terranes, eastern Alaska Range, Alaska: Geological Society of America Bulletin, v. 96, no. 10, p. 1251–1270, https://doi.org/10.1130/0016-7606(1985)96-1251:OATEOT>2.0.CO:2.
- Nokleberg, W.J., Aleinikoff, J.N., Lange, I.M., Silva, S.R., Miyaoka, R.T., Schwab, C.E., and Zehner, R.E., 1992a, Preliminary geologic map of the Mount Hayes quadrangle, eastern Alaska Range, Alaska: U.S. Geological Survey Open File Report 92–594, scale 1:250,000, 1 sheet, 39 p.
- Nokleberg, W.J., Aleinikoff, J.N., Dutro, J.T., Jr., Lanphere, M.A. Silberling, N.J., Silva, S.R., Smith, T.E., and Turner, D.L., 1992b, Map, tables, and summary of fossil and istopic age data, Mount Hayes quadrangle, eastern Alaska Range, Alaska: U.S. Geological Survey Miscellaneous Field Studies Map 1996-D, scale 1:250,000, 1 sheet, 43 p.
- Nokleberg, W.J., Aleinikoff, J.N., Bundtzen, T.K., and Hanshaw, M.N., 2013, Geologic strip map along the Hines Creek Fault showing evidence for Cenozoic displacement in the western Mount Haves and northeastern

- Healy quadrangles, eastern Alaska Range, Alaska: U.S. Geological Survey Scientific Investigations Map 3238, scale 1:63,360, 29 p., http://pubs.usgs.gov/sim/3238/.
- scale 1:63,360, 29 p., http://pubs.usgs.gov/sim/3238/.
  Nokleberg, W.J., Aleinikoff, J.N., Bond, G.C., Ferrians, O.J., Jr., Herzon, P.L., Lange, I.M., Miyaoka, R.T., Richter, D.H., Schwab, C.E., Silva, S.R., Smith, T.E., and Zehner, R.E., 2015, Geologic maps of the eastern Alaska Range, Alaska (44 quadrangles, 1:63,360 scale), with descriptions and interpretations of map units: Alaska Division of Geological and Geophysical Surveys Report of Investigation 2015-6, scale 1:63,360, 45 sheets, 64 p., https://doi.org/10.14509/29444.
- O'Driscoll, L.J., and Miller, M.S., 2015, Lithospheric discontinuity structure in Alaska, thickness variations determined by Sp receiver functions: Tectonics, v. 34, no. 4, p. 694–714, https://doi.org/10.1002/2014TC003669.
- O'Neill, M., Ridgway, K.D., and Eastham, K.R., 2001, Mesozoic sedimentation and deformation along the Talkeetna Thrust Fault, South-Central Alaska—New insights and their regional tectonic significance, in Galloway, J.P., ed., Studies by the U.S. Geological Survey in Alaska: U.S. Geological Survey Professional Paper 1678, 203 p.
- Pavlis, T.L., Chapman, J.B., Bruhn, R.L., Ridgway, K., Worthington, L.L., Gulick, S.P., and Spotila, J., 2012, Structure of the actively deforming fold-thrust belt of the St. Elias orogen with implications for glacial exhumation and three-dimensional tectonic processes: Geosphere, v. 8, no. 5, p. 991–1019, https://doi .org/10.1130/GES00753.1.
- Pecha, M.E., Gehrels, G.E., McClelland, W.C., Giesler, D., White, C., and Yokelson, I., 2016, Detrital zircon U-Pb geochronology and Hf isotope geochemistry of the Yukon-Tanana terrane, Coast Mountains, southeast Alaska: Geosphere, v. 12, no. 5, p. 1556–1574, https:// doi.org/10.1130/GES01303.1.
- Piercey, S.J., and Colpron, M., 2009, Composition and provenance of the Snowcap assemblage, basement to the Yukon-Tanana terrane, northern Cordillera: Implications for Cordilleran crustal growth: Geosphere, v. 5, no. 5, p. 439–464, https://doi.org/10.1130/GES00505.S3.
- Plafker, G., and Berg, H.C., 1994, The Geology of Alaska: Boulder, Colorado, Geological Society of America, 1068 p., https://doi.org/10.1130/DNAG-GNA-G1.
  Preece, S.J., and Hart, W.K., 2004. Geochemical variations
- Preece, S.J., and Hart, W.K., 2004, Geochemical variations in the <5 Ma Wrangell Volcanic Field, Alaska: Implications for the magmatic and tectonic development of a complex continental arc system: Tectonophysics, v. 392, no. 1–4, p. 165–191, https://doi.org/10.1016/ j.tecto.2004.04.011.
- Ranalli, G., 2000, Rheology of the crust and its role in tectonic reactivation: Journal of Geodynamics, v. 30, no. 1, p. 3–15, https://doi.org/10.1016/S0264-3707(99)00024-1.
- Rasendra, N., Bonnin, M., Mazzotti, S., and Tiberi, C., 2014, Crustal and upper-mantle anisotropy related to fossilized transpression fabric along the Denali Fault, northern Canadian Cordillera: Bulletin of the Seismological Society of America, v. 104, no. 4, p. 1964–1975, https:// doi.org/10.1785/0120130233.
- Regan, S.P., Benowitz, J.A., and Holland, M.E., 2020, A plutonic brother from another magma mother: Disproving the Eocene Foraker-McGonagall pluton piercing point and implications for long-term slip on the Denali Fault: Terra Nova, v. 32, p. 66–74, https://doi.org/10.1111/ter.12437.
- Renne, P.R., Deino, A.L., Walter, R.C., Turrin, B.D., Swisher, C.C., Becker, T.A., Curtis, G.H., Sharp, W.D., and Jaouni, A.R., 1994, Intercalibration of astronomical and radioisotopic time: Geology, v. 22, p. 783–786, https://doi.org/10.1130/0091-7613(1994)022<0783:IOAART >2.3.CO;2.
- Renne, P.R., Mundil, R., Balco, G., Min, K., and Ludwig, K.R., 2010, Joint determination of <sup>40</sup>K decay constants and <sup>40</sup>Ar\*/<sup>40</sup>K for the Fish Canyon sanidine standard, and improved accuracy for <sup>40</sup>Ar/<sup>59</sup>Ar geochronology: Geochimica et Cosmochimica Acta, v. 74, p. 5349, https://doi.org/10.1016/j.gca.2010.06.017.
- Riccio, S.J., Fitzgerald, P.G., Benowitz, J.A., and Roeske, S.M., 2014, The role of thrust faulting in the formation of the eastern Alaska Range: Thermochronological constraints from the Susitna Glacier Thrust Fault region of the intracontinental strike-slip Denali Fault

- $system:\ Tectonics,\ v.\ 33,\ p.\ 2195-2217,\ https://doi.org/10.1002/2014TC003646.$
- Richter, D.H., and Dutro, J.T., Jr., 1975, Revision of the type Mankommen Formation (Pennsylvanian and Permian), Eagle Creek area, eastern Alaska Range, Alaska: U.S. Geological Survey Bulletin, v. 1395-B, p. B1–B25.
- Richter, D.H., and Matson, J.A., 1971, Quaternary faulting in the eastern Alaska Range: Bulletin of the Geological Society of America, v. 82, p. 1529–1540, https:// doi.org/10.1130/0016-7606(1971)82[1529:QFITEA] 2.0 CO:2
- Richter, D.H., Smith, J.G., Lanphere, M.A., Dalrymple, G.B., Reed, B.L., and Shew, N., 1990, Age and progression of volcanism, Wrangell volcanic field, Alaska: Bulletin of Volcanology, v. 53, no. 1, p. 29–44, https:// doi.org/10.1007/BF00680318.
- Ridgway, K.D., Trop, J.M., Nokleberg, W.J., Davidson, C.M., and Eastham, K.R., 2002, Mesozoic and Cenozoic tectonics of the eastern and central Alaska Range: Progressive basin development and deformation in a suture zone: Bulletin of the Geological Society of America, v. 114, p. 1480–1504, https://doi.org/10.1130/0016-7606(2002)114<1480:MACTOT>2.0.CO;2.
- Ridgway, K.D., Thoms, E.E., Layer, P.W., Lesh, M.E., White, J.M., and Smith, S.V., 2007, Neogene transpressional foreland basin development on the north side of the central Alaska Range, Usibelli Group and Nenana Gravel, Tanana basin, in Ridgway, K.D., Trop, J.M., Glen, J.M.G., and O'Neill, M.O., eds., Tectonic Growth of a Collisional Continental Margin: Crustal Evolution of Southern Alaska: Geological Society of America Special Paper 431, p. 507–547, https://doi.org/10.1130/2007.2431(20).
- Rioux, M., Hacker, B., Mattinson, J., Kelemen, P., Blusztajn, J., and Gehrels, G., 2007, Magmatic development of an intra-oceanic are: High-precision U-Pb zircon and whole-rock isotopic analyses from the accreted Talkeetna arc, south-central Alaska: Geological Society of America Bulletin, v. 119, no. 9–10, p. 1168–1184, https://doi.org/10.1130/B25964.1.
- Roeske, S.M., Mattinson, J.M., and Armstrong, R.L., 1989, Isotopic ages of glaucophane schists on the Kodiak Islands, southern Alaska, and their implications for the Mesozoic tectonic history of the Border Ranges fault system: Geological Society of America Bulletin, v. 101, no. 8, p. 1021–1037, https://doi.org/10.1130/0016-7606(1989)101<1021:1AOGSO>2.3.CO;2.
- Roeske, S.M., Snee, L.W., and Pavlis, T.L., 2003, Dextral strike-slip reactivation of an arc-forearc boundary during Late Cretaceous-early Eocene oblique convergence in the northern Cordillera, in Sisson, V.B., Roeske, S.M., and Pavlis, T.L., eds., Geology of a Transpressional Orogen Developed during Ridge-Trench Interaction along the North Pacific Margin: Geological Society of America Special Paper 371, p. 141–170, https://doi .org/10.1130/0-8137-2371-X.141.
- Romero, M.C., Ridgway, K.D., and Gehrels, G.E., 2020, Geology, U-Pb geochronology, and Hf isotope geochemistry across the Mesozoic Alaska Range suture zone (south-central Alaska): Implications for Cordilleran collisional processes and tectonic growth of North America: Tectonics, v. 39, no. 3, e2019TC005946.
- Rose, A.W., 1965, Geology and mineral deposits of the Rainy Creek areas, Mt. Hayes Quadrangle, Alaska: Alaska Division of Mines and Minerals Geologic Report 14, scale 1:36,000, 1 sheet, 57 p., https://doi.org/10.14509/343.
- Rose, A.W., 1966, Geological and geochemical investigations in the Eureka Creek and Rainy Creek areas, Mt. Hayes Quadrangle, Alaska: Alaska Division of Mines and Minerals Geologic Report 20, scale 1:40,000, 3 sheets, 41 p., https://doi.org/10.14509/349.
  Rubin, C.M., and Saleeby, J.B., 1991, The Gravina se-
- Rubin, C.M., and Saleeby, J.B., 1991, The Gravina sequence: Remnants of a mid-Mesozoic oceanic arc in southern southeast Alaska: Journal of Geophysical Research: Solid Earth, v. 96, p. 14,551–14,568, https://doi.org/10.1029/91JB00591.
- Rubin, C.M., Saleeby, J.B., Cowan, D.S., Brandon, M.T., and McGroder, M.F., 1990, Regionally extensive mid-Cretaceous west-vergent thrust system in the northwestern Cordillera: Implications for continent-margin tectonism: Geology, v. 18, no. 3, p. 276–280, https:// doi.org/10.1130/0091-7613(1990)018<0276:REMCW V>2.3.CO;2.

- Ruppert, N.A., 2008, Stress map for Alaska from earthquake focal mechanisms, in Freymueller, J.T., Haeussler, P.J., Wesson, R., and Ekström, G., eds., Active Tectonics and Seismic Potential of Alaska: Washington, D.C., American Geophysical Union Geophysical Monograph Series, v. 179, p. 351–367.
- Rusmore, M.E., 1987, Geology of the Cadwallader Group and the Intermontane–Insular superterrane boundary, southwestern British Columbia: Canadian Journal of Earth Sciences, v. 24, no. 11, p. 2279–2291, https://doi .org/10.1139/e87-213.
- Saleeby, J.B., 1992, Age and tectonic setting of the Duke Island ultramafic intrusion, southeast Alaska: Canadian Journal of Earth Sciences, v. 29, no. 3, p. 506–522, https://doi.org/10.1139/e92-044.
- Saltus, R.W., and Hudson, T.L., 2007, Regional magnetic anomalies, crustal strength, and the location of the northern Cordilleran fold-and-thrust belt: Geology, v. 35, no. 6, p. 567–570, https://doi.org/10.1130/G23470A.1.
- Saltus, R.W., Hudson, T.L., and Wilson, F.H., 2007, The geophysical character of southern Alaska—Implications for crustal evolution, in Ridgway, K.D., Trop, J.M., Glen, J.M.G., and O'Neill, M.O., eds., Tectonic Growth of a Collisional Continental Margin: Crustal Evolution of Southern Alaska: Geological Society of America Special Paper 431, p. 1–20, https://doi .org/10.1130/2007.2431(01).
- Saltus, R.W., Stanley, R.G., Haeussler, P.J., Jones, J.V., III, Potter, C.J., and Lewis, K.A., 2016, Late Oligocene to present contractional structure in and around the Susitna basin, Alaska—Geophysical evidence and geological implications: Geosphere, v. 12, no. 5, p. 1378–1390, https://doi.org/10.1130/GES01279.1.
- Samson, S.D., and Alexander, E.C., 1987, Calibration of the interlaboratory <sup>40</sup>Ar/<sup>39</sup>Ar dating standard, MMhb1: Chemical Geology, v. 66, p. 27–34.
- Samson, S.D., Patchett, P.J., Gehrels, G.E., and Anderson, R.G., 1990, Nd and Sr isotopic characterization of the Wrangellia terrane and implications for crustal growth of the Canadian Cordillera: The Journal of Geology, v. 98, no. 5, p. 749–762, https://doi.org/10.1086/629438.
- Sibson, R.H., 1985, A note on fault reactivation: Journal of Structural Geology, v. 7, no. 6, p. 751–754, https://doi.org/10.1016/0191-8141(85)90150-6.
- Smith, J.G., and MacKevett, E.M., Jr., 1970, The Skolai Group in the McCarthy B-4, C-4, C-5 Quadrangles, Wrangell Mountains, Alaska: U.S. Geological Survey Bulletin, v. 1274-Q, p. Q1–Q26.
- Smith, T.E., 1981, Geology of the Clearwater Mountains, south-central Alaska: Alaska Division of Geological and Geophysical Surveys Geologic Report 60, scale 1:63,360, 3 sheets, 72 p., https://doi.org/10.14509/406.
- 1:63,360, 3 sheets, 72 p., https://doi.org/10.14509/406.
  Snyder, D.C., and Hart, W.K., 2007, The White Mountains
  Granitoid Suite: Isotopic constraints on source reservoirs for Cretaceous magmatism within the Wrangellia terrane, in Ridgway, K.D., Trop, J.M., Glen,
  J.M.G., and O'Neill, M.O., eds., Tectonic Growth
  of a Collisional Continental Margin: Crustal Evolution of Southern Alaska: Geological Society of
  America Special Paper 431, p. 379–399, https://doi.org/10.1130/2007.2431(15).
- St. Amand, P., 1957, Geological and geophysical synthesis of the tectonics of portions of British Columbia, the Yukon Territory, and Alaska: Geological Society of America Bulletin, v. 68, no. 10, p. 1343–1370, https://doi.org/10.1130/0016-7606(1957)68[1343:GAGSOT]2.0.CO;2.
- Stout, J.H., 1965, Bedrock Geology between Rainy Creek and the Denali fault, Eastern Alaska Range, Alaska [M.S. thesis]: Fairbanks, University of Alaska, 75 p.
- Stout, J.H., 1976, Geology of the Eureka Creek area, east-central Alaska Range: State of Alaska Department of Natural Resources, Division of Geological and Geophysical Surveys Geologic Report 46, scale 1:63,360, 1 sheet, 32 p.
- Stout, J.H., and Chase, C.G., 1980, Plate kinematics of the Denali fault system: Canadian Journal of Earth Sciences, v. 17, no. 11, p. 1527–1537, https://doi.org/10.1139/ e80-160
- Stout, J.H., Brady, J.B., Weber, F., and Page, R.A., 1973, Evidence for Quaternary movement on the McKinley strand of the Denali fault in the Delta River area,

- Alaska: Geological Society of America Bulletin, v. 84, no. 3, p. 939–948, https://doi.org/10.1130/0016-7606(1973)84<939:EFQMOT>2.0.CO;2.
- Surpless, K.D., Sickmann, Z.T., and Koplitz, T.A., 2014, East-derived strata in the Methow basin record rapid mid-Cretaceous uplift of the southern Coast Mountains batholith: Canadian Journal of Earth Sciences, v. 51, no. 4, p. 339–357, https://doi.org/10.1139/cjes-2013-0144.
- Sykes, L.R., 1978, Intraplate seismicity, reactivation of preexisting zones of weakness, alkaline magmatism, and other tectonism postdating continental fragmentation: Reviews of Geophysics, v. 16, no. 4, p. 621–688, https://doi.org/10.1029/RG016i004p00621.
- Taylor, M., Yin, A., Ryerson, F.J., Kapp, P., and Ding, L., 2003, Conjugate strike-slip faulting along the Bangong-Nujiang suture zone accommodates coeval east-west extension and north-south shortening in the interior of the Tibetan Plateau: Tectonics, v. 22, https://doi .org/10.1029/2002TC001361.
- Terhune, P.J., Benowitz, J.A., Trop, J.M., O'Sullivan, P.B., Gillis, R.J., and Freymueller, J.T., 2019, Cenozoic tectono-thermal history of the southern Talkeetna Mountains, Alaska: Insights into a potentially alternating convergent and transform plate margin: Geosphere, v. 15, no. 5, p. 1539–1576, https://doi.org/10.1130/ GES02008.1.
- Tikoff, B., Kelso, P., Manduca, C., Markley, M.J., and Gillaspy, J., 2001, Lithospheric and crustal reactivation of an ancient plate boundary: The assembly and disassembly of the Salmon River suture zone, Idaho, USA, in Holdsworth, R.E., Strachan, R.A., Macloughlin, J.F., and Knipe, R.J., eds., The Nature and Tectonic Significance of Fault Zone Weakening: Geological Society, London, Special Publication 186, p. 213–231.
- Tommasi, A., Knoll, M., Vauchez, A., Signorelli, J.W., Thoraval, C., and Logé, R., 2009, Structural reactivation in plate tectonics controlled by olivine crystal anisotropy: Nature Geoscience, v. 2, no. 6, p. 423, https://doi.org/10.1038/ngeo528.
- Trop, J.M., and Ridgway, K.D., 2007, Mesozoic and Cenozoic tectonic growth of southern Alaska: A sedimentary basin perspective, in Ridgway, K.D., Trop, J.M., Glen, J.M.G., and O'Neill, M.O., eds., Tectonic Growth of a Collisional Continental Margin: Crustal Evolution of Southern Alaska: Geological Society of America Special Paper 431, p. 55–94, https://doi.org/10.1130/2007.2431(04).
- Trop, J.M., Benowitz, J., Cole, R.B., and O'Sullivan, P., 2019, Cretaceous to Miocene magmatism, sedimentation, and exhumation within the Alaska Range su-

- ture zone: A polyphase reactivated terrane boundary: Geosphere, v. 15, no. 4, p. 1066–1101, https://doi.org/10.1130/GES02014.1.
- Trop, J.M., Benowitz, J.A., Koepp, D.Q., Sunderlin, D., Brueseke, M.E., Layer, P.W., and Fitzgerald, P.G., 2020, Stitch in the ditch: Nutzotin Mountains (Alaska) fluvial strata and a dike record ca. 117–114 Ma accretion of Wrangellia with western North America and initiation of the Totschunda fault: Geosphere, v. 16, no. 1, p. 82– 110, https://doi.org/10.1130/GES02127.1.
- Turner, D.L., and Smith, T.E., 1974, Geochronology and generalized geology of the Central Alaska Range, Clearwater Mountains, and Northern Talkeetna Mountains: Alaska Division of Geological and Geophysical Surveys Open File Report 72, scale 1:250,000, 1 sheet, 13 p.
- Twelker, E., Waldien, T.S., Newberry, R.J., Freeman, L.K., Sicard, K.R., Lande, L.L., Wypych, A., Reioux, D.A., and Bachman, E.N., 2020, Bedrock geologic map of the eastern Denali Highway area, Mount Hayes, Healy, and Talkeetna Mountains quadrangles, Alaska: Alaska Division of Geological and Geophysical Surveys Report of Investigation 2020-7, scale 1:100,000, 1 sheet, http:// doi.org/10.14509/30469.
- Veenstra, E., Christensen, D.H., Abers, G.A., and Ferris, A., 2006, Crustal thickness variation in south-central Alaska: Geology, v. 34, no. 9, p. 781–784, https://doi.org/10.1130/G22615.1.
- Vermeesch, P., 2004, How many grains are needed for a provenance study?: Earth and Planetary Science Letters, v. 224, no. 3–4, p. 441–451, https://doi.org/10.1016/j.epsl.2004.05.037.
- Vermeesch, P., 2012, On the visualization of detrital age distributions: Chemical Geology, v. 312–313, p. 190– 194, https://doi.org/10.1016/j.chemgeo.2012.04.021.
- Wahrhaftig, C., Turner, D.L., Weber, F.R., and Smith, T.E., 1975, Nature and timing of movement on Hines Creek strand of Denali fault system, Alaska: Geology, v. 3, no. 8, p. 463–466, https://doi.org/10.1130/0091-7613(1975)3<463:NATOMO>2.0.CO;2.
- Waldien, T.S., Roeske, S.M., Benowitz, J.A., and Stockli, D.F., 2017, Cenozoic reactivation of Cretaceous terrane accretionary structures in the eastern Alaska Range, Alaska: Geological Society of America Abstracts with Programs, v. 49, no. 6, https://doi.org/10.1130/ abs/2017AM-307791.
- Waldien, T.S., Roeske, S.M., Benowitz, J.A., Allen, W.K., Ridgway, K.D., and O'Sullivan, P.B., 2018, Late Miocene to Quaternary evolution of the McCallum Creek thrust system, Alaska: Insights for range-boundary

- thrusts in transpressional orogens: Geosphere, v. 14, no. 6, p. 2379–2406, https://doi.org/10.1130/GES01676.1.
- Wallace, W.K., Hanks, C.L., and Rogers, J.F., 1989, The southern Kahiltna terrane: Implications for the tectonic evolution of southwestern Alaska: Geological Society of America Bulletin, v. 101, p. 1389–1407, https://doi .org/10.1130/0016-7606(1989)101<1389:TSKTIF>2. 3.CO:2.
- White, C., Gehrels, G.E., Pecha, M., Giesler, D., Yokelson, I., McClelland, W.C., and Butler, R.F., 2016, U-Pb and Hf isotope analysis of detrital zircons from Paleozoic strata of the southern Alexander terrane (southeast Alaska): Lithosphere, v. 8, no. 1, p. 83–96, https://doi.org/10.1130/L475.1.
- Whitney, D.L., and Evans, B.W., 2010, Abbreviations for names of rock-forming minerals: The American Mineralogist, v. 95, no. 1, p. 185–187, https://doi. org/10.2138/am.2010.3371.
- Wilson, F.H., Hults, C.P., Mull, C.G., and Karl, S.M., comps., 2015, Geologic map of Alaska: U.S. Geological Survey Scientific Investigations Map 3340, scale 1:1,584,000, 2 sheets, 196 p., http://dx.doi.org/10.3133/sim3340.
- Wyld, S.J., Umhoefer, P.J., and Wright, J.E., 2006, Reconstructing northern Cordilleran terranes along known Cretaceous and Cenozoic strike-slip faults: Implications for the Baja British Columbia hypothesis and other models, in Haggert, J.W., Enkin, R.J., and Monger J.W.H., eds., Paleogeography of the North American Cordillera: Evidence for and Against Large-Scale Displacements: Geological Association of Canada Special Paper 46, p. 277–298.
- Yokelson, I., Gehrels, G.E., Pecha, M., Giesler, D., White, C., and McClelland, W.C., 2015, U-Pb and Hf isotope analysis of detrital zircons from Mesozoic strata of the Gravina belt, southeast Alaska: Tectonics, v. 34, p. 2052–2066, https://doi. org/10.1002/2015TC003955.
- York, D., Hall, C.M., Yanase, Y., Hanes, J.A., and Kenyon, W.J., 1981, 40Ar/39Ar dating of terrestrial minerals with a continuous laser: Geophysical Research Letters, v. 8, p. 1136–1138, https://doi.org/10.1029/ GL/08i011p01136.

SCIENCE EDITOR: ROB STRACHAN ASSOCIATE EDITOR: BERNHARD GRASEMANN

Manuscript Received 11 February 2020 Revised Manuscript Received 8 May 2020 Manuscript Accepted 2 June 2020

Printed in the USA